# 科技部補助

# 大專學生參與專題研究計畫研究成果報告

計畫名稱：黃酮醇、Zidovudine 與 Ticagrelor 對 PriA 與 DnaB 解旋?的抑制機制與藥物優化

執行計畫學生：彭偉峰

學生計畫編號：NSC 102-2815-C-040-014-B
研究期間：102 年 07 月 01 日至 103 年 02 月 28 日止，計 8 個月

指導教授：黃晟洋

處理方式：本計畫涉及專利或其他智慧財產權,2 年後可公開查詢

執行單位：中山醫學大學生物醫學科學學系（所）

中華民國 103 年 03 月 24 日

# 目錄

# 摘要

常見的細菌院內感染常造成嚴重的症狀，甚至死亡；雖可用抗生素治療，但臨床治療常發現這些細菌多已帶有多重抗抗生素的能力，包括各地頻頻傳出的"超級細菌"。之前的研究指出，部分黃酮醇化合物 (flavonols) 具有可抑制細菌酵素如 DNA 解旋酶以及其他 DNA 結合蛋白質的能力，進而阻斷細菌 DNA 複製以及影響其生長，因此，這些與 DNA 結合和反應的蛋白質與解旋酶應該是一個可供新型抗生素研發的分子標靶。另外，黃酮醇化合物也可能會是其他細菌酵素的抑制劑。在此計劃，我們分析了細菌所特有的引子合成體蛋白質群，分別從金黃色葡萄球菌與克雷白氏肺炎桿菌選殖而來，包含了 PriA 解旋酶、PriB、PriC、DnaT、DnaC、DnaB 解旋酶、DnaD、DnaI 與 SSB 蛋白質跟各種黃酮醇交互作用的能力之外，也對細菌所特有的酵素：尿囊素水解酵素 (allantoinase) 與二氫乳清酸水解酶(dihydroorotase) 作結合與抑制的分析。除了黃酮醇之外，我們亦使用已核准使用的臨床藥物 Zidovudine (為抗愛滋病病毒的核苷酸反轉錄酶抑制劑)進行是否可老藥新用於抗菌的試篩。我們發現黃酮醇對以上所述的這些蛋白質擁有良好的結合與抑制能力，尤其是黃酮醇中的 kaempferol 對尿囊素水解酵素與二氫乳清酸水解酶有極強的抑制能力。然而，利用酵素抑制動力學模型得知 kaempferol 對此兩酵素的抑制型態卻有所不同： kaempferol 對尿囊素水解酵素為競爭型抑制劑但對二氫乳清酸水解酶則為非競爭型抑制劑；透過 docking 與電腦模擬的實驗也發現此與酵素抑制的結果相符。綜觀以上結果，我們認為黃酮醇尤其是 kaempferol ，不單單為一優質的天然抗氧化物，也是一良好的抗生素研發的前導物 (lead compound)。此研究部分的結果已發表至 *Biochimie* (Peng, W.F., Huang, C.Y.* (2014) Allantoinase and dihydroorotase binding and inhibition by flavonols and the substrates of cyclic amidohydrolases. ***Biochimie***, accepted and published online, doi: 10.1016/j.biochi.2014.01.001., SCI)，其中本人為第一作者。未來我們更希望優化含各種醣基的黃酮醇衍生物等，希能找尋出更強的抑制劑作為不同於抑制細胞壁生成等傳統機制的新型抗生素。

# 第一章：緒論 (introduction)

## 1.1 金黃色葡萄球菌（*Staphylococcus aureus*）介紹及致病機制

金黃色葡萄球菌 (*Staphylococcus aureus*) 為一種革蘭氏陽性球菌 (gram positive coccus)，在顯微鏡下成葡萄串狀，無鞭毛及內孢子，具有 catalase，為常見引起食物中毒的病原菌，存在於皮膚及黏膜上，葡萄球菌為表皮上正常之菌種，可能會引起伺機性感染 (opportunistic infection)，金黃色葡萄球菌會引起不同程度之感染症，如毛囊炎、心內膜炎、骨髓炎等 [1]。

金黃色葡萄球菌之感染為院內感染 (nosocomial infection) 非常常見的菌種，會引起嚴重的症狀，如菌血症 (bacterimia)，甚至死亡，經驗上使用 β-lactam 類抗生素進行治療，例如：oxacillin, cephalosporins 等，但由於抗生素使用氾濫，造成細菌產生 β-lactamase, PBP (Penicillin Binding Protein), efflux transporter 等抗菌機制，MRSA (Methicillin resistant *Staphyloccocus aureus*) 於 1961 年首次在英國發現，其擁有 β-lactamase 並對於 β-lactam 類藥物產生抗性，在醫院中被稱為「超級細菌」，對於 MRSA，萬古黴素(vancomycin) 通常為最後一線之藥物，其機制為抑制細菌細胞壁之合成，但近年來，VRSA (Vancomycin resistant *Staphyloccocus aureus*) 也開始在醫院中出現 [2-5]。

金黃色葡萄球菌具有多種的致病機轉，包含如 (A)結構因子：英膜 (capsule) 及肽聚醣 (peptidoglycan) 可以促進發炎，抑制趨化作用 (chemotaxis) 及吞噬作用 (phagocytosis)，protein A 為金黃色葡萄球菌特有之成份，具有吸附抗體及補體的作用；(B)毒素：cytotoxin 會造成 β 型溶血， exfoliative toxin 為 serine protease，會造成 SSSS (脫皮症候群)，enterotoxin 為一超級抗原 (superantigen)，作用於人體中會使 T cell 分泌大量 cytokine，造成嚴重的系統性發炎反應，臨床表徵即為食物中毒，TSST (Toxic shock syndrome toxin) 亦為超級抗原，會破壞腎小管內皮細胞，並引起腎衰竭；(C)酵素：玻尿酸酶 (hyaluronidase)、纖維蛋白溶解酶 (fibrinolysin) 等可以幫助細菌在組織間移動 [6,7]。

## 1.2 克雷白氏肺炎菌（*Klebsiella pneumoniae*）介紹及致病機制

克雷白氏肺炎菌 (*Klebsiella pneumoniae*) [8] 為僅次於大腸桿菌 (*Escherichia coli*)

亦造成菌血症之腸內菌 (Enterobactericeae)，主要之致病機轉為其高變異性的莢膜，能抵抗巨噬細胞的吞噬作用；纖毛 (fibriae) 為一種細菌黏附因子，其提供了感染的專一；螯鐵系統 (iron acquisition system)：以螯鐵蛋白 (siderophore) 為主，細菌借此與宿主競爭生物生存所需的三價鐵離子。克雷白氏菌在人體中為常在菌種，存在於呼吸道、消化道、泌尿道等黏膜性上皮，在醫院中，克雷白氏肺炎菌亦為院內感染常見之菌種，ESBL 型 (Extended-spectrum of β-lactamase ) 為最常見的，其具有能分解廣效性頭孢菌素水解酶，因而造成嚴重的抗藥性，NDM-1 (New Delhi metallo-β-lactamase) 抗菌株的發現也使得克雷白氏菌的抗藥性問題日益增加 [9-11]。

## 1.3 DNA 複製系統

### 1.3.1 解旋酶 (helicase)

解旋酶是一類可解開 DNA 上兩兩鹼基配對氫鍵的酶，藉由水解 ATP 供給能量來解開雙股螺旋 DNA（unwinding DNA）[12-15]。本計畫會研究兩種解旋酶，分別為 DnaB [16,17] 與 PriA [18,19]。

#### 1.3.1.1 DnaB 解旋酶

DnaB 解旋酶是所有生物體維持生命所必需的酵素，其主要的功能是能將緊密黏合的雙股螺旋 DNA 進行解旋，並形成兩條單股 DNA，以利於 DNA 聚合酶 (polymerase) 的結合，促使 DNA 的複製。不管在一般 DNA 的複製，又或者是進行 DNA 修復（DNA repair）時，都是不可或缺的。在先前的研究提出，DnaB 會事先的與單股 DNA 進行結合，而後再將 ATP 進行水解反應，以獲取能量並進行移動與解旋。由於先前一連串蛋白質交互作用，而吸引 DnaB 結合到 DNA 上使 DNA 解旋，並使 DNA 模板 (DNA template) 所裸露出來，此時引子合成蛋白 DnaG 便會合成引子 (primer) 在模板 DNA 上，並引導 DNA 聚合酶複製出另外一股 DNA，已完成 DNA 的複製或修復 [12-14,20]。

DnaB 依照解旋酶家族的分類，可區分出許多不同的家族，依照其解旋的方向性，分為 3’-5’方向解旋的 A 型解旋酶，以及 5’-3’的 B 型解旋酶，而 DnaB 為 B 型解旋酶。另外 DnaB 在其結構上，分為三個主要區域，分別為 αβγ，其這三個區域結存在於大部份的細菌解旋之中，其中 β 區域只要為核甘酸（nucleotide）結合位並對核甘酸進行水解反應以獲的能量，而 γ 區域是吸引單股 DNA 與其結合，並具有與其他 DnaB 進

行交互作用，使 DnaB 形成六套體（hexamer）結構。α 區域主要是解旋酶對 DNA 進行解旋的主要功能區域，但經由與其他菌種進行序列比對時其相似並不高，這還待其他學家進行研究 [21]。

#### 1.3.1.2 PriA 解旋酶

在眾多的解旋酶之中，PriA 是被分類在 3’-5’方向解旋的 A 型解旋酶 [15,22-24]。PriA 解旋酶為引子合成體（primosome）中的一員，對於 DNA 的複製相當重要，且已証證時當 DNA 的複製叉（replication fork）受到外在環境破壞，造成 DNA 無法繼續進行複製時，為主要因子去重新開啟 DNA 的複製。它可辨識受到損害的 DNA 所形成的特殊二級結構（second structure），並且與之結合並延長展露出單股 DNA 區域，並吸引單股 DNA 結合蛋白（single strand DNA binding protein）抓住裸露的 DNA，等待其它蛋白前來進行換手動作。假使將其去除，細菌在充滿 UV 光的照射下，其存活率會大大的下降 [25-32]。

在先前的研究發現已知，PriA 解旋酶內含有兩個區域，為單股 DNA 結合區，以及 nucleotide 結合區 [18,33]。而 PriA 的 DNA 結合區分為兩個，一個對 DNA 有微弱的結合能力，另一個對 DNA 有強力的結合反應 [34]。在無 ADP 存在的環境下，DNA 只會被 PriA 的強力 DNA 結合區進行結合，但當 ADP 與 PriA 相互結合時，便會改變 PriA 的蛋白質構型，使微弱 DNA 結合區打開，幫助 PriA 與 DNA 作結合，大大增強與 DNA 結合的能力 [34]。

### 1.3.2 DNA 複製再啟動（DNA replication restart）

引子合成體 (primosome)，其最早的機制是在嗜菌體中被發現 [35-39]。在嗜菌體 ϕX174 的 DNA 上有特殊的 DNA 序列，稱之為 *pas* (primosome assembly site)，會吸引引子合成體靠近並進行 DNA 複製，因此被發現到。在原核生物體中，其 DNA 模板受到細菌體中的氧化壓力或紫外線照射等外在化學性傷害時，其 DNA 複製便會暫停，等到 DNA 修復完成之後，才會重新進行 DNA 的複製 [40,41]。要將其以停止的 DNA 複製重新啟動，便需要引子合成體來合成引子，便於 DNA 複製繼續進行。引子合成體是由一連串的蛋白質相互結合而形成的蛋白質-DNA 複合體，在革蘭氏陰性菌與陽性菌並不相同 [42-48]。革蘭氏陽性菌如今黃色葡萄球菌的引子合成體其組成的蛋白質為： PriA, DnaD, DnaB, DnaC, DnaI, 與 DnaG [49]。一開始 PriA 會結合到 DNA

目標區域上，DnaD、DnaI 與 DnaC 會先後的與 PriA 進行結合，其中的機制雖然還不清楚，但可以確定的是 DnaD 會先與 PriA 先行結合，其 DnaI 與 DnaC 會相互結合形成複合物 $DnaI_6$-$DnaC_6$，並與 DnaD 進行結合，後再吸引 DnaB 與之結合，DnaI-DnaC 複合物便會幫助 DnaB 結合裝載（loading）到 DNA 上 [50]。當 DnaB 結合在 DNA 上時，其 DnaG 便會一同的結合上來，並在模板 DNA 上合成新的引子，最終 DNA 聚合酶結合上來繼續未完成的複製。在先前的研究指出，DnaI 會先與 ATP 進行結合，後與 DnaB 進行交互作用並一同與 DnaB 形成六聚體（$DnaB_6$-$DnaI_6$），同時 DnaI 的蛋白構形發生改變，以易於將 DnaB 結合組裝到 DNA 上，後再進行 ATP 水解反應，使其蛋白構行回復到先前未與 ATP 結合時的狀態，並從 DnaB 身上離開完成 DnaB 與 DNA 的組裝 [51-58]。

## 1.4 類黃酮介紹及醫療用途

類黃酮 (flavonoids) 是個獨特卻又常見於光合作用植物中，常現在水果、蔬菜、花、茶、酒、蜂蜜當中被分離出，目前科學家鑑定出約 4000 種不同的類黃酮 [59-65]。在幾世紀以來，他常被用於治療人類的疾病，並且發現這天然的產物，具有抗人類感染（anti-infaction）的效用。依照其結構上分類，可分為：黃酮類 (flavones)、黃酮醇類 (flavonol)、黃烷酮類 (flavanone)、異黃酮類 (isoflavone)、新類黃酮 (neoflavonoid)，並依照其種類，具有可抗菌（anti-bacterial），抗黴（anti-fungal），抗病毒（anti-viral）等活性 [63-70]。它也具有抗發炎與抗氧化反應，例如在抗發炎方面，黃酮類化合物能夠抑制轉錄因子 $NF_kB$ 的和 AP-1 與上游的傳遞路徑進行結合，如：MAPK，IKK 和 PI3K/Akt 訊息傳遞路徑，使降低發炎性物質的產生或使降低促發炎性物質（TNF，IL-A，PGE2）和活化發炎酵素（COX-2 和 iNOS）的活動，達到降低發炎的效果。在抗氧化方面，也有論文指出，類黃酮具有抑制 NADPH oxidase 的活性，以避免身體產生過多的過氧化物質。另外，也發現到類黃酮具有直接抑制 DNA 的生成、影響細胞膜穩定性與能量代謝的能力。類黃酮的結構有三個六角環的構造，為其基本結構，並在 A 環與 C 環上依不同種類在不同位置接上數量不同的氫氧基，這與類黃酮有抗氧化能力息息相關，也會在 B 環上接上不同數量的氫氧基，使其產生不同的化學和物理特性。

## 1.5 Zidovudine 介紹及醫療用途

Zidovudine 又名 Azidothymidine (AZT)，是一個已臨床使用的核苷酸反轉錄酶抑制劑 (Nucleoside Reverse-transcriptase Inhibitor, NRTI)，用於治療後天免疫不全症 (AIDS) [71]。AZT 可以抑制 HIV 病毒合成 viral DNA，並減緩病毒的複製與散播，目前與其他抗 HIV 藥物組合進行合併療法(Highly Active Antiretroviral Therapy, HAART)，AZT 選擇性的抑制 HIV 的反轉錄酶，使得 HIV 無法將其 RNA 反轉錄為 DNA，進而影響 viral DNA 嵌入宿主 DNA 形成 provirus；AZT 之疊氮基 (Azido group) 可以增加其親脂性 (lipophilic)，並使它能順利通過受感染細胞之細胞膜及血腦障壁 (Blood-Brain Barrier)，細胞中的酵素會將其轉變為帶有三個磷酸的形式，並對 HIV 反轉錄酶產生抑制。

## 1.6 Ticagrelor 介紹及醫療用途

近年來，急性冠心症 (Acute Coronary Syndrome, ACS)的發生率逐漸上升，冠狀動脈血管內膜的斑塊突然破裂，導致血栓的產生，使得心肌供氧量不足，若血栓只塞住部分之血管，血流減少但仍能通過時，稱為不穩定型心絞痛 (Unstable Angina)；若血栓將血流完全阻斷，導致心肌缺氧時則稱為心肌梗塞 (Myocardial Infarction)。預防 ACS 的再發生有賴於抗血小板藥物，如 asprin , clopidogrel 等，ticagrelor 是一個 ADP receptor antagonist [72,73]，並經由可逆且非競爭性的與血小板上 $P2Y_{12}$ ADP receptor 結合後，並藉由抑制由 ADP 活化之 GbIIb/IIIa 附合體活化降低血小版活化與凝集，由於其對於上 $P2Y_{12}$ ADP receptor 為可逆的拮抗，凝集功能的回復依照血清中 ticagrelor 及其活性代謝物的濃度而定 [72,73]。

## 1.7 Cyclic Amidohydrolase 介紹

### 1.3.1 Cyclic Amidohydrolase

Amidohydrolase superfamily 為一群可以催化碳或磷骨架上 amide 及 ester functional group 之酵素[74-77]，尿囊素水解酶 (allantoinase) [78-82], 二氫乳清酸水解酶 (dihydroorotase) [83-87], 海因酶 (hydantoinase) [88-95] 及二氫嘧啶酶 (dihydropyrimidinase) [94-101] 都屬於 cyclic amidohydrolase 家族。另外，imidase 與 imidase-hydrolyzing enzyme 也屬於此家族 [95,99,101-105]，他們具有結構及功能相似性，但在胺基酸序列上卻缺少相似性，這些酵素具有 metal center，大致分為單金屬中

心與雙金屬中心兩種，並催化在嘧啶及嘌呤代謝中五元及六元環受質之 cyclic amide bond 之水解及開環反應。

allantoinase 與 dihydroorotase 之 active site 均含有四個 histidine,一個 aspartate 及一個 post-carboxylated lysine 或是第二個 aspartate，羧化的 lysine 與活化位中金屬 cofactor 的結合及催化活性均有關 [78,80,81]。Cyclic amidohydrolase 目前認為之催化機制為：參與親核水解反應的水分子必須被活化；受質的 amide bond 必須經由旁邊 carbonyl group 的極化而變得更加親電 (electrophilic)；而在 leaving group 中的 N 必須被質子化，最後酵素將 C-N bond 水解開環。此類酵素雖然催化機制相似，但具有受質專一性，其機制尚未清楚。

#### 1.3.1.1 尿囊素水解酶 (Allantoinase, ALLase)

尿囊素水解酶 (allantoinase) 為 homotetrameric dinuclear metalloenzyme，廣泛存在於各類生物中，包含細菌、植物到部分動物均有之 [106-112]，allantoinase 催化尿囊素 (allantoin)與 allantoic acid 之間可逆的水解及開環，此反應在醯脲 (Ureide)代謝中扮演重要的角色，並影響生物對於嘌呤代謝物中氮元素的利用。

#### 1.3.1.2 二氫乳清酸水解酶 (Dihydroorotase, DHOase)

二氫乳清酸水解酶 (dihydroorotase) [113-116] 與 allantoinas 相似，皆為 metalloenzyme，催化 carbamoyl aspartate 與 dihydroorotate 之間的可逆水解反應，此反應位於 de novo pyrimidine synthesis 之第三步，在哺乳類中，dihydroorotate 為 CAD (Carbamoyl phosphate synthetase/ Aspartate transcarbamoylase/ Dihydroorotase) 蛋白質複合體的一部分，CAD 在哺乳類中負責嘧啶的生合成，但在原核細胞中，CAD 複合體中的三個酵素則會各自表現 [115,117,118]。

## 1.8 研究動機

近年來，因為過於氾濫的使用抗生素，已導致細菌演化出了可以抵抗多種抗生素的能力，使形成多重抗藥性。”超級細菌”一詞頻頻出現於新聞媒體的報導，除之前印度所傳出的腸道菌 (克雷白氏菌與大腸桿菌)已蔓延至各地，最近在英國亦爆發出”超級金黃色葡萄球菌”。這些細菌所引發的感染症原可以使用青黴素或頭孢菌素等抗生素來治療，然由於這些細菌經由突變或交換基因等方式亦發展出對抗這些傳統抗生素的能力，尤其是以其細胞壁合成或核醣體蛋白質為標靶的藥物，且已有多重抗藥性

的細菌不斷被發現與報導，成為臨床治療時甚面臨無藥可醫的情況。因此若能開發出新的標靶，也許對此棘手的問題將能有所幫助。此計劃提出的 PriA 與 DnaB，雖是細菌 DNA 複製時所必需的解旋酶，然其結構與功能與高等動物的解旋酶相比則有顯著的不同，因此亦可能據此所開發出之藥物對人體較無副作用。另外，之前我們已發現部分黃酮醇物質對克雷白氏肺炎桿菌 DnaB 解旋酶的解旋能力有明顯的抑制效果[16,119]；此抑制效果主要是經由抑制其 ATP 的結合。由於許多不同的黃酮醇物質也已被報導可抑制許多的細菌來源的酵素，因此我們也有興趣將我們實驗室兩個細菌特有的酵素，dihydroorotase 與 allantoinase 一起分析。由於臨床上已有許多藥物其藥理機轉是抑制酵素或激酶等的核苷酸的結合，因此也許有其他更多已可臨床使用但仍未在抗菌項目中所嘗試的天然物或藥物有抑制解旋酶的活性，值得試著篩選與優化出來。因此此計劃測試與優化各種類黃酮物質對細菌的 PriA 與 DnaB 解旋酶的抑制之外，包括原使用於抗愛滋與抗凝血的核苷酸類似藥物，Zidovudine 與 Ticagrelor，對這些解旋酶與其他的 DNA 結合蛋白質有系統性的做抑制與結合之分析。部份的結果今年已發表在生化領域的 SCI 期刊 ***Biochimie*** [Peng, W.F. (彭偉峯), Huang, C.Y.* (2014) Allantoinase and dihydroorotase binding and inhibition by flavonols and the substrates of cyclic amidohydrolases. ***Biochimie***, accepted, and published online, doi: 10.1016/j.biochi.2014.01.001., SCI]，其中本人為第一作者。

# 第二章：材料與方法

# （Materials and Methods）

## 2.1 實驗材料

(1) 聚合酶連鎖反應(PCR)中所使用的 buffer 以及 *Taq* polymerase 購買自 MDBio (Frederick, MD, USA)。

(2) PCR 產物純化，所使用的 kit 購買自 VIOGENE (Taipei, Taiwan)。

(3) 質體抽取所使用的 kit 購買自 MDBio (Frederick, MD, USA)。

(4) Gel extraction 所使用的 kit 購買自 GE Healthcare (Piscataway, NJ, USA)。

(5) 製備 Clone 的限制酶購買自 NEB (Ipswich, MA, USA)。

(6) 所使用的勝任細胞 (competent cell) 為 *ECOS*™ 21、*ECOS*™ 101 購買自 YEASTERN (Taipei, Taiwan)。

(7) 接合反應所使用的T4 DNA ligase 和 buffer 購買自 Promega (Madison, WI, USA)。

(8) 細菌生長所使用的 LB 購買自BD (Franklin Lakes, NJ, USA)。

(9) 抗生素 Ampicillin 購買自MDBio (Frederick, MD, USA)。

(10) 蛋白質表現是使用isopropyl β-D-1-thiogalactopyranoside (IPTG)，購買自MDBio (Frederick, MD, USA)。

(11) 純化所使用的膠體管柱為 HisTrap™ HP 購買自GE Healthcare (Piscataway, NJ, USA)。

(12) SDS-PAGE 所使用的 SDS、TEMED、Tris-HCl (pH 8.8)、Tris-HCl (pH 6.8)、30% Acrylamide/Bis、APS、Stain buffer 皆購買自BIO-RAD (Hercules, CA, USA)。

(13) 螢光偵測實驗所使用的六種類黃酮：myricetin、quercetin、galangin、kaempferol、myricitrin、dihydromyricetin 皆購買自Sigma ( St. Louis, MO, USA)

(14) Bacterial agar 購買自 AMRESCO (Solon, OH, USA)。

- Ampicillin LB 培養盤製作：

  12.5 g 的 LB 和 7.5 g 的 bacterial agar 加入 500 ml 的 $ddH_2O$，高溫高壓滅菌，冷卻至 55 ℃，加入 250 µl 的 100 mg/ml ampicillin 後倒盤。

(15) DNA 電泳使用的 Agarose I™ 購買自 AMRESCO (Solon, OH, USA)。

- 1 % 瓊脂膠製作配方：

12.5 g 的 agarose 加入 70 ml 的 0.5X TAE 中，沸騰至透明呈清狀，冷卻至 55 ℃後倒入鑄膠槽中。

(16) SDS PAGE 製作配方：

- 10X running buffer (1 L) 製作配方 (使用時稀釋為 1X)：

| | | | |
|---|---|---|---|
| 1. | Tris | 32.3 g | （final concentration = 250 mM） |
| 2. | Glycine | 144 g | （final concentration = 1.92 M） |
| 3. | SDS | 20 g | （final concentration = 1 %） |

- Stacking gel (4 %)：

| | |
|---|---|
| 1. $ddH_2O$ | 1.50 ml |
| 2. 30 % Acrylamide/Bis | 0.33 ml |
| 3. 1.5 M Tris-HCl (pH 6.8) | 0.63 ml |
| 4. 10 % SDS | 25 µl |
| 5. 10 % APS | 25 µl |
| 6. TEMED | 1 µl |

- Resolving gel (12 %)：

| | |
|---|---|
| 1. $ddH_2O$ | 1.65 ml |
| 2. 30 % Acrylamide/Bis | 2.00 ml |
| 3. 1.5 M Tris-HCl (pH 8.8) | 1.25 ml |
| 4. 10 % SDS | 50 µl |
| 5. 10 % APS | 50 µl |
| 6. TEMED | 1.5 µl |

- Destain buffer (1 L)製作配方：

| | |
|---|---|
| 1. Methanol | 200 ml |
| 2. Acetic acid | 100 ml |
| 3. $ddH_2O$ | 700 ml |

## 2.2 蛋白質取得與處理相關之技術

### 2.2.1 聚合酶連鎖反應

加入下列之 PCR 實驗反應物至200 µl 微量離心管中並混和均勻，使用的儀器是 BIO-RAD Thermocycler，反應條件如下所示。

Reagent：

| | | |
|---|---|---|
| 1. | Template DNA | 0.5ul |
| 2. | Primer-forward | 1ul |
| 3. | Primer-revers | 1ul |
| 4. | 10mM dNTP mix | 1ul |
| 5. | 10X Taq buffer | 5ul |
| 6. | Taq DNA Polymerase | 0.7ul |
| 7. | Sterile deionized water | 40.8ul |

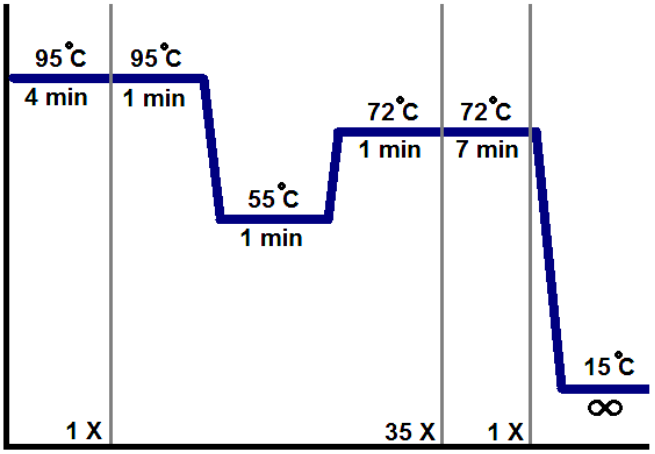


取 4 µl 反應後混合液產物與 1 µl 的 6X loading dye 混合後，將其注入到 1 % 瓊脂膠(0.5X TAE buffer and 1 % agarose)並進行電泳（electrophoresis），於 0.5X TAE buffer 中給予電流 110 mV 分離產物約 20 分鐘，經 EtBr 染色 10~15 分鐘後用紫外光照膠確認反應後產物大小是否正確。

### 2.2.2 PCR 產物的純化

(1) 將PCR產物 （總體積50 µl） 加入 500 µl PX buffer 混合均勻。

(2) 將混合好產物加入 Clean up column，13000 rpm 離心，1分鐘。

(3) 去掉下層液，加入500 µl WF Buffer，以13000 rpm 離心，1分鐘。

(4) 去掉下層液，加入500 µl WS Buffer，以13000 rpm 離心，1分鐘。

(5) 再以 13000 rpm 離心2分鐘 (使WS buffer 內的 ethanol 加以去除乾淨)。

(6) 換至新的 tube 後加入 50 µl 的 dd$H_2O$，放置室溫約10分鐘，再以 13000 rpm 離心2分鐘，並保存至-20 ℃。

### 2.2.3 質體抽取及質體製備

質體抽取步驟為：

(1) 將含有 pET21b 質體之單一菌落挑起，加入含有 4 µl 100 mg/ml ampicillin 的 4 ml LB 培養液中，置於 37℃培養箱，搖晃培養到 $OD_{600}$ 約為 1.0 。

(2) 後在 Tube 中分次加入 1000 µl 菌液，離心 12000 rpm，1 分鐘，去除上清液，並重覆 4 次。

(3) 加入 250 µl 的 Solution I，並將離心下來的菌塊溶散，後在冰上反應 2 分鐘。

(4) 加入 250 µl Solution II，用手緩慢搖晃均勻，室溫反應 1 分鐘。

(5) 加入 250 µl Solution III，用手緩慢搖晃均勻，室溫反應 1 分鐘。

(6) 離心 11000 rpm，10 分鐘，並將其上清液取出 (勿吸取到細胞碎片的白色沉澱物)。

(7) 將 750 µl 上清液吸至 Collect tube 中，在室溫靜置 2 分鐘，離心 6400 rpm，1 分鐘。

(8) 除去 column 之過濾液，加入 500µl Wash Solution，離心 7200 rpm，1 分鐘，重複兩次。

(9) 再以 8800 rcf 離心 2 分鐘 (將 Wash Solution 中的 ethanol 加以去除乾淨)。

(10) 最後加入 50 µl 的 elution buffer 放置 37℃ 反應 5 分鐘，以 8800 rcf 離心 2 分鐘，完成質體抽取。

### 2.2.3 蛋白質表現測試與蛋白質表現菌體儲存

(1) 將定序結果正確的質體轉型至 (*ECOS*™ 21)中。

(2) 用挑菌棒取出 plate 中的單一菌落，種入含 4 µl 100 mg/ml ampicillin 的 4 ml LB 培養液中，置於 37 ℃培養箱，搖晃培養至 $OD_{600}$=1.0。

(3) 將 O.D 1.0 的菌液平分成兩管，一管做蛋白表現測試，一管做菌液儲存，各加入 2 ml LB 培養液，搖晃培養至 $OD_{600}$=1.6。

(4) 從蛋白表現測試管中取 200 µl 菌液至 eppendorf 中，原菌液加入 1 M isopropyl β-D-1-thiogalactopyranoside (IPTG) 4 µl，再培養 4 小時後取 150 µl 表現後菌液至 eppendorf 中。

(5) 用 12000 rpm 離心，1 分鐘，用 20 µl $ddH_2O$ 回溶菌塊後跑 SDS-PAGE 進行確認，步驟如下：

1. 加入 4X loding dye 10 µl 混合均勻，以 98 ℃加熱 1 小時。
2. 將 marker 與 sample 注入 SDS-PAGE 之後，以 70 mV 跑膠約 2 小時。
3. 跑膠完成後，將膠片置於 stain solution (coomassie blue)中染色 1 小時。
4. 染色完後以 destain solution，退染約 1 小時。

5. 最後以玻璃紙封膠，風乾後確認結果。

(6) 取菌液儲存管，在 tube 中分次加入 1000 µl 菌液，離心 12000 rpm，1 分鐘，去除上清液，重覆 4 次。

(7) 加入 400 µl LB 培養液回溶菌塊，再加入 50% glycerol 100 µl 後，保存至-80 ℃，完成菌液儲存。

### 2.2.4 細菌大量培養與蛋白質表現

(1) 取出儲存菌液 10 µl，加入含 4 µl 100 mg/ml ampicillin 的 4 ml LB 培養液中，置於 37 ℃培養箱，搖晃培養至菌液濃度達到 $OD_{600}$=1.2。

(2) 將培養至 $OD_{600}$=1.2 的菌液加入含 200 µl 100 mg/ml ampicillin 的 500 ml LB 培養液中，此次共培養 2 瓶共 1 L 細菌培養液，置於 37 ℃培養箱，搖晃培養至菌液濃度達到 $OD_{600}$=1.6 (時間約 4~6 小時)。

(3) 於濃度約為 $OD_{600}$=1.6 時加入 1 M IPTG 125 µl 誘導表現蛋白生成，在 25 ℃環境下繼續培養 8 小時。

### 2.2.5 蛋白質純化

(1) 將培養好的菌液分置於 250 ml 離心瓶，以高速冷凍離心機 (Beckman) 12000 rpm 於 4 ℃低溫離心 20 分鐘。

(2) 除去上清液，每瓶以 10 ml 的 binding buffer (5 mM imidazole, 500 mM NaCl, pH 7.4) 將底部菌塊重新回溶，將回溶的菌液放入 50 ml 離心管。

(3) 使用超音波破碎機 (sonicator) 將溶於 binding buffer 內的菌體均勻震碎。

(4) 之後以 14000 rpm 於 4 ℃低溫離心 20 分鐘，收集上清液。

(5) 將純化用 column His Trap™ HP 依序通入 30 ml 的 $ddH_2O$、30 ml 的 50 mM $NiSO_4$、30 ml 的 $ddH_2O$ 及 30 ml 的 5 mM imidazole, 500 mM NaCl, pH 7.4) buffer。

(6) 接著將含有蛋白質之上清液以慢速通入 column 中。

(7) 通完上清液後，依序使用含有 500 mM NaCl pH 7.4 的不同濃度 imidazole (5 mM、60 mM、100 mM、200 mM、500 mM) 通入 column。並收集洗出之蛋白質各 50 ml。

(8) 最後使用 100 mM EDTA pH 8.00 清洗 column，並用 20 % EtOH 通入 column 保存。後以 SDS-PAGE 確認蛋白質狀況，至此蛋白質純化完成。

### 2.2.6 蛋白質透析

實驗使用之透析膜為 Thermo Snake Skin® Pleated Dialysis Tubing。

(1) 剪下適當長度後，將透析膜浸濕於蛋白質要置換之 buffer(此實驗使用之 buffer 為 20 mM Tris–HCl, 200 mM NaCl, pH 8.0)，大約 2 分鐘。

(2) 將浸濕的透析膜拉平，以長型夾子夾住下端密封，放入欲置換 buffer 之蛋白質約 20ml，將上端也以長型夾子夾住密封，並預留約 1 公分之置換空間。

(3) 將蛋白質懸掛於欲置換之 buffer 中，體積約為 1000ml，以磁石攪動 buffer，轉速約 160 rpm，置於 4 ℃環境下置換 6 小時，即完成蛋白質透析。

### 2.2.7 蛋白質濃縮

- 實驗使用之濃縮管為 Millipore Amicon ultra-10K。

(1) 取出濃縮管後，以酒精和 dd$H_2O$ 小心沖洗 (以免破壞過濾膜)。

(2) 清洗完畢後，加入 10 ml 透析完的蛋白質溶液，3000 rpm 於 4 ℃低溫離心 30 分鐘，重覆此步驟至蛋白質濃度達到實驗條件為止 (需注意蛋白質狀態是否有聚集沉澱)。

(3) 使用完畢後，以 dd$H_2O$ 和酒精小心沖洗，保存至 20 % 酒精中。

## 2.3 蛋白質-小分子交互作用之螢光淬滅

本計畫所使用的螢光偵測儀器為 Hitachi-2700，實驗條件如下

### 2.3.1 用螢光淬滅偵測蛋白在不同類黃酮及臨床藥物的情況下：

(1) 環境 buffer：HEPES 50mM, Tris 50mM, NaCl 50mM　pH7

(2) 蛋白濃度約為 0.1~1uM

(3) 類黃酮濃度：為 1-30 uM

(4) 偵測時間間隔為 1 min

(5) 反應環境溫度為：25 ℃

(6) 偵測波長為(ex/em)：280/330 nm

## 2.4 蛋白質-小分子電腦模擬交互作用：分子對接(Molecular docking)

### 2.4.1 分子對接使用之配體 (ligand) 及蛋白質模型 (model)：

(1) 分子對接使用之配體(docking ligand)是從 PubChem 及 DrugBank 以.pdb 或.sdf 檔案格式下載

(2) KpPriA N 端之模型是利用 SWISS MODEL 並基於 2D7H (aa. 4-104)

(3) KpPriA 全長之模型(4NL4)下載自 PDB (Protein Data Bank)

(4) SaDnaB 之模型是利用 SWISS MODEL 並基於 Geobacillus kaustophilus DnaC (2R6C) 之結構

(5) Sty Allantoinase 之模型是利用 SWISS MODEL 並基於 Bacillus halodurans allantoinase (3HM7: 42% identity)之結構

(6) Kp Dihydroorotase 之模型是利用 SWISS MODEL 並基於 Salmonella enterica dihydroorotase (3JZE : 93% identity)之結構

### 2.4.2 分子對接(HEX-Server)：

(1) HEX-Server 網址為 http://hexserver.loria.fr/index.php

(2) 將 ligand 及 receptor 以.pdb 檔案格式上傳

(3) 選擇 Correlation type (Shape only, Shape+Electrostatic)

(4) 將檔案 submit 後，等待結果並下載之

### 2.4.3 分子對接(PATCH DOCK)：

(1) PATCH DOCK 網址為 http://bioinfo3d.cs.tau.ac.il/PatchDock/

(2) 將 ligand 及 receptor 以.pdb 檔案格式上傳

(3) 填入 e-mail，將 RMSD 設為 1.5，選擇 Complex type 為 Protein-small ligand

(4) 將檔案 submit 後，等待結果並下載之

## 2.5 利用 Malachite Green Assay 分析蛋白質之 ATPase activity

(1) 根據不同的實驗條件準備 sample

(2) 將 UV/VIS 光譜儀(Hitachi U3300)暖機 15 分鐘

(3) 選擇 Rate 模式並調整測定波長為 610nm 及測定時間為 30 sec

(4) 將 125 λ sample、1250 λ ddH2O 及 430 λ Ammonium Heptamolybdate (28uM) in 2.1 uM H2SO4 加入 6 孔細胞盤中反應十分鐘後，加入 320 λ 0.35% PVA+

0.035% Malachite Green 再反應十分鐘

(5) 反應後加入 Cuvette 後放入機器中(注意光路位置)

(6) 按 Run 並讀取實驗數據。

## 2.6 利用水解酶實驗分析黃酮醇對於水解酶活性之抑制

(1) 本實驗使用 UV/VIS 光譜儀，前置步驟與 malachite green assay 相同

(2) Allantoinase 之受質 allantoin 的水解由 258nm 吸光值下降測定；dihydroorotase 之受質 dihydroorotate 的水解由 230nm 吸光值下降測定

(3) 光譜儀設定恆溫 25℃，將 protein solution (1-30 μg)加入含有 100mM Tris-HCl pH=8.0 buffer 及受質之 2mL 石英管中

(4) 選擇 Rate 模式並調整測定波長及測定時間為 120 sec

(5) Allantoin 之消光係數(extinction coefficient)為 0.0261 $mM^{-1}cm^{-1}$ at 258nm；dihydroorotate 之消光係數為 0.92 $mM^{-1}cm^{-1}$ at 230 nm

(6) 將數值收集後套用至 Michaelis-Menten equation 並計算相關動力學常數

## 2.7 利用 Native PAGE 分析 Protein-Protein Interaction

(1) 將電泳玻璃片用 75%酒精和 ddH2O 洗淨並擦拭乾淨（註：使用完後的電泳玻璃片，要以清潔劑清洗並擦拭乾淨）

(2) 並架到電泳座上固定（註：架設電泳玻璃片時，需左右調整使兩塊玻璃底部成一平面，再將固定扣扣上固定）

(3) 先配置下層的 Resolving gel（12%）於離心管中。

(4) 將配膠所需物質混合均勻－Vortex machine。

(5) 將下層膠溶液注入兩電泳玻璃片之間。

(6) 加入酒精覆蓋，靜置 20~30 分鐘（註：加酒精時須平均受力，以維持膠平面的水平）。

(7) 待膠體凝固後，將水倒出或吸乾（註：可觀察離心管中剩餘的膠是否凝固作為比對）

(8) 再配置上層膠 Stacking gel（4%）於離心管中，將配膠所需物質混合均勻。

(9) 將上層膠溶液注入兩電泳玻璃片之間，加到滿後，插入電泳齒梳（註：若有氣泡，可稍微將齒梳上下移動，使氣泡脫離）

(10) 待上層膠凝固後，抽出齒梳

(11) 將整組電泳玻璃膠體，置入電泳槽中

(12) 首先將 Running Buffer 倒入電泳槽內槽中

(13) 處理好的 Sample(rxn o/n)，以 10 μl 注入到凹槽中

(14) Sample load 完後，在內槽持續加入 running buffer 直到內側玻璃片的邊緣，外槽則是加到指示界線即可

(15) 連接電泳槽與電源供應器 （註：正接正，負接負，可以看顏色）

(16) 打開電源，用上下鈕將電壓調為 150V/150min，按 Run 開始跑膠

(17) 將膠取出後，加入 Staining solution 染色，震盪約 1 小時

(18) 再用 Destaining solution 退染，第一次約 30 分鐘，之後視情況調整時間

(19) Native Gel 膠體制備方法：

- Stacking gel (4 %)：

| | |
|---|---|
| 1. $ddH_2O$ | 1.35 ml |
| 2. 30 % Acrylamide/Bis | 0.33 ml |
| 3. 1.5 M Tris-HCl (pH 6.8) | 0.63 ml |
| 4. Glycerol | 100 µl |
| 5. 10 % APS | 100 µl |
| 6. TEMED | 2.5 µl |

- Resolving gel (12 %)：

| | |
|---|---|
| 1. $ddH_2O$ | 2.1 ml |
| 2. 30 % Acrylamide/Bis | 1.45 ml |
| 3. 1.5 M Tris-HCl (pH 8.8) | 1.25 ml |
| 4. Glycerol | 100 µl |
| 5. 10 % APS | 100 µl |
| 6. TEMED | 2 µl |

## 2.8 利用螢光共振能量轉移 (Fluorescence Resonance Energy Transfer,FRET) 觀察蛋白質-DNA interaction

本計畫所使用的螢光偵測儀器為 Hitachi-2700，實驗條件如下

(1) 制備 5uM 5’-Cy3-dT42-s’-Cy5 in 20 mM Tris, 50 mM NaCl buffer

(2) 螢光光譜儀使用方式與 Fluorescence quench 相同

(3) 將 5’-Cy3-dT42-s’-Cy5 加入石英管中,final concentration=5 nM

(4) 將不同蛋白之加入滴定之，反應 1 分鐘後以 Ex:515,Em:530-700 掃描

(5) 將 data 以 sigma plot 分析

## 2.9 利用奈米金粒子 (Gold NTA-NanoParticle) 觀察蛋白質-DNA interaction

(1) 將欲使用之蛋白質以 PBS+0.01% Tween 20 稀釋至 40 nM (實驗適用範圍 10 nM~100 nM)，

(2) 蛋白質以 1:1 比例與 already nickel-activated nanoparticle (Φ=30nm)混合，並在室溫中反應 10 分鐘

(3) 將欲測試交互作用之兩個蛋白質以 1:1 比例混和後，於室溫反應 10-30 分鐘

(4) 照相後根據其呈色分析蛋白質之間之交互作用

# 第三章：結果與討論

# （Results and Discussion）

**(I) 黃酮醇抑制解旋酶**

Nucleotide 可藉由水解反應提供解旋酶 DnaB 與 PriA 在解旋雙股 DNA 時所需要的能量，另亦使蛋白質構效產生變化。因此假使有一個小分子化合物，能有效地結合在解旋酶的 nucleotide binding site 上，或是結合在解旋酶的異位調控區 (allosteric binding site)，阻止 nucleotide 結合或影響到結構變化，使解旋酶無法進行動態移動，便可以抑制解旋酶的活性，進而達到抑制細菌複製的目的，此將可能成為新型抗生素之前驅物。我們根據之前的研究結果，利用四種類黃酮，以螢光淬滅方式觀察其與解旋酶的結合狀況，螢光淬滅法主要是藉由蛋白質中芳香環類胺基酸：tryptophan, tyrosine, phenylalanine 吸收波長而發出螢光，若此類胺基酸因小分子與蛋白質作用而被遮蔽，螢光強度便會減弱，造成螢光淬滅現象。我們選用 myricetin, quercetin, kaempferol, galangin 這四種類黃酮進行實驗，並經由計算 $K_d$ 值並互相比較其結合能力，若結合越強則可能會佔據解旋酶之 ATP 結合區，達到抑制效果。X 軸為黃酮醇的濃度變化，Y 軸為$(F_0\text{-}F)/F_0$，表示螢光強弱的變化，$F_0$ 為單純蛋白質的螢光數值，而 F 為蛋白質與黃酮醇進行結合時所產生的螢光數值。

由實驗結果作圖分析，並計算其解離常數 $K_d$，$K_d$ 為蛋白質與受質及其複合體之乘積比例[E][S]/[ES] (E: enzyme, S: substrate, ES: enzyme-substrate complex )，當 $K_d$ 越小，表示[ES]濃度很高，也就是蛋白質與受質的結合作用越強，使反應趨向於形成複合體，在螢光線性分析中，我們使用公式 $\Delta F=\Delta F_{max}\text{-}K_d(\Delta F_{max}/[S])$計算出 $K_d$ 值。圖二、圖九、圖十分別為 KpPriA, SaPriA, SaDnaB 螢光淬滅光譜之整理分析，由計算結果可得知對於 SaPriA 四種黃酮醇分子之 $K_d$ 值如下：galangin 之 $K_d$ 值為 11.01 ± 2.66 μM，kaempferol 之 $K_d$ 值為 9.14 ± 3.32 μM，myricetin 之 $K_d$ 值為 3.30 ± 0.41 μM，quercetin 之 $K_d$ 值為 11.75 ± 2.46 μM，故 SaPriA (金黃色葡萄球菌的 PriA) 與四種黃酮醇之結合能力強弱為 myricetin > kaempferol > galangin > quercetin; 對於 SaDnaB 四種黃酮醇分子之 $K_d$ 值如下：galangin 之 $K_d$ 值為 15.32 ± 0.88 μM，kaempferol 之 $K_d$ 值為 7.32 ± 0.39 μM，myricetin 之 $K_d$ 值為 7.96 ± 0.70 μM，quercetin 之 $K_d$ 值為 21.04 ± 4.45 μM，故 SaPriA 與四種黃酮醇之結合能力強弱為 Myricetin ~ Kaempferol > Galangin > Quercetin。

ATP 在解旋酶活性中扮演著提供能量的角色，若能利用小分子化合物去影響解旋酶的 ATPase 活性，便能有效抑制解旋酶的活性，我們利用 Malachite Green Assay 呈色法觀察 PriA 的 ATPase activity，並加入類黃酮觀察其對於 PriA 水解 ATP 的抑制情形。ATP 經過水解後產生磷酸根 Pi，Malachite Green Assay 是利用 Pi 與鉬酸鹽(Molybdate)結合產生 complex 並與染劑 Malachite Green 反應後呈色，若 sample 中有 Pi 的產生，試劑便會由黃色轉為綠色，藉由 UV/VIS 光譜儀測量 610nm 之吸光值，再帶入標準曲線中便可以了解 sample 中 Pi 的濃度。

圖十三為 Machite Green Assay 之標準曲線及實驗條件的決定，我們利用配製好的磷酸鹽溶液當成標準品 (濃度由 0-16 μM)，Malachite Green Assay 在此區間皆呈線性上升 ($R^2$=0.992, y=0.084x-0.017)，顯示此標準在此區間可受信賴，我們將以此標準曲線對所有的 ATPase 水解活性所得出的 Pi 進行定量，並換算其 ATPase activity.。在決定實驗條件的過程中，我們改變 PriA 反應之環境，利用不同的 $Mg^{2+}$及 ATP 濃度，並得到 PriA 之 ATPase 活性隨著 $Mg^{2+}$及 ATP 濃度的升高而增加，圖十四(A)中，隨著 PriA 濃度的上升，顏色由黃色轉為藍綠色，此上升由於們的分析及可能就是 PriA 分解 ATP 所得到的 Pi，PriA 之 ATPase activity 隨著濃度上升而增加，我們藉由以上結果訂出以下實驗條件→ $Mg^{2+}$: 5mM, ATP: 1mM, 反應時間：1hr，SaPriA 濃度為 4 μM。

圖十四(B)中顯示， PriA 在 ssDNA 及 ADP 存在的情況下，解旋酶 SaPriA 的 ATPase 活性會增加，且 ssDNA 與 ADP 具有加成的效果。在圖十五中顯示，在有黃酮醇分子存在的情況下， SaPriA 的 ATPase 活性受到抑制，kaempferol 之抑制效果大於 myricetin 之抑制效果，myricetin 抑制了 30% SaPriA 之 ATPase activity，kaempferol 則抑制了 60%之 ATPase activity；但若同時加入 ssDNA，myricetin 及 kaempferol 對於 SaPriA 之 ATPase 活性反而有促進的效果，其機制仍在討論中。另外，圖十六中我們利用 Malachite Green Assay 測試引子合成體蛋白之 ATPase activity，結果顯示文獻中具有 ATPase 活性之 primosomal protein (SaPriA, KpDnaB) 均會水解 ATP，此結果顯示 malachite green assay 為一個具有 Sensitivity (敏感度)及 Specificity (特異度)之方法。

**(II) 黃酮醇抑制 ALLase 與 DHOase**

目前的抗生素設計較少著眼於鹼基代謝，大部分之抗生素標的為細菌之細胞壁及核醣體次單元，然而在抗病毒藥物及抗腫瘤藥物中則十分常見，如抗 HSV-1 藥物 Acyclovir 及 5-FU 等。本計劃中發現黃酮醇可以抑制解旋酶 PriA 的 ATPase 活性，若黃酮醇能在 DNA 代謝的更上游抑制細菌生存必須之生化反應，黃酮醇便可能經由藥物優化成為 multi-target 之抗生素前驅物。尿囊素水解酶 (ALLase)及二氫乳清酸水解

酶 (DHOase)在嘌呤及嘧啶的代謝中扮演重要角色，我們選用四種黃酮醇：myricetin, quercetin, kaemoferol, galangin 進行抑制 allantoinase 及 dihydroorotase 水解反應之實驗，並利用螢光淬滅法了解黃酮醇與 allantoinase 及 dihydroorotase 之結合。

圖十七為黃酮醇對於 allantoinase 及 dihydroorotase 之水解酶抑制實驗，由實驗作圖得知，kaempferol 對於 allantoinase 有最強的抑制效果，黃酮醇對於 allantoinase 的抑制強弱為：kaempferol > galangin > quercetin > myricetin；另外，kaempferol 對於 dihydroorotase 亦具有最強的抑制效果，黃酮醇對於 dihydroorotase 之抑制強弱為：kaempferol > myricetin > galangin > quercetin。kaempferol 對於 allantoinase 及 dihydroorotase 具有良好的抑制效果，黃酮醇化合物對於水解酶之抑制效果 ($IC_{50}$) 均位於 μM range，相對於水解酶之受質類似物 (抑制效果位於 mM range)有更佳的抑制效果，經過計算後，kaempferol 對於 allantoinase 之 $IC_{50}$ 為 35 ± 3 μM；而 kaempferol 對於 dihydroorotase 之 $IC_{50}$ 為 31 ± 2 μM。

Kaempferol 對於 allantoinase 及 dihydroorotase 有良好的抑制效果，利用螢光淬滅法可以了解 kaempferol 與水解酶之結合狀況，並可以推斷其抑制效果是否與其結合能力有關，圖十八為 kaempferol 對於 allantoinase 及 dihydroorotase 之螢光淬滅光譜之整理分析，經計算其對於水解酶之解離常數 $K_d$，可得知 kaempferol 對於 allantoinase 之 $K_d$ 為 28.3 ± 3.8 μM，對於 dihydroorotase 之 $K_d$ 則為 20.9 ± 3.9 μM，從水解酶抑制實驗及螢光淬滅實驗中發現，kaempferol 可以抑制及結合至 allantoinase 及 dihydroorotase ，且 $IC_{50}$ 及 $K_d$ 均在 μM range，相對於受質類似物之常數均位於 mM range，因此黃酮醇，尤其是 kaempferol，展現出極優的抑制(大概 3 個 order)，對比於以受質為基礎的抑制劑設計。

**(III) 黃酮醇抑制引子合成體蛋白質群**

本計劃中發現黃酮醇可以與多種解旋酶結合，並對於解旋酶之 ATPase 活性產生抑制，在細菌重啟複製叉 (Replication restart) 機制中，多個蛋白質參與引子合成體的組合 (assembly)，當小分子與黃酮醇結合後便有機會阻止引子合成體蛋白質之間的組合及引子合成體與 DNA 的結合，本實驗中利用三種黃酮醇：myricetin, quercetin, kaemoferol 進行實驗，並利用螢光淬滅法了解黃酮醇與引子合成體蛋白之結合。藉由了解黃酮醇與引子合成體的結合，可以對黃酮醇進行優化，並設計對於引子合成體蛋白群均有抑制效果之化合物。

圖三至圖八、圖十一、圖十二為引子合成體蛋白螢光淬滅光譜之整理分析，根據實驗作圖分析，並計算其解離常數 $K_d$，quercetin 對於引子合成體蛋白之解離常數約在

1-10 μM range，顯示 quercetin 對於引子合成體蛋白質有強的結合，另外 myricetin 與 kaempferol 對於引子合成體蛋白之解離常數約在 15-25 μM range，相較於 quercetin 對於引子合成體蛋白之結合能力較弱。Quercetin 對於引子合成體蛋白具有較強的結合能力，但其螢光淬滅程度在本實驗中使用之黃酮醇中相比偏低；反之，myricetin 與 kaempferol 雖螢光淬滅程度較高，但對於引子合成體蛋白之結合能力較弱，此結果顯示 quercetin 與 myricetin / kaempferol 對於引子合成體之結合及抑制模式可能不同。

**(IV) 臨床藥物抑制解旋酶**

老藥新用 (drug repurposing) 是指已被核准做為臨床使用之藥物，利用比對藥物、受體及疾病之間的關連性，近而預測藥物之效果，近而從已核准之藥物中發現新的適應症用途或是新的用法，老藥新用的好處除了具有完整的藥物動力學、代謝途徑、副作用等數據，在改變新劑型或劑量後也較容易推測安全性。本實驗中使用抗愛滋用藥 AZT (Zidovudine) 進行實驗，並以螢光淬滅實驗探討 AZT 是否會與解旋酶結合。

圖二至圖十二為整個引子合成體蛋白之螢光淬滅光譜之整理分析，根據實驗作圖分析，並計算其解離常數 $K_d$，AZT 與 SaPriA 之 $K_d$ 為 16.19 ± 3.88 μM；AZT 與 SaDnaB 之 $K_d$ 為 19.35 ± 1.67 μM，相較於黃酮醇有較弱的結合能力，而 AZT 與引子合成體蛋白的解離常數約在 5 μM 處，顯示其對於引子合成體蛋白有強的結合，相較於先前實驗中所使用之黃酮醇有較強的結合能力，此結果顯示 AZT 對於解旋酶的結合模式與其他引子合成體蛋白不同。另外，在 Malachite Green Assay 中，AZT 也具有抑制 SaPriA 水解 ATP 之效果，顯示 AZT 與解旋酶的結合可能與其 ATPase 之 active site 有關連。

**(V) 類黃酮之優化以抑制解旋酶**

在本計劃中發現 myricetin 對於解旋酶產生強的螢光淬滅，顯示其對於解旋酶具有結合能力，另外在 malachite green assay 中也發現 myricetin 可以抑制 PriA ATPase 的活性，因此我們對於黃酮醇進行優化，將與 myricetin 結構相似之類黃酮分子利用分子對接快速篩選具有高結合能獲 docking score 之化合物。根據分子對接的結果，我們選擇在 myricetin 3-O 位置修飾 rhamnose (rhamnose 修飾普遍見於植物的糖苷衍生物中)，即 myricitrin，探討 C 環所需空間與作用情形；及將 Myricetin 的 C 環上之雙鍵還原，即 dihydromyricetin，探討 C 環上的 OH 是否需特定方位，藉由優化 myricetin 了解 myricetin 之構效關係(Structure-Activity Relationship, SAR)。

圖二、圖九、圖十分別為 KpPriA, SaPriA, SaDnaB 螢光淬滅光譜之整理分析，經

實驗作圖分析後，對於 KpPriA，myricetin 及其衍生物在螢光淬滅程度上大小如下：myricetin > dihydromyricetin > myricitrin，myricetin 在螢光淬滅程度上與 dihydromyricetin 在 8 μM 前相當，而 myricetin 濃度超過 8 μM 後則相較於 dihydromyricetin 淬滅較多的光；對於 SaPriA，myricetin 及其衍生物在螢光淬滅程度上大小如下：dihydromyricetin > myricitrin > myricetin，計算其解離常數 $K_d$，myricetin < dihydromyricetin <myricitrin；對於 SaDnaB，myricetin 及其衍生物在螢光淬滅程度上大小如下：myricetin > dihydromyricetin > myricitrin，計算其解離常數 $K_d$，myricetin < myricitrin < dihydromyricetin；另外，在 Malachite Green Assay 中，myricetin 及其衍生物不等程度抑制 SaPriA 之 ATPase activity，抑制程度大小如下：myricetin ~ myricitrin > dihydromyricetin，綜合螢光淬滅實驗及 ATPase activity assay，myricetin 對於解旋酶 ATPase 之抑制能力相對於其衍生物強，並顯示 Flavonol 之 C 環上 2,3 號碳之間的雙鍵還原及 3 號碳上糖基修飾均會減弱其抑制 PriA 其 ATPase Activity 之效果。

圖三至圖八、圖十一、圖十二為引子合成體蛋白螢光淬滅光譜之整理分析，myricetin 及其衍生物對於引子合成體蛋白之結合程度，從螢光淬滅程度上，myricetin 及其衍生物在螢光淬滅程度上大小如下：myricetin > dihydromyricetin > myricitrin，而計算其解離常數 $K_d$，myricitrin < dihydromyricetin < myricetin，myricitrin 在螢光淬滅實驗中淬滅較少的螢光，但具有較小的 $K_d$ 顯示；dihydromyricetin 及 myricetin 在螢光淬滅實驗中淬滅較多的螢光，但具有較大的 $K_d$，此結果顯示 myricitrin 與 myricetin, dihydromyricetin 之結合模式不同，另外 myricitin 與引子合成體蛋白具有較強的結合能力，myricetin 與解旋酶具有較強的結合能力，此結果顯示 myricetin 及其衍生物結構之官能基對於解旋酶及其他引子合成體有不同模式之交互作用。

**(VI) 黃酮醇抑制解旋酶之模式探討**

本計劃中解旋酶 PriA 與黃酮醇之結合與抑制模式分兩部分探討：在 *K.pneumoniae* PriA 結晶結構尚未解除及發表之前，我們利用 SWISS MODEL 模擬 KpPriA 之模型 (基於 EcPriA aa. 4-104; 2D7H)，並利用 HEX-SERVER (shape model 與 Shape + electrostatic model) 及 PATCH DOCK 兩個線上分子對接軟體探討四種黃酮醇：galangin, kaempferol, myricetin, quercetin 與 PriA 可能之結合區位，並推測可能的抑制模式。每個黃酮醇與三種分子對接方法進行模擬，並取其前三個最佳解，利用 PyMol 分子視覺化軟體進行分析，並觀察位於黃酮醇分子周圍 3Å 之胺基酸分布狀況，以及預測其氫鍵鍵長，圖二十九中，統計 36 個 solution 後結果顯示：黃酮醇與 E50 及 L20 兩個胺基酸產生氫鍵的次數最多，平均每個 solution 中黃酮醇均會與此二殘基產生一

個氫鍵，另外，D17,Y18,I44,V45,V48 殘基也會與黃酮醇中的 OH 產生氫鍵，這些殘基位於 PriA 之 3'BD (3' DNA Binding Domain)，此區域負責 PriA 與 DNA 之交互作用，docking 結果顯示黃酮醇可能藉由抑制 DNA 與 PriA 結合影響 PriA 之 DNA unwinding，及影響 PriA 之構形，PriA 與 ATP 之結合位置位於 N 端，但 Docking 結果中，黃酮醇皆未結合於 ATP 結合位，黃酮醇對於 ATPase activity 之抑制機制是否不藉由占據 ATP 結合位，此抑制機制仍須探討。

Bhattacharyya *et al.* 在本人此國科會大專生計畫快結案之時，今年一月多解出了 KpPriA 全長結構(圖三十) [18]，因此本人亦對 KpPriA 之 domain 結構進行分析： 3'BD (3' binding domain) ─ WH (Winged helix) ─ Helicase lobe 1 ─ Helicase lobe 2 ─ CTD，3' BD 負責與 DNA 之 3' interaction)及與 SSB interaction，WH domain 以前之 N- terminus (~ 200 residue)屬於 DBD (DNA binding domain)，此後之 C- terminus (~ 530 residue)屬於 HD (Helicase domain)，於 Helicase lobe 2 中夾有另一 domain 稱為 CRR (Cystenine Rich Region) domain，CRR 中含有 2 個 $Zn^{2+}$，功能為 binding dsDNA。利用 KpPriA 全長結構 PDB: 4NL4，我們將六種黃酮醇：dihydromyricetin, galangin, kaempferol, myricetin, myricitrin, quercetin 及兩種臨床藥物：AZT, ticagrelor 同樣利用 HEX-SERVER (shape model 與 Shape + electrostatic model) 及 PATCH DOCK 兩個線上分子對接軟體探討化合物與 PriA 可能的結合區位，並與 N-terminus KpPriA model 之結果比較。

圖三十一至圖五十四為利用分子對接工具 (HEX SERVER,PATCH DOCK) 與六種黃酮醇：dihydromyricetin, galangin, kaempferol, myricetin, myricitrin, quercetin 及兩種臨床藥物：AZT, ticagrelor 之結合模式。綜合三種分子對接方法之結果，在各方法結合能前六高的結合模式中：AZT 與 KpPriA 之結合模式可能是與 helicase lobe 1 結合；dihydromyricetin 與 KpPriA 之結合模式可能是與 helicase lobe 2 及 CRR 結合；galangin 與 KpPriA 之結合模式之預測在三種方法中則較為分歧，HEX SERVER (shape model) 與 PATCH DOCK 模擬之結合模式顯示 galangin 與 KpPriA 的結合可能於 helicase lobe 1/2 及 CRR，HEX SERVER (shape +electrostatic model)模擬之結合模式則顯示 galangin 結合於 3'BD 處；kaempferol 與 KpPriA 之結合模式可能是與 helicase lobe 2 及 3'BD；myricetin 與 KpPriA 之結合模式可能是與 helicase lobe 2 及 3'BD；myricitrin 與 KpPriA 之結合模式在三種方法中則較為分歧，HEX SERVER (shape model)與 PATCH DOCK 模擬之結合模式顯示 myricitrin 與 KpPriA 的結合可能於 helicase lobe 1/2，HEX SERVER (shape +electrostatic model)模擬之結合模式則顯示 myricitrin 結合於 CRR 及 3'BD 處；quercetin 與 KpPriA 之結合模式可能是與 CRR 及 helicase lobe 2 結合，另外

也有結合模式顯示與 ADP binding site 結合；ticagrelor 與 KpPriA 之結合模式可能是與 3’BD 及 helicase lobe 2 結合，另外，在 HEX SERVER (shape model )最高結合能的模式顯示 ticagrelor 與 ADP binding site 結合，此結果與 ticagrelor 臨床上之藥物標的位相同。

從以上結果可發現黃酮醇與 KpPriA 之結合模式多與 helicase 1/2 結合，顯示其抑制 PriA 之機制可能與抑制解旋酶的活性有關；具有較高的螢光淬滅效果及較強的 ATPase activity 抑制效果之 kaempferol 及 myricetin，兩者之結合模式多結合於 3’BD 及 helicase lobe 2，從以上模式推測其抑制 PriA 之機制可能為抑制解旋及影響 3’BD 與 leading strand binding 造成 replacation restart 無法進行，另外，binding 於 3’BD 也有可能造成 PriA N-terminus 構形產生改變而改變其 ATPase acitivity；quercetin 及 galangin 之結合模式與 kaempferol 及 myricetin 不同，這也與螢光淬滅實驗結果相當，結合於 CRR 可能造成 PriA unwinding acitivity 之下降；AZT 與 KpPriA 之結合模式顯示與 helicase lobe 1 結合，由此模擬結果顯示 AZT 抑制 KpPriA 之模式可能與其臨床藥理機制不同；ticagrelor 及 quercetin 均有結合模式顯示其與 ADP binding site 結合，ADP 與 PriA 可以增加其 ATPase 及解旋酶活性，顯示 ADP binding site 亦有可能是優化此二化合物之標的

我們利用 SWISS MODEL 以 homology modeling 模擬 SaDnaB 模型(圖五十五)，並基於 Geobacillus kaustophilus DnaC (2R6C) 之結構，SaDnaB 之 N-terminus 與 DNA binding 及解旋酶活性較無關，而與 DnaB 之 dimerization 有關，SaDnaB 在細菌中為六聚體，主要與 DnaI-DnaC complex 交互作用，並對 dsDNA 解旋，C-terminus 之 DNA binding loop 會幫助 SaDnaB 與 DNA 結合，Walker A 及 Walker B 則會與 nucleotide 結合，並與 nucleotide 結合後影響 SaDnaB 之構形。圖五十六至圖六十七中，綜合三種分子對接方法之結果，在各方法結合能前六高的結合模式中：galangin 與 SaDnaB 之結合模式可能是與 Walker A 及 DNA binding loop 結合；kaempferol 與 SaDnaB 之結合模式可能是與 DNA binding loop 結合；myricetin 與 SaDnaB 之結合模式可能是與 DNA binding loop 結合；myricetin 與 SaDnaB 之結合模式可能是與 Walker A 結合，綜合以上結果，黃酮醇與 SaDnaB 之結合模式大多結合於 DNA Binding loop 及 Walker A 上，顯示黃酮醇對於 SaDnaB 抑制機制為抑制其與 DNA 結合，並導致無法解旋，在部份的結合模式中，黃酮醇結合於靠近 N-terminus 位置，此模式顯示黃酮醇亦可能藉由抑制 SaDnaB 之 dimerization 或是與其他 primosomal protein 之交互作用。

**(VII) 黃酮醇抑制 ALLase 與 DHOase 之模式探討**

在本計劃中發現黃酮醇 kaempferol 對於allantoinase及dihydroorotase具有抑制效果，為了研究 kaempferol 對於 allantoinase 及 dihydroorotase 為何種模式之抑制劑，我們利用固定濃度之 kaempferol (40μM) 並改變受質濃度，進行水解酵素實驗，圖十九為 kaempferol 與 allantoinase 及 dihydroorotase 之抑制實驗，並藉由此結果分析動力學常數，水解酶之動力常數利用雙倒數 Lineweaver-Burk 作圖整理後：kaempferol 對於 allantoinase 之抑制在 Lineweaver-Burk plot 中，作圖線條交會於 y 軸之相似點，此結果顯示 kaemferol 對於 allantoinase 為競爭型抑制劑 (competitive inhibitor)；kaempferol 對於 dihydroorotase 之抑制在 Lineweaver-Burk plot 中，作圖線條呈現平行，在 y 軸上各自具有不同之截距，此結果顯示 kaemferol 對於 dihydroorotase 為非競爭型抑制劑 (uncompetitive inhibitor)，dihydroorotase 在 40μM Kaempferol 存在之下之 $V_{max}$ 為 4.24±0.06 μmol/mg/min，$K_m$ 則為 0.048±0.004 mM，根據動力學實驗的結果，kaempferol 對於 dihydroorotate-dihydroorotase complex 產生抑制，而非對於 dihydroorotase free enzyme 產生抑制，Kaempferol 異位調控了 dihydroorotase。根據實驗結果，Kaempferol 對於 allantoinase 為競爭型抑制劑，對於 dihydroorotase 為非競爭型抑制劑。

在水解酶抑制實驗及動力學實驗中，我們得到 kaempferol 為 allantoinase 及 dihydroorotase 之抑制劑，為了進一步了解其抑制機制，我們利用 SWISS MODEL 以 homology modeling 模擬 allantoinase 及 dihydroorotase 之結構，並利用 PATCH DOCK 將 Kaempferol 以分子對接 (molecular docking) 方式放入模擬之結構，我們選取了 docking score 最高之三個 solution 進行分析。圖二十為 Kaempferol 與 allantoinase 之結合模式，對於 kaempferol 與 allantoinase 之結合模式，根據具有最高分數的 solution 1，kaempferol 之 hydroxyl group 與 allantoinase 之 Ser286 及 Ser317 交互作用，docking 之位置亦位於 active site 中，Ser317 為 allantoinase 受質質結合位中重要之殘基；圖二十一為 kaempferol 與 dihydroorotase 之結合模式，對於 Kaempferol 與 dihydroorotase 之結合模式，根據具有最高分數的 solution 1，kaempferol 之 hydroxyl group 與 dihydroorotase 之 E35, G277 及 V346 交互作用，此三個殘基位於 active 外面。Kaempferol 與 allantoinase 及 dihydroorotase 之根據分子對接所得到之結合模式與動力學的實驗結果相互印證。

**(VIII) 解旋酶 PriA 與引子合成體蛋白及 DNA 之交互作用**

解旋酶與引子合成體蛋白及 DNA 的交互作用亦是另一個可以著眼於設計抑制 Replication Restart 機制的 target，在本實驗中，利用螢光共振能量傳遞 (FRET) 觀察 KpPriB 與 SaPriA 之交互作用，我們利用螢光光譜儀發展了一套即時觀測引子合成體蛋白與 DNA 交互作用之方法，一段 42dT 的 ssDNA 片段在 3’端帶有 Cy5，5’端帶有

Cy3；Cy3 為 FRET 之螢光能量 Donor(產生者)；Cy5 為 FRET 之螢光能量 Acceptor(接受者)，當帶有螢光探針的 dT42 與蛋白質產生交互作用，使得 Cy3 與 Cy5 靠近，便會產生螢光共振能量傳遞現象，在螢光光譜儀上可以發現 567nm 處螢光強度的下降伴隨 665nm 處螢光強度的上升。藉由螢光光譜儀觀測 530-700nm 螢光強度的消長，即可分析引子合成體蛋白與 DNA 的交互作用，並了解在結合過程中 DNA 構形之變化與蛋白質間的距離。

圖二十二為以 FRET 分析 KpPriB 與 DNA 之交互作用，以 PriA 為首的重啟複製叉路徑中，KpPriB 為引子合成體的第二個成員，當其結合到 PriA 上時，會刺激 PriA 之解旋酶及 ATPase 活性，並穩定 DNA 與 PriA 之結合，PriB 主要以兩套體(dimer)存在，與 DNA 結合時以三明治包夾方式纏繞 DNA，並具有正協同效應，圖中 KpPriB 纏擾 dT42 並產生螢光共振能量傳遞現象，並在 665nm 處產生 acceptor (Cy5)之波峰，圖二十三為以 FRET 分析 SaPriA 與 DNA 之交互作用，當 SaPriA 與 dT42 反應時，隨著 dT42 濃度的上升，在 567nm 處的波峰呈現藍移(blue shift)現象，圖二十四為以 FRET 分析 SaPriA-KpPriB 與 DNA 之交互作用，SaPriA 對於 dT42 本身會產生藍移現象，當同時加入 KpPriB 時，隨著 KpPriB 濃度的上升，則出現螢光共振能量傳遞現象，顯示 PriB 結合上 PriA-DNA 複合體時，PriB 會優先往 PriA 接觸，並拉扯 DNA 趨於緊密，這可從 Cy3,Cy5 十分靠近以至於產生 FRET 現象得知，最後，PriA,PriB 將共結合於 DNA 上，完成初步引子合成體組裝。

圖二十五為以 FRET 分析 SaDnaB 與 DNA 之交互作用，SaDnaB 為一解旋酶，對於 ssDNA 不易產生 interaction，而 dT42 為 ssDNA，故在光譜圖中 Cy3 螢光未見明顯下降，圖二十六為以 FRET 分析 SaDnaI 與 DNA 之交互作用，DnaI 為革蘭氏陽性菌獨有之 primosomal protein，為 helix loader，DnaI 會帶著 DnaC 附著至複製叉上，DnaI 具有 binding DNA 之能力，從光譜圖可見 DnaI 與 dT42 產生交互作用，並使得 Cy3 之產生螢光共振能量傳遞現象，造成 567nm 處螢光下降，並可見 665nm 處隨著 DnaI 濃度的上昇而產生波峰，圖二十七為以 FRET 分析 SaDnaB-SaDnaI 與 DNA 之交互作用，SaDnaB 本身與 dT42 不易產生作用，當同時加入 SaDnaI 時，隨著 SaDnaI 濃度的上升，則出現螢光共振能量傳遞現象，顯示 DnaI-DnaB complex 會與 DNA 結合，並造成 DNA 構形的改變，並拉扯 DNA 趨於緊密。

除了著眼於抑制解旋酶本身之 ATPase 活性或 Helicase 活性，解旋酶與其他引子合成體蛋白之交互作用也是設計解旋酶抑制劑的 target 之一，DnaD，一個獨特存在於革蘭氏陽性菌引子合成體的蛋白，具有促進 DnaB 與 DNA 之結合能力，圖二十八以 Native PAGE 分析 SaPriA 與 SaDnaD 之交互作用，從 Native PAGE 結果可以發現其 a.a

1-204 片段會與 SaPriA 產生交互作用，但其 a.a 1-195 片段則不會與 SaPriA 產生交互作用，顯示 SaDnaD C 端可能為與 PriA 交互作用之位置。

如何高速的篩選藥物標靶之抑制劑為藥物研發非常重要的一環 (High-Throughput Screening, HTS )，我們利用奈米金粒子實驗了解 primosomal protein 之間的交互作用，並加入黃酮醇及其他可能之化合物進行高速篩選，奈米金粒子隨粒徑上昇而改變顏色，由桃紅色轉變為淺紫色，在圖六十八中，我們以奈米金粒子分析 KpPriA 與 KpPriB 及 KpSSB 之交互作用，KpPriA 與金粒子混和後為深紫色，顯示其 PriA 與奈米金粒子結合後粒徑上昇，KpPriB 及 KpSSB 與奈米金粒子結合後則未明顯改變金粒子之粒徑；將 KpPriA 與 KpPriB 及 KpSSB 混和後，奈米金粒子顏色均轉為淺紫色，顯示 KpPriA 與 KpPriB 及 KpSSB 之交互作用；加入 myricetin 後發現顏色與控制組未有明顯差異，顯示 myricetin 對於 KpPriA 之抑制標的並非 KpPriA 與其他 primosomal protein 之結合，此方法我們將用來高速篩選本計畫結論所延伸後續藥物優化所得到之化合物。

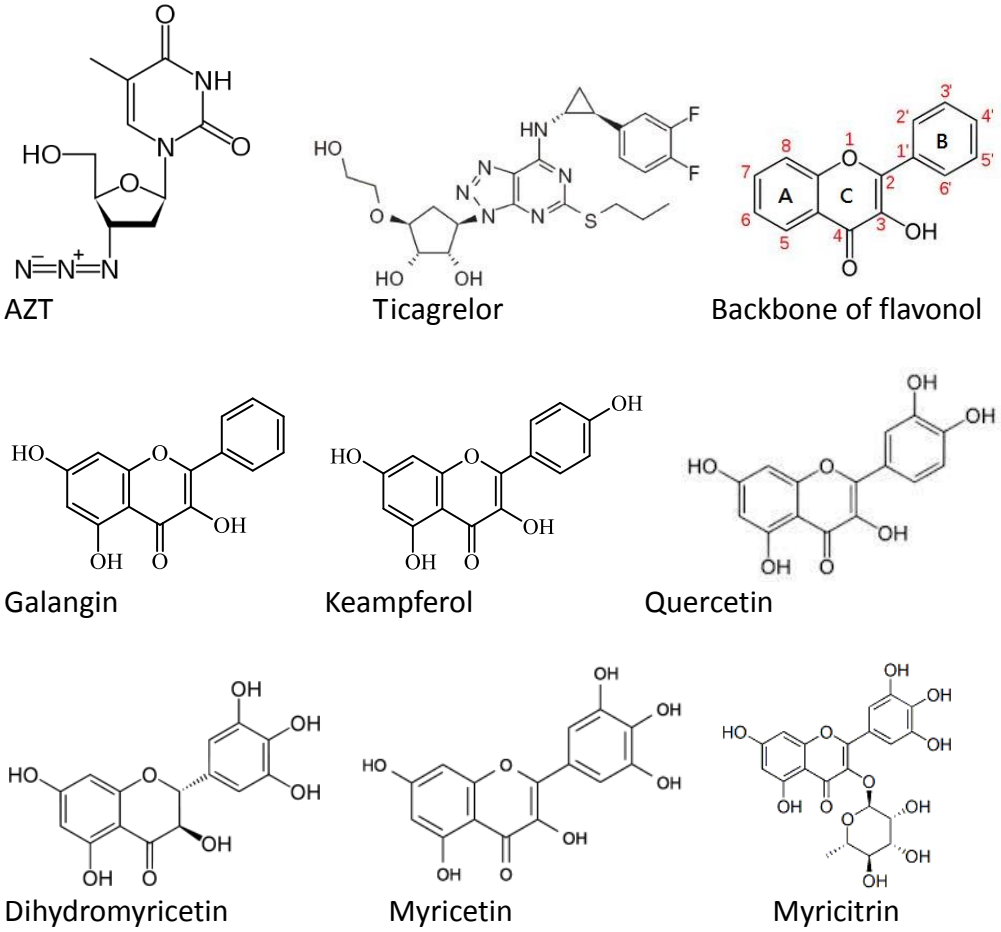


**圖一：本實驗使用之小分子化合物**

AZT 為核苷酸反轉錄酶抑制物；Ticagrelor 為 ADP receptor 抑制劑，用於抑制血小板凝集。類黃酮的基本結構以 A,B,C 三個環為主體，並且在 A 環與 B 環上有不同數量的 OH 基修飾，並衍生出不同的類黃酮物質及其生物特性，以上六種黃酮醇為本實驗使用之類黃酮衍生物，Galangin, Kaempferol, Quercetin, Myricetin 分別在 B 環上帶有 0,1,2,3 個不同數量的 OH 基；Myricitrin 為 Myricetin 之 3-O-rhamnoside (即探討 C 環所需空間與作用情形)；Dihyromyricetin 則是將 Myricetin 的 C 環上之雙鍵還原(即探討 C 環上的 OH 是否需特定方位)。

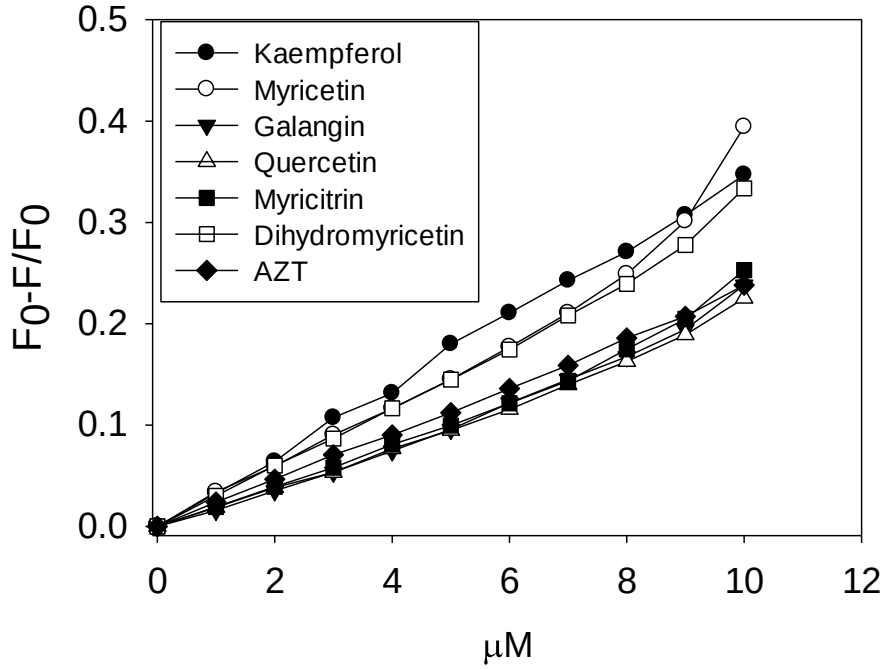


KpPriA 濃度：0.05 μM
Buffer: 50mM Tris , 50mM NaCl , 50mM HEPES　Ex/Em : 280/330 nm
反應時間：1 min　環境溫度：25℃

**圖二：以螢光淬滅實驗(quenching)分析 KpPriA 與小分子之交互作用**。在淬滅螢光的程度上，myricetin > kaempferol > dihydromyricetin > myricitrin ~ AZT ~ Galangin > AZT，顯示 myricetin 與 KpPriA 之結合能力最強，myricetin 與 dihydromyricetin 在 8 μM 前具有相當的結合能力，而超過 8 μM，myricetin 具有較佳之螢光淬滅的效果。

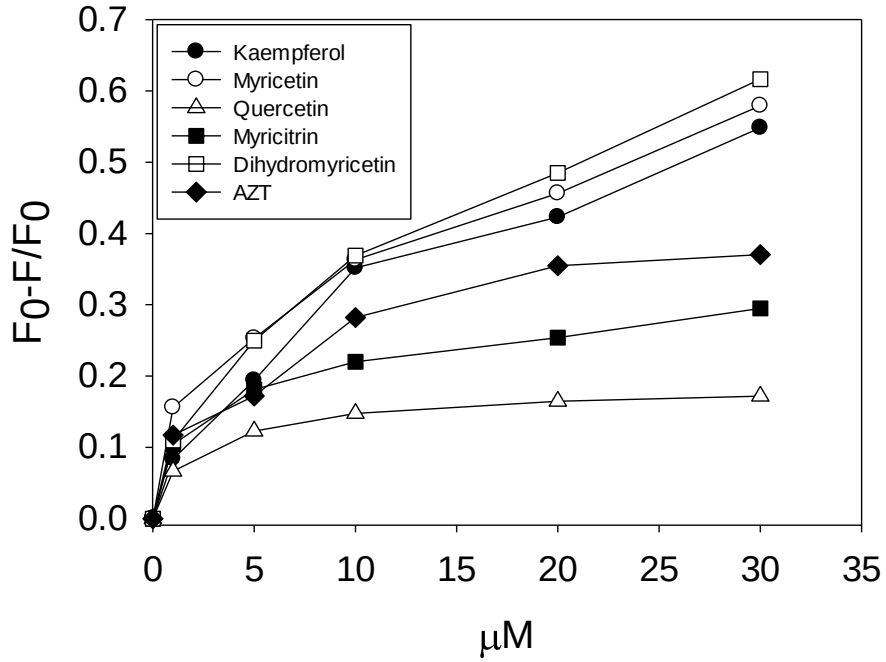


KpPriB 濃度：6 μM

Buffer: 50mM Tris , 50mM NaCl , 50mM HEPES　　Ex/Em : 280/330 nm

反應時間：1 min　　環境溫度：25℃

| Flavonol | $K_d$ (μM) | StdErr |
|---|---|---|
| Kaempferol | 12.98 | 3.58 |
| Myricetin | 7.92 | 3.23 |
| Quercetin | 1.94 | 0.23 |
| Myricitrin | 2.62 | 0.79 |
| Dihydromyricetin | 11.70 | 3.02 |
| AZT | 5.75 | 2.15 |

**圖三：以螢光淬滅實驗(quenching)分析 KpPriB 與小分子之交互作用。**在淬滅螢光的程度上，dihydromyricetin > myricetin > kaempferol > AZT > myrcitrin > quercetin；而在解離常數 $K_d$ 上，quercetin < myricitrin < AZT < myricetin < dihydromyricetin < kaempferol，此結果顯示 myricitrin, quercetin 與 myricetin , kaempferol 有不同的結合模式。

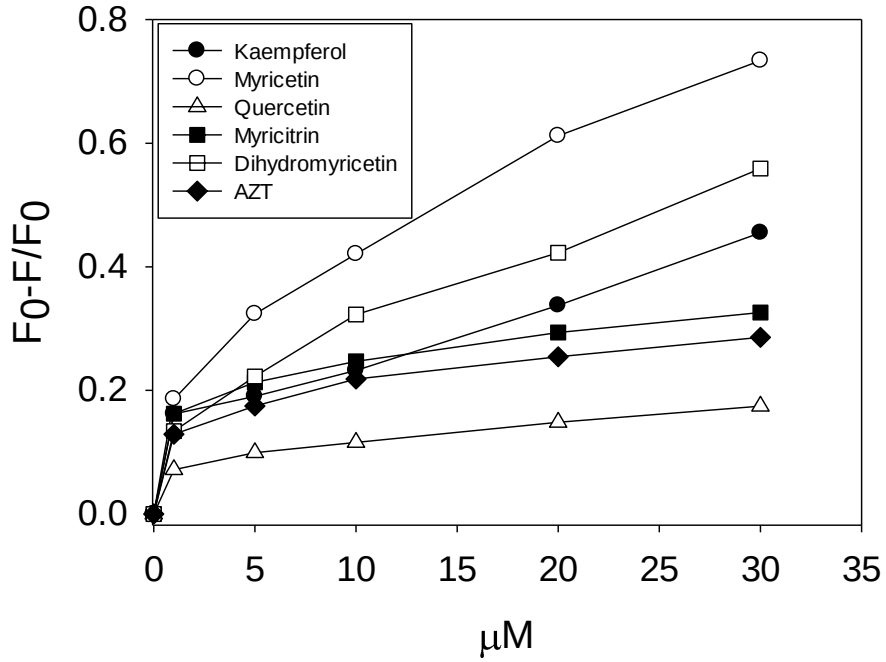


KpPriC 濃度：0.3 μM
Buffer: 50mM Tris , 50mM NaCl , 50mM HEPES　Ex/Em : 280/330 nm
反應時間：1 min　環境溫度：25℃

| Flavonol | $K_d$ (μM) | StdErr |
|---|---|---|
| Kaempferol | 9.60 | 7.15 |
| Myricetin | 9.72 | 3.81 |
| Quercetin | 2.36 | 1.24 |
| Myricitrin | 1.20 | 0.51 |
| Dihydromyricetin | 11.27 | 4.86 |
| AZT | 1.68 | 0.70 |

**圖四：以螢光淬滅實驗(quenching)分析 KpPriC 與小分子之交互作用。**在淬滅螢光的程度上， myricetin > dihydromyricetin > kaempferol > myrcitrin > AZT > quercetin；而在解離常數 $K_d$ 上，myricitrin < AZT < quercetin < kaempferol < myricetin < dihydromyricetin，此結果顯示 myricitrin, quercetin 與 myricetin , kaempferol 有不同的結合模式。

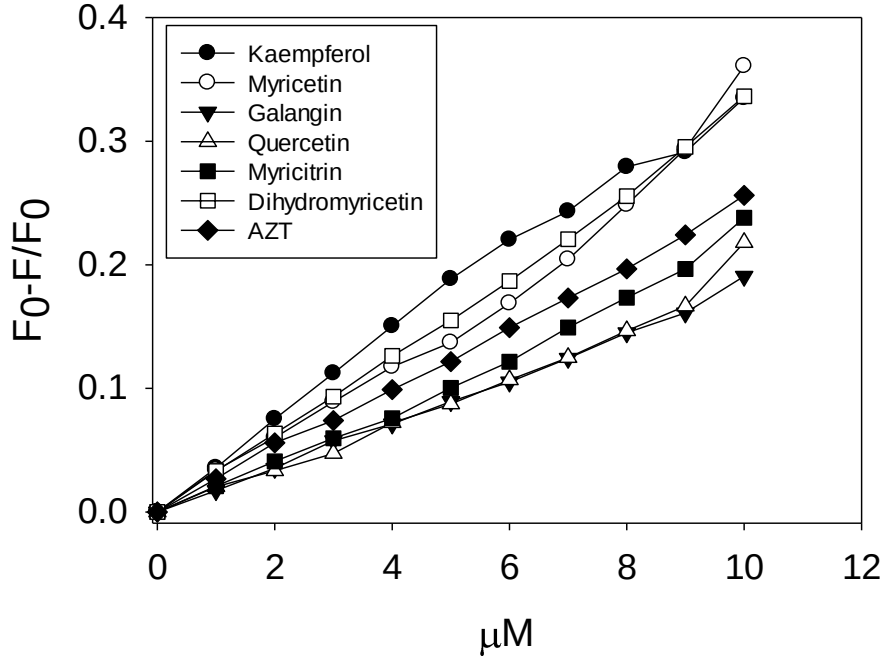


KpDnaC 濃度：0.03 μM
Buffer: 50mM Tris , 50mM NaCl , 50mM HEPES　Ex/Em : 280/330 nm
反應時間：1 min　環境溫度：25℃

**圖五：以螢光淬滅實驗(quenching)分析 KpDnaC 與小分子之交互作用。**在淬滅螢光的程度上， myricetin > dihydromyricetin ~ kaempferol > AZT > myrcitrin > quercetin > galangin，在 8 μM 前，kaempferol 與 dihydromyricetin 淬滅螢光之能力大於 myricetin，在黃酮醇濃度大於 8 μM 後，myricetin 則具有較佳的螢光淬滅能力。

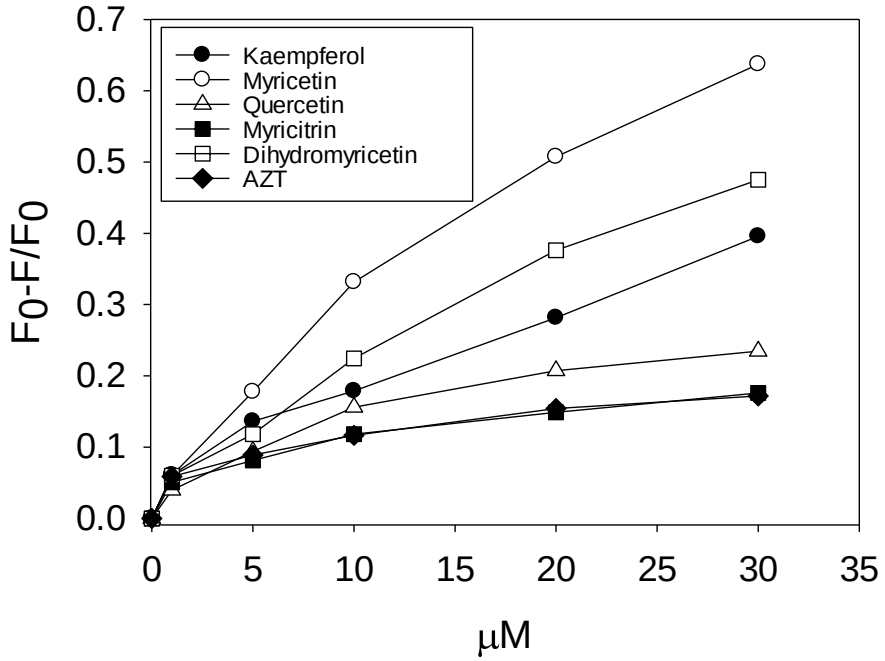


KpDnaG 濃度：0.3 μM

Buffer: 50mM Tris , 50mM NaCl , 50mM HEPES　Ex/Em : 280/330 nm

反應時間：1 min　環境溫度：25℃

| Flavonol | $K_d$ (μM) | StdErr |
|---|---|---|
| Kaempferol | 27.72 | 13.24 |
| Myricetin | 27.43 | 3.14 |
| Quercetin | 10.68 | 1.60 |
| Myricitrin | 6.50 | 2.35 |
| Dihydromyricetin | 36.66 | 9.87 |
| AZT | 4.60 | 1.89 |

**圖六：以螢光淬滅實驗(quenching)分析 KpDnaG 與小分子之交互作用。**在淬滅螢光的程度上， myricetin > dihydromyricetin > kaempferol > quercetin> myrcitrin ~ AZT；而在解離常數 $K_d$ 上，AZT < myricitrin < quercetin < myricetin < kaempferol < dihydromyricetin，此結果顯示 myricitrin, quercetin 與 myricetin , kaempferol 有不同的結合模式。

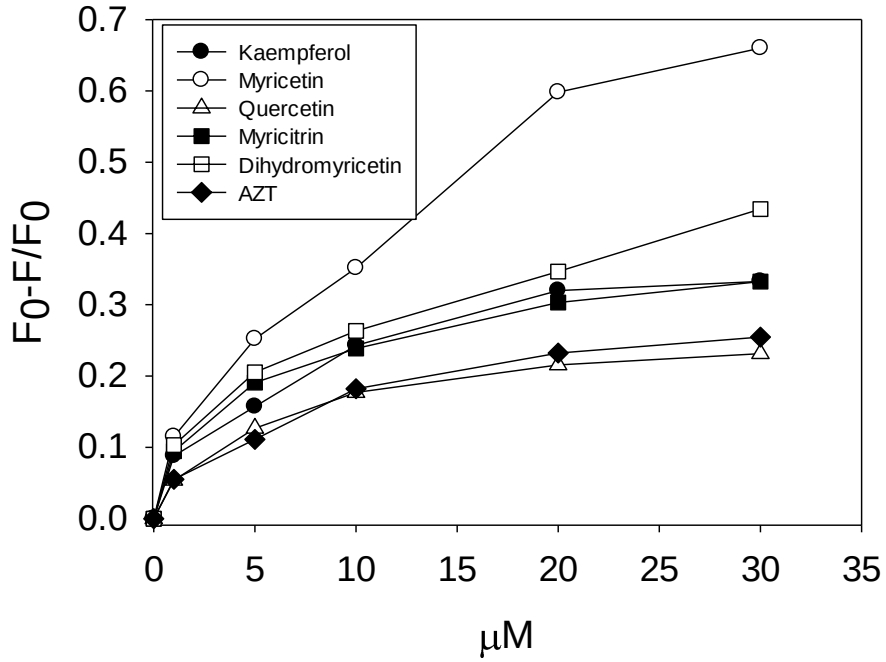


KpDnaT 濃度：0.3 μM
Buffer: 50mM Tris , 50mM NaCl , 50mM HEPES　Ex/Em : 280/330 nm
反應時間：1 min　環境溫度：25℃

| Flavonol | $K_d$ (μM) | StdErr |
|---|---|---|
| Kaempferol | 6.65 | 1.83 |
| Myricetin | 16.08 | 4.89 |
| Quercetin | 5.17 | 0.59 |
| Myricitrin | 4.32 | 0.99 |
| Dihydromyricetin | 7.84 | 2.75 |
| AZT | 8.06 | 1.70 |

**圖七：以螢光淬滅實驗(quenching)分析 KpDnaT 與小分子之交互作用。**在淬滅螢光的程度上， myricetin > dihydromyricetin > kaempferol ~ myrcitrin >AZT > quercetin；而在解離常數 $K_d$ 上， myricitrin < quercetin < kaempferol < dihydromyricetin < AZT < myricetin，此結果顯示 myricitrin, quercetin 與 myricetin 有不同的結合模式。

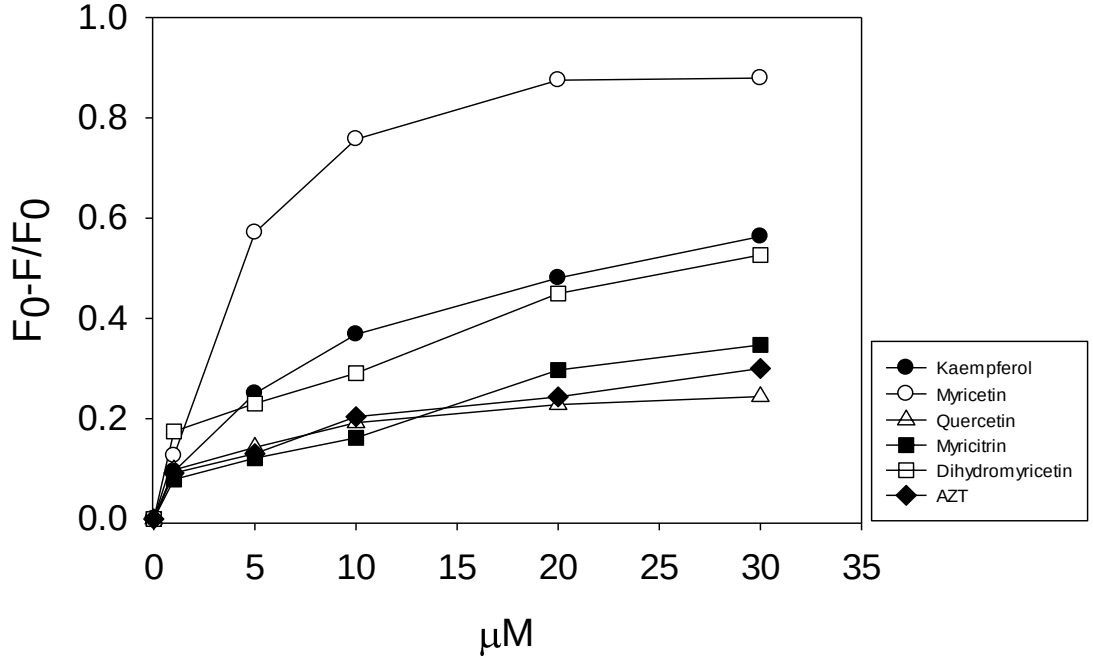


KpSSB 濃度：0.4 μM
Buffer: 50mM Tris , 50mM NaCl , 50mM HEPES　Ex/Em : 280/330 nm
反應時間：1 min　環境溫度：25℃

| Flavonol | $K_d$ (μM) | StdErr |
|---|---|---|
| Kaempferol | 9.36 | 1.23 |
| Myricetin | 4.55 | 0.91 |
| Quercetin | 2.54 | 0.92 |
| Myricitrin | 21.12 | 10.94 |
| Dihydromyricetin | 8.98 | 5.16 |
| AZT | 6.58 | 2.89 |

**圖八：以螢光淬滅實驗(quenching)分析 KpSSB 與小分子之交互作用。**在淬滅螢光的程度上， myricetin > kaempferol > dihydromyricetin >myrcitrin >AZT > quercetin；而在解離常數 $K_d$ 上，quercetin< myricetin < AZT < dihydromyricetin< kaempferol <myricitrin 。

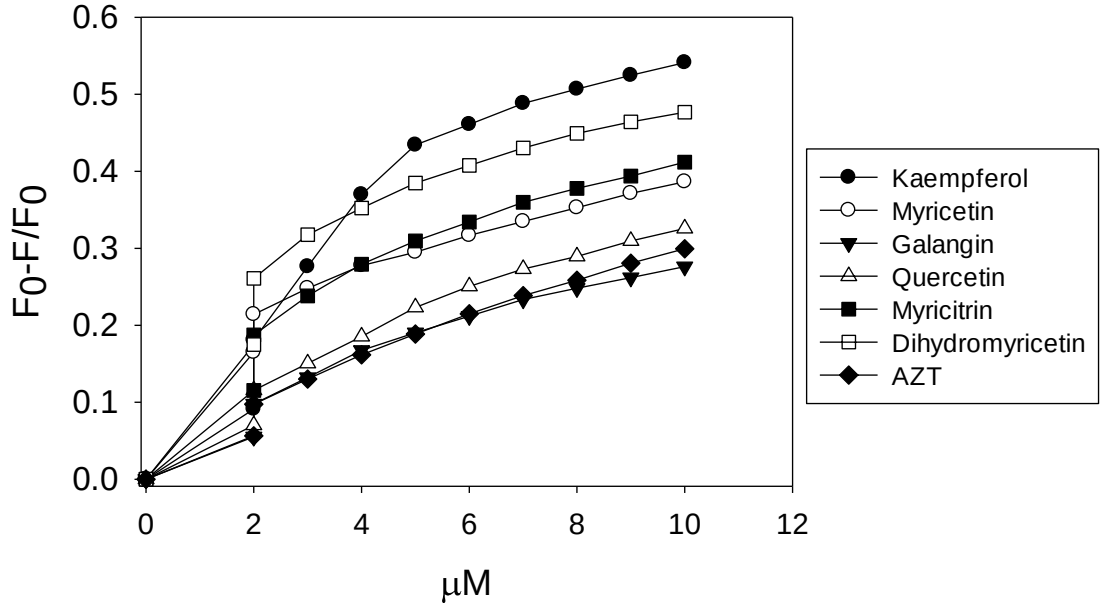


SaPriA 濃度：0.03 μM

Buffer: 50mM Tris , 50mM NaCl , 50mM HEPES　Ex/Em : 280/330 nm

反應時間：1 min　環境溫度：25℃

| Flavonol | $K_d$ (μM) | StdErr |
|---|---|---|
| Kaempferol | 9.14 | 3.32 |
| Myricetin | 3.30 | 0.41 |
| Galangin | 11.01 | 2.66 |
| Quercetin | 11.75 | 2.46 |
| Myricitrin | 5.85 | 1.13 |
| Dihydromyricetin | 3.63 | 0.63 |
| AZT | 16.19 | 3.88 |

**圖九：以螢光淬滅實驗(quenching)分析 SaPriA 與小分子之交互作用。**在淬滅螢光的程度上， kaempferol > dihydromyricetin > myrcitrin> myricetin >quercetin >AZT >galangin；而在解離常數 $K_d$ 上，myricetin< dihydromyricetin< myricitrin <kaempferol <galangin< quercetin< AZT 。

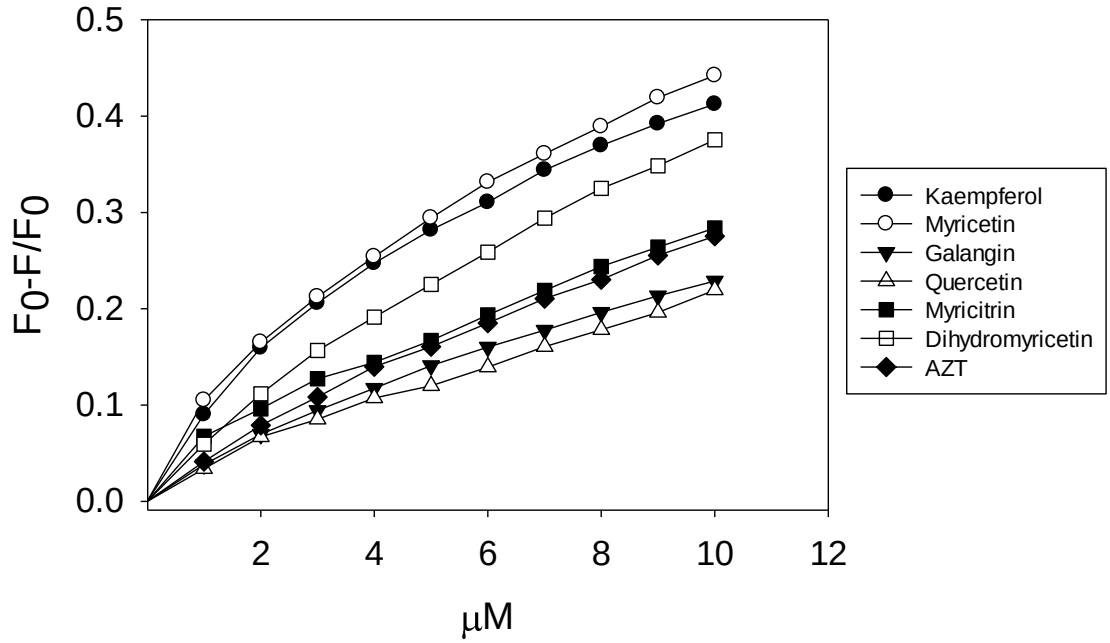


SaDnaB 濃度：0.25 μM

Buffer: 50mM Tris , 50mM NaCl , 50mM HEPES　Ex/Em : 280/330 nm

反應時間：1 min　環境溫度：25℃

| Flavonol | $K_d$ (μM) | StdErr |
|---|---|---|
| Kaempferol | 7.32 | 0.39 |
| Myricetin | 7.96 | 0.70 |
| Galangin | 15.32 | 0.88 |
| Quercetin | 21.04 | 4.45 |
| Myricitrin | 12.15 | 2.53 |
| Dihydromyricetin | 16.43 | 1.03 |
| AZT | 19.35 | 1.67 |

**圖十：以螢光淬滅實驗(quenching)分析 SaDnaB 與小分子之交互作用。**在淬滅螢光的程度上，myricetin >kaempferol > dihydromyricetin > myrcitrin> AZT >galangin >quercetin；而在解離常數 $K_d$ 上，kaempferol< myricetin< myricitrin< galangin< dihydromyricetin< AZT<quercetin 。

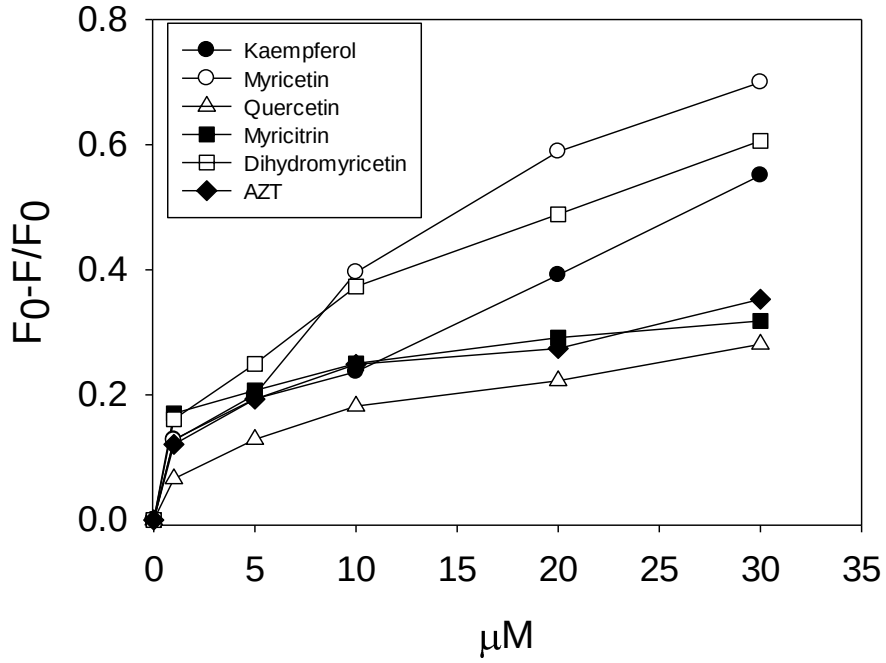


SaDnaD 濃度：0.6 μM
Buffer: Heparin (500mM NaCl,10mM Sodium Phosphate,pH=7)  Ex/Em : 280/330 nm
反應時間：1 min　　環境溫度：25℃

| Flavonol | $K_d$ (μM) | StdErr |
|---|---|---|
| Kaempferol | 26.25 | 18.39 |
| Myricetin | 20.01 | 6.58 |
| Quercetin | 7.50 | 2.39 |
| Myricitrin | 1.01 | 0.45 |
| Dihydromyricetin | 9.31 | 3.75 |
| AZT | 3.14 | 1.39 |

**圖十一：以螢光淬滅實驗(quenching)分析 SaDnaD 與小分子之交互作用。**在淬滅螢光的程度上，myricetin > dihydromyricetin >kaempferol > AZT > myrcitrin> quercetin；而在解離常數 $K_d$ 上，myricitrin< AZT< quercetin< dihydromyricetin <myricetin < kaempferol，此結果顯示 myricitrin, quercetin 與 myricetin, kaempferol 有不同的結合模式。

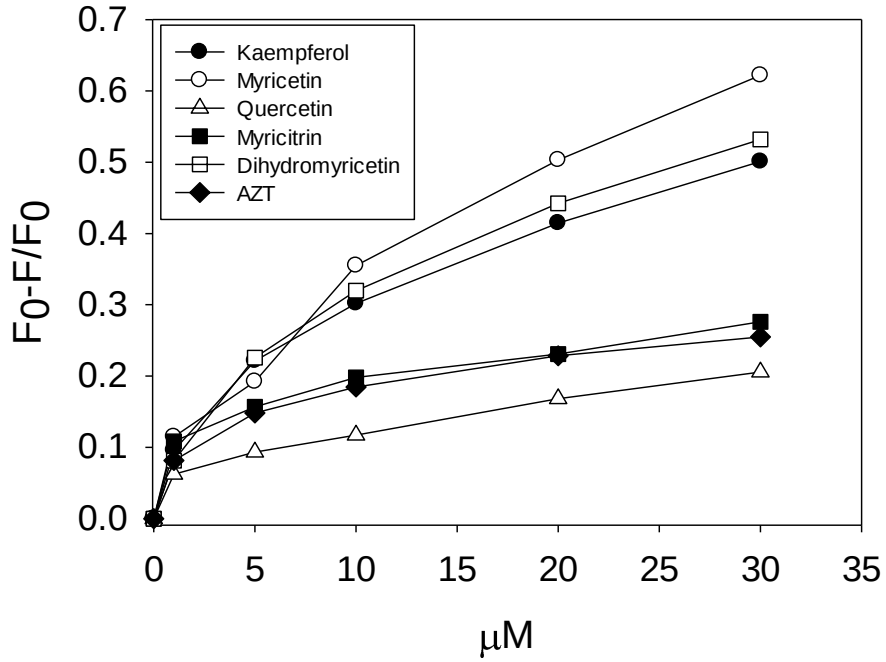


SaDnaI 濃度：2.4 μM

Buffer: 50mM Tris , 50mM NaCl , 50mM HEPES　　Ex/Em : 280/330 nm

反應時間：1 min　　環境溫度：25℃

| Flavonol | $K_d$ (μM) | StdErr |
|---|---|---|
| Kaempferol | 10.08 | 2.41 |
| Myricetin | 18.15 | 5.67 |
| Quercetin | 8.11 | 4.08 |
| Myricitrin | 2.47 | 1.09 |
| Dihydromyricetin | 11.52 | 1.87 |
| AZT | 3.61 | 1.01 |

**圖十二：以螢光淬滅實驗(quenching)分析 SaDnaI 與小分子之交互作用。**在淬滅螢光的程度上，myricetin > dihydromyricetin > kaempferol > myrcitrin> AZT > quercetin；而在解離常數 $K_d$ 上，myricitrin< AZT< quercetin <kampferol< dihydromyricetin< myricetin，，此結果顯示 myricitrin, quercetin 與 myricetin,kaempferol 有不同的結合模式。

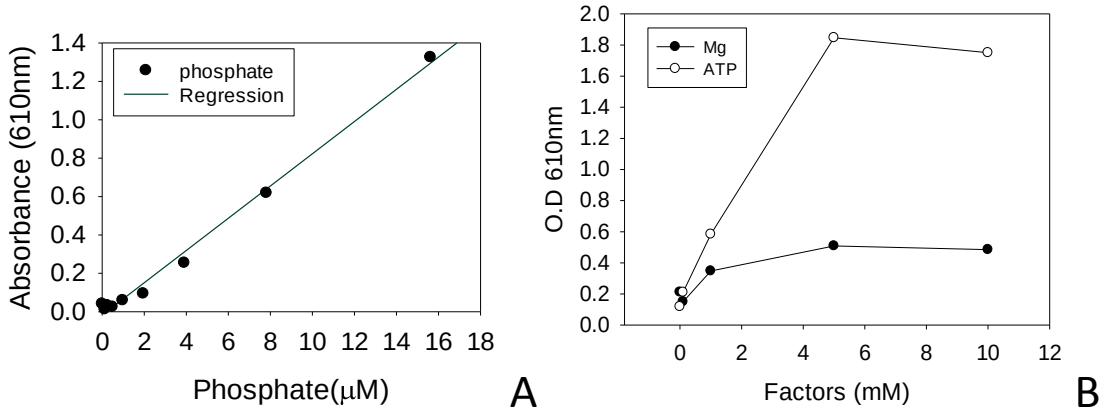


**圖十三：**(A)Malachite Green Assay 之標準曲線，我們利用配置好的磷酸鹽溶液當成標準品(濃度由 0-16 $\mu$ M)，Malachite Green Assay 在此區間皆呈線性上升($R^2$=0.992, y=0.084x-0.017)，顯示此標準在此區間可受信賴，我們將以此標準曲線對所有的 ATPase 水解活性所得出的 Pi 進行定量，並換算其 ATPase activity.。(B) 改變 PriA 反應之環境，利用不同的 $Mg^{2+}$及 ATP 濃度，並得到 PriA 之 ATPase 活性隨著 $Mg^{2+}$及 ATP 濃度的升高而增加，並藉由以上結果訂出以下實驗條件→ $Mg^{2+}$: 5mM, ATP: 1mM 。

A

$Mg^{2+}$:5mM
ATP:1mM
Rxn time:3hr
DNA: -

| Protein(μM) | 0 | 0.3 | 0.6 | 1.2 | 2.4 |
|---|---|---|---|---|---|
| Abs | 0.340 | 0.364 | 0.361 | 0.449 | 0.521 |

B

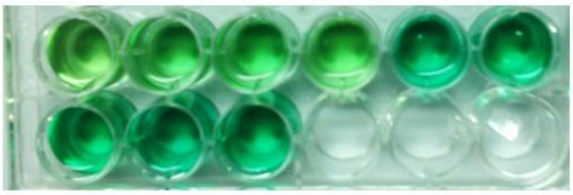

$Mg^{2+}$:5mM
ATP:1mM
ADP:2mM
DNA:1λ
Rxn time:3hr

DNA: -
ADP: -

| Protein(μM) | 0 | 1 | 2 |
|---|---|---|---|
| Abs | 0.351 | 0.442 | 0.460 |

DNA: -
ADP: +

| Protein(μM) | 0 | 1 | 2 |
|---|---|---|---|
| Abs | 0.410 | 0.925 | 0.801 |

DNA:+
ADP:+

| Protein(μM) | 0 | 1 | 2 |
|---|---|---|---|
| Abs | 0.823 | 1.077 | 1.050 |

**圖十四：**(A) 隨著 PriA 濃度的上升，顏色由黃色轉為藍綠色，此上升由於們的分析及可能就是 PriA 分解 ATP 所得到的 Pi，PriA 之 ATPase activity 隨著濃度上升而增加(B) PriA 在 ssDNA 及 ADP 存在的情況下，解旋酶 SaPriA 的 ATPase 活性會增加，且 ssDNA 與 ADP 具有加成的效果。

A

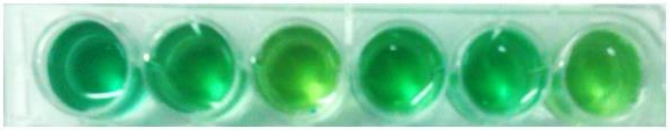

$Mg^{2+}$:5mM
ATP:1mM
Rxn time:1hr
Flavonoids: 35 uM
SaPriA : 4 μM

| | 0 | M | K | Mtrin | DM | AZT |
|---|---|---|---|---|---|---|
| Abs | 0.740 | 0.581 | 0.380 | 0.579 | 0.642 | 0.425 |

B

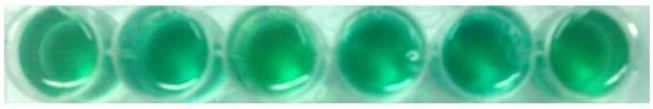

$Mg^{2+}$:5mM
ATP:1mM
Rxn time:1hr
Flavonoids: 35 uM
DNA: +
SaPriA : 4 μM

| | 0 | M | K | Mtrin | DM | AZT |
|---|---|---|---|---|---|---|
| Abs | 0.692 | 0.852 | 0.714 | 0.875 | 0.987 | 0.792 |

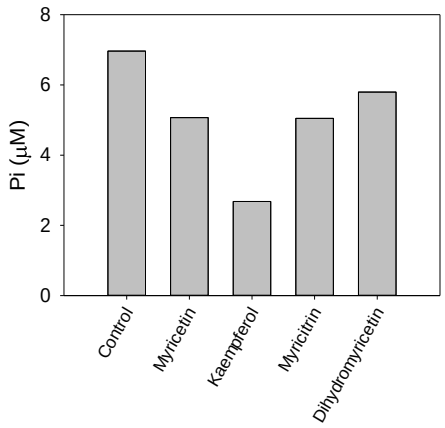


**圖十五：**在有黃酮醇分子存在的情況下(A) SaPriA 的 ATPase 活性受到抑制，kaempferol 之抑制效果大於 myricetin 之抑制效果，myricetin 抑制了 30% SaPriA 之 ATPase activity，kaempferol 則抑制了 60%之 ATPase activity；但若同時加入 ssDNA(B)，myricetin 及 kaempferol 對於 SaPriA 之 ATPase 活性反而有促進的效果。

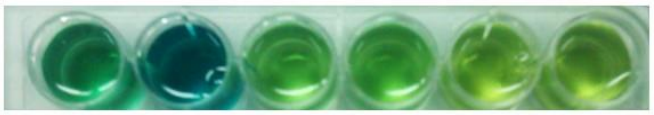

$Mg^{2+}$:5mM
ATP:1mM
Rxn time:2hr

| | SaPriA 4 μM | KpDnaB 15 μM | KpDnaC 0.1 μM | SaDnaD 8 μM | SaSSB 10 μM | SaDnaB 4 μM |
|---|---|---|---|---|---|---|
| Abs | 0.633 | 1.843 | 0.349 | 0.391 | 0.240 | 0.251 |

**圖十六：**利用 Malachite Green Assay 測試引子合成體蛋白之 ATPase activity，結果顯示文獻中具有 ATPase 活性之 primosomal protein (SaPriA, KpDnaB) 均會水解 ATP，此結果顯示 malachite green assay 為一個具有 Sensitivity (敏感度)及 Specificity (特異度)之方法。

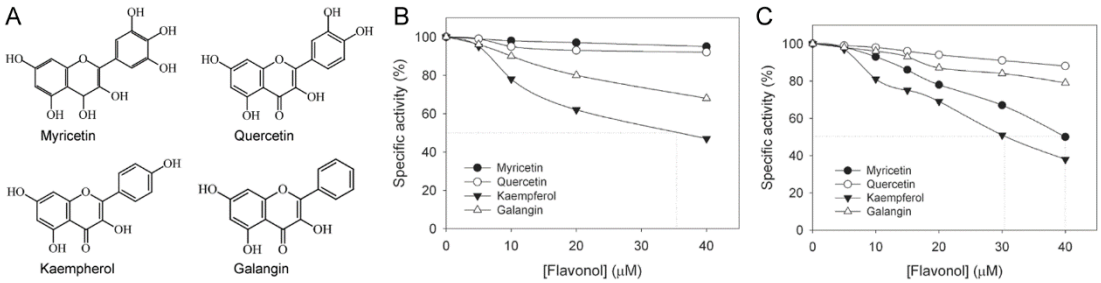


**圖十七：**(A)實驗中使用之黃酮醇, (B)kaempferol 對於 allantoinase 有最強的抑制效果，黃酮醇對於 allantoinase 的抑制強弱為：kaempferol>galangin>quercetin>myricetin；(C)Kaempferol 對於 dihydroorotase 亦具有最強的抑制效果，黃酮醇對於 dihydroorotase 之抑制強弱為：kaempferol > myricetin > galangin > quercetin。kaempferol 對於 allantoinase 及 dihydroorotase 具有良好的抑制效果，黃酮醇化合物對於水解酶之抑制效果 ($IC_{50}$) 均位於 μM range，相對於水解酶之受質類似物 (抑制效果位於 mM range) 有更佳的抑制效果，經過計算後，kaempferol 對於 allantoinase 之 $IC_{50}$ 為 35 ± 3 μM；而 kaempferol 對於 dihydroorotase 之 $IC_{50}$ 為 31 ± 2 μM。

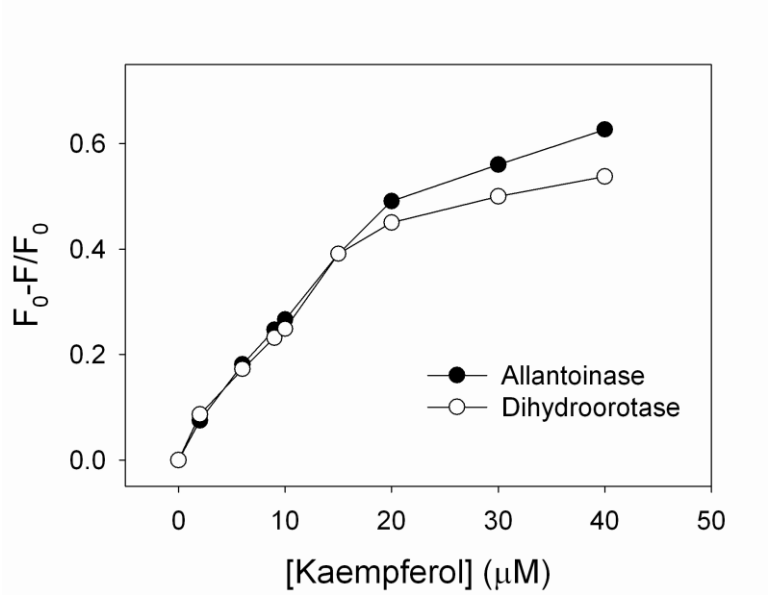


**圖十八：**Kaempferol 對於水解酶之解離常數 $K_d$，可得知 kaempferol 對於 allantoinase 之 $K_d$ 為 28.3±3.8 μM，對於 dihydroorotase 之 $K_d$ 則為 20.9±3.9 μM，從水解酶抑制實驗及螢光淬滅實驗中發現，Kaempferol 可以抑制及結合至 allantoinase 及 dihydroorotase，且 $IC_{50}$ 及 $K_d$ 均在 μM range，相對於受質類似物之常數均位於 mM range。

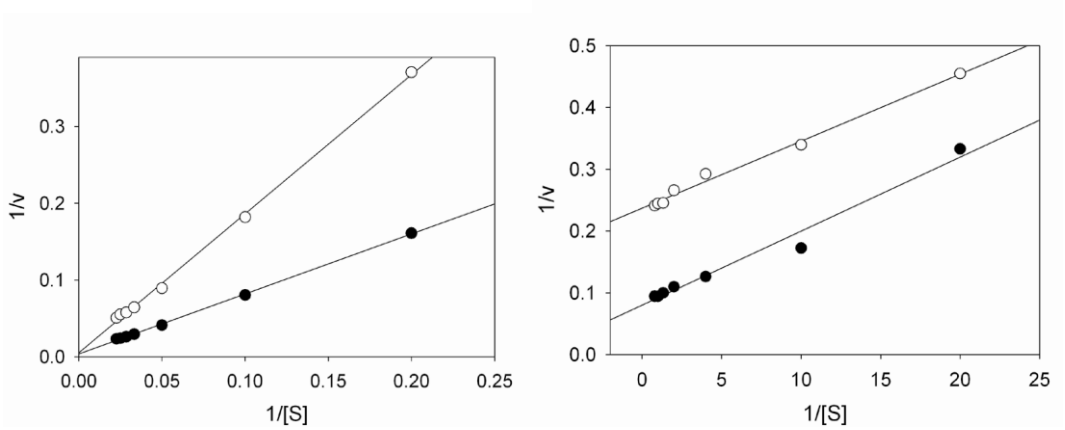


**圖十九：**(左)kaempferol 對於 allantoinase 之抑制在 Lineweaver-Burk plot 中，作圖線條交會於 y 軸之相似點，此結果顯示 kaemferol 對於 allantoinase 為競爭型抑制劑 (competitive inhibitor)；(右)kaempferol 對於 dihydroorotase 之抑制在 Lineweaver-Burk plot 中，作圖線條呈現平行，在 y 軸上各自具有不同之截距，此結果顯示 kaemferol 對於 dihydroorotase 為不競爭型抑制劑 (uncompetitive inhibitor) 。

A

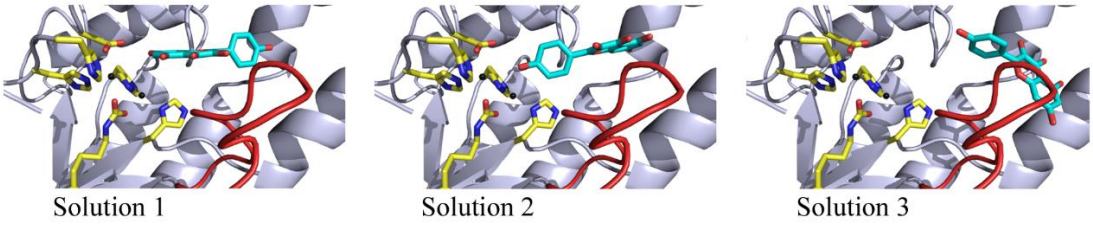


B

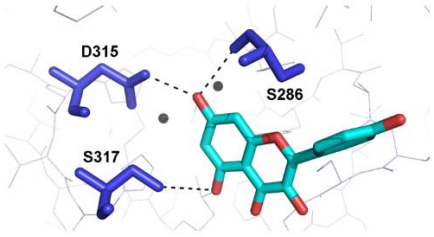


**圖二十：**Kaempferol 與 allantoinase 之結合模式 (A)結合能最高的 3 個結合模式，active site residue 以黃色標示；substrate binding loop 以紅色標注 (B)解一的 Binding environment， kaempferol 之 hydroxyl group 與 allantoinase 之 Ser286 及 Ser317 交互作用，docking 之位置亦位於 active site 中，Ser317 為 allantoinase 受質質結合位中重要之殘基，與酵素學實驗結果符合。

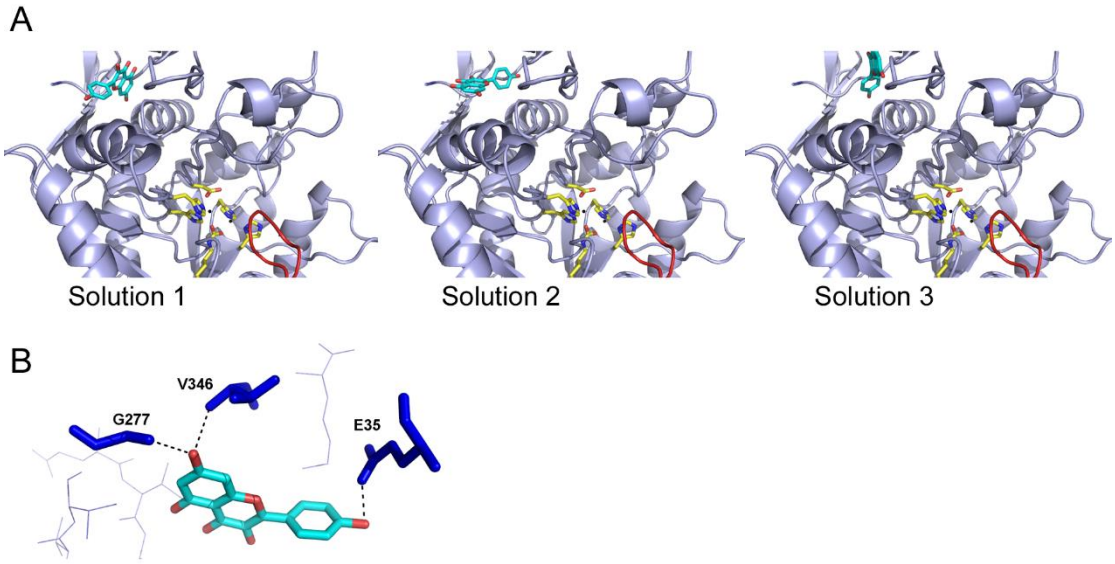


**圖二十一：**Kaempferol 與 dihydroorotase 之結合模式 (A)結合能最高的 3 個結合模式，active site residue 以黃色標示；substrate binding loop 以紅色標注 (B)解一的 Binding environment， kaempferol 之 hydroxyl group 與 dihydroorotase 之 E35, G277 及 V346 交互作用，此三個殘基位於 active site 外面。

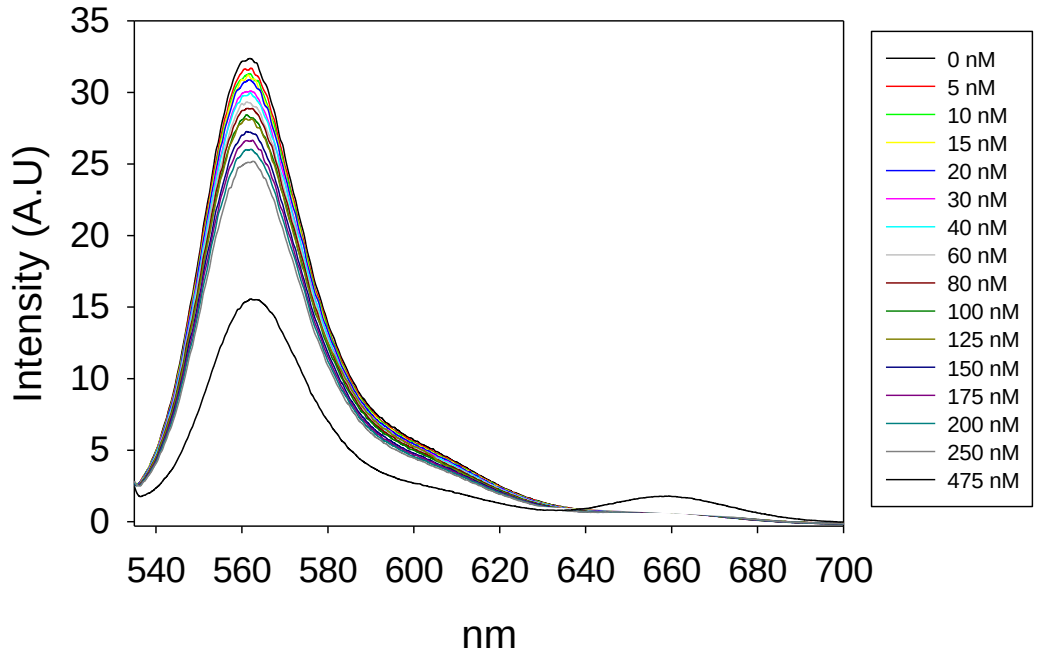


Cy3-5’-dT42-3’-Cy5 : 5 nM
Buffer: 20 mM Tris, 50 mM NaCl　Ex/Em : 515/530-700 nm
反應時間：1 min　　環境溫度：25℃

**圖二十二：**以 FRET 分析 KpPriB 與 DNA 之交互作用。在不同濃度下可觀察到波峰的改變與能量的變化。

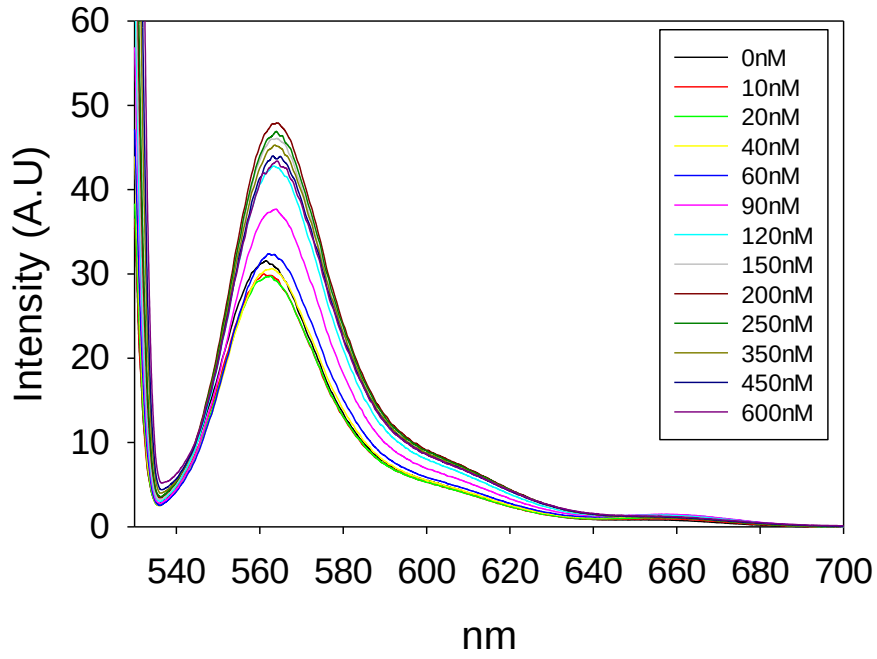


Cy3-5’-dT42-3’-Cy5 : 5 nM
Buffer: 20 mM Tris, 50 mM NaCl　Ex/Em : 515/530-700 nm
反應時間：1 min　　環境溫度：25℃

**圖二十三：**以 FRET 分析 SaPriA 與 DNA 之交互作用隨著 dT42 濃度的上升，在 567nm 處的波峰呈現藍移 (blue shift) 現象。

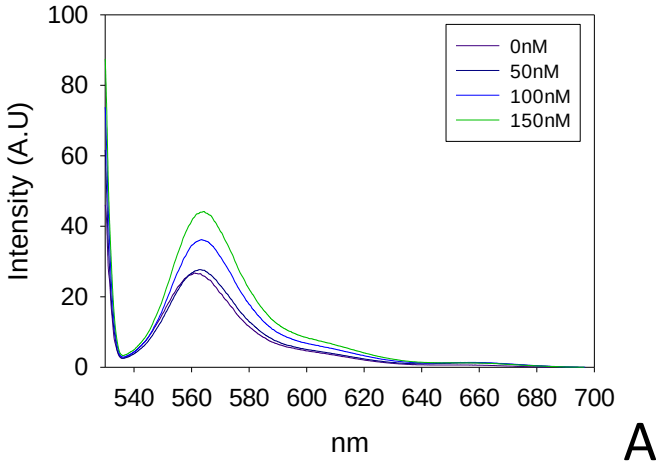


A

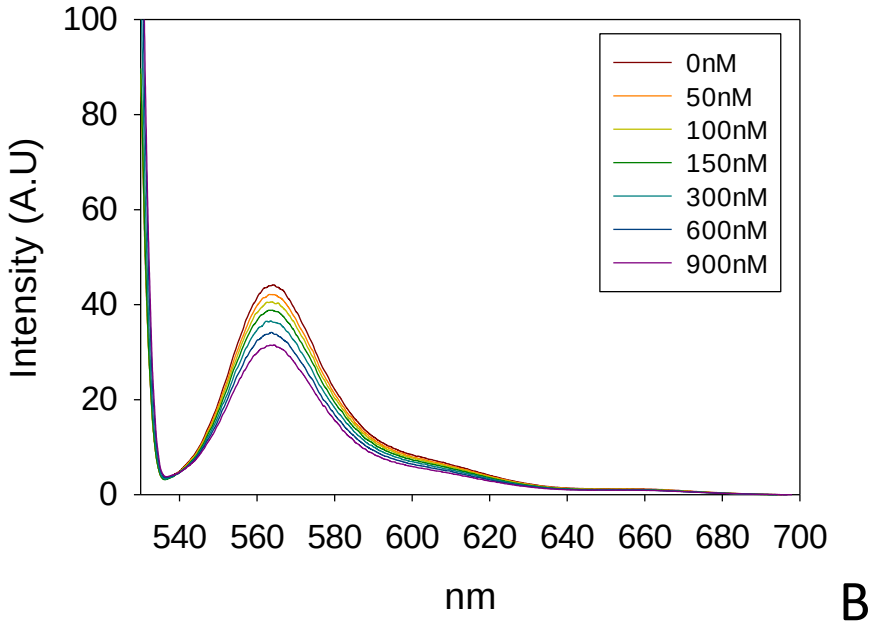


B

Cy3-5’-dT42-3’-Cy5 : 5 nM
Buffer: 20 mM Tris, 50 mM NaCl　Ex/Em : 515/530-700 nm
反應時間：1 min　　環境溫度：25℃

**圖二十四：**SaPriA 與 dT42 反應時，隨著 dT42 濃度的上升，在 567nm 處的波峰呈現藍移(blue shift)現象(A)；當同時加入 KpPriB 時，隨著 KpPriB 濃度的上升，則出現 FRET 現象，顯示 PriB 結合上 PriA-DNA 複合體時，PriB 會優先往 PriA 接觸，並拉扯 DNA 趨於緊密，這可從 Cy3,Cy5 十分靠近以至於產生 FRET 現象得知，最後，PriA,PriB 將共結合於 DNA 上，完成初步引子合成體組裝。

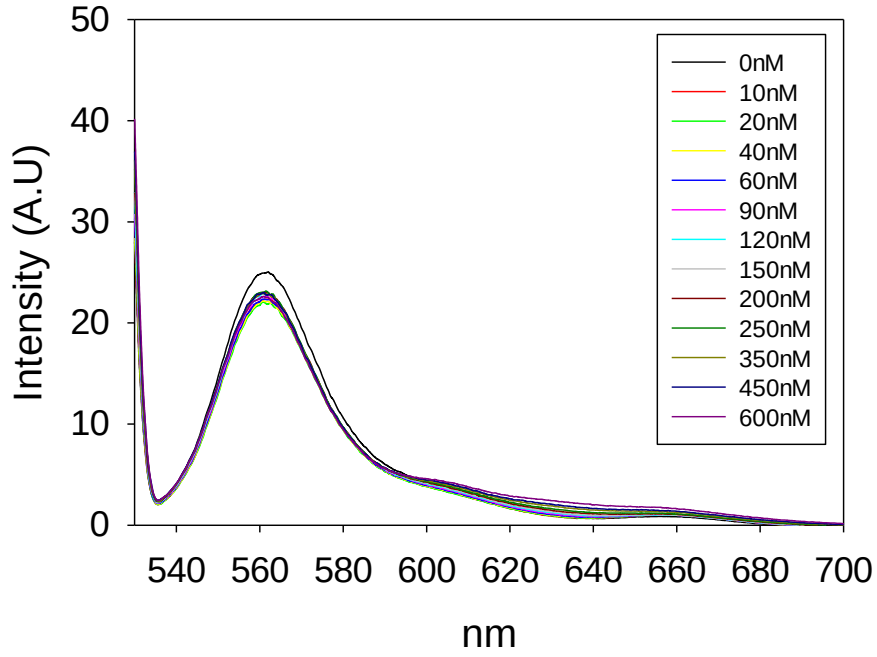


Cy3-5’-dT42-3’-Cy5 : 5 nM
Buffer: 20 mM Tris, 50 mM NaCl　Ex/Em : 515/530-700 nm
反應時間：1 min　　環境溫度：25℃

**圖二十五：**以 FRET 分析 SaDnaB 與 DNA 之交互作用，SaDnaB 為一解旋酶，對於 ssDNA 不易產生 interaction，而 dT42 為 ssDNA，故在光譜圖中 Cy3 螢光未見明顯下降。

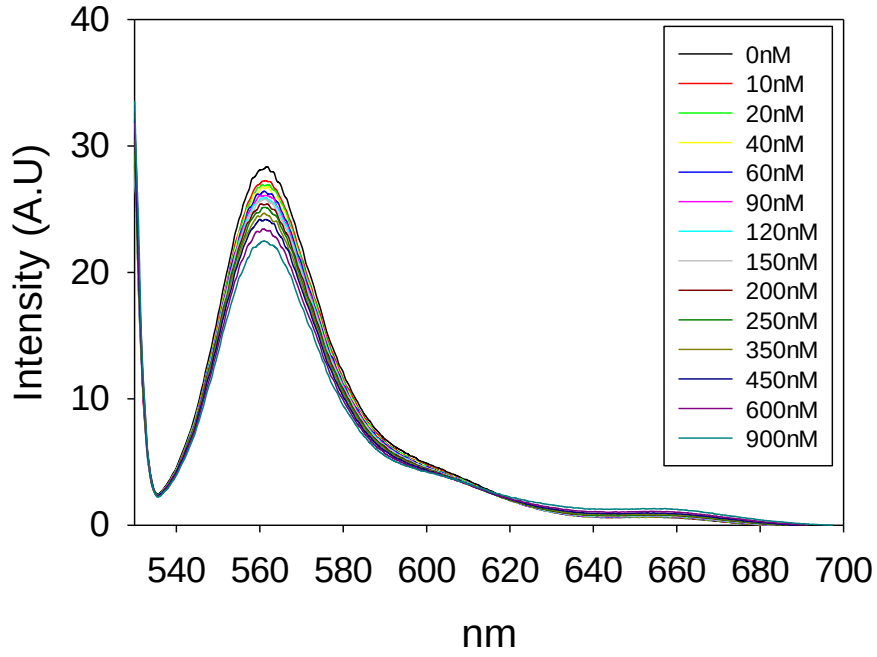


Cy3-5’-dT42-3’-Cy5 : 5 nM
Buffer: 20 mM Tris, 50 mM NaCl　Ex/Em : 515/530-700 nm
反應時間：1 min　　環境溫度：25℃

**圖二十六：**以 FRET 分析 SaDnaI 與 DNA 之交互作用，DnaI 為革蘭氏陽性菌獨有之 primosomal protein，為 helix loader，DnaI 會帶著 DnaC 附著至複製叉上，DnaI 具有 binding DNA 之能力，從光譜圖可見 DnaI 與 dT42 產生交互作用，並使得 Cy3 之產生螢光共振能量傳遞現象，造成 567nm 處螢光下降，並可見 665nm 處隨著 DnaI 濃度的上昇而產生波峰。

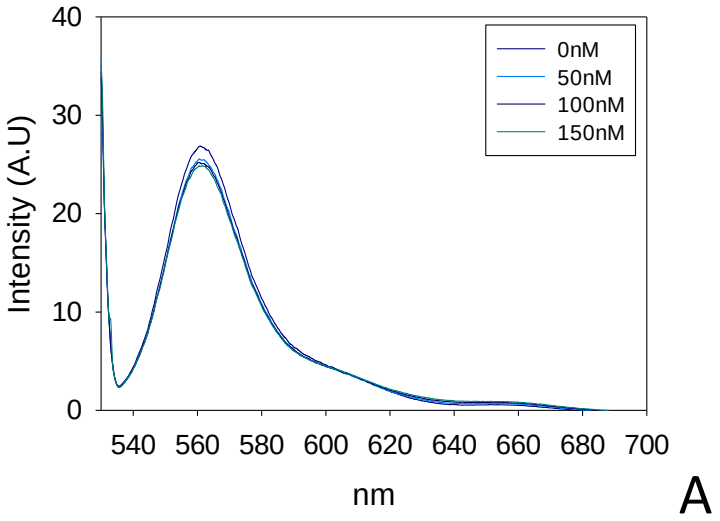


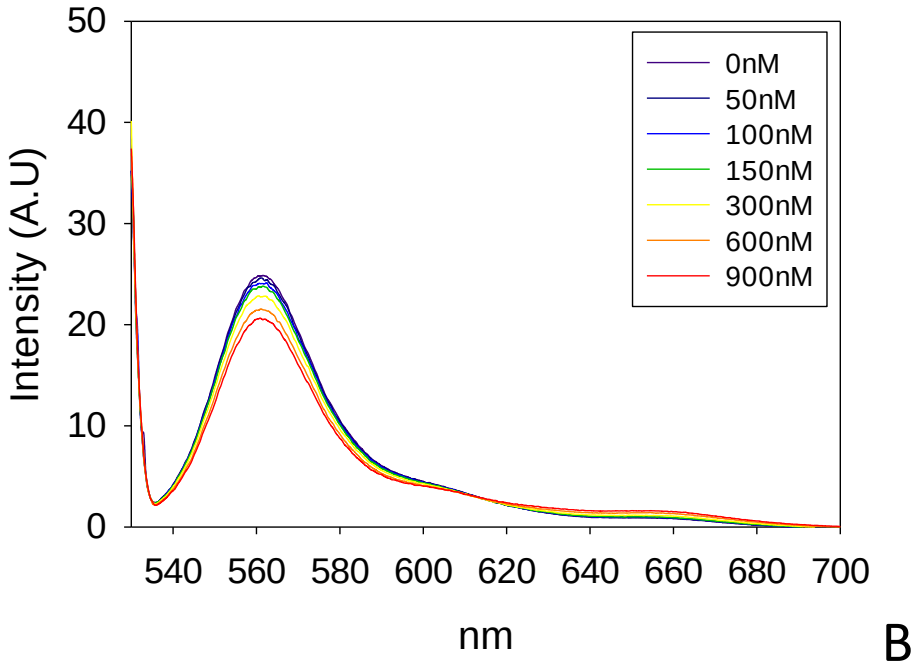


Cy3-5’-dT42-3’-Cy5 : 5 nM
Buffer: 20 mM Tris, 50 mM NaCl　Ex/Em : 515/530-700 nm
反應時間：1 min　　環境溫度：25℃

**圖二十七：**以 FRET 分析 SaDnaB-SaDnaI 與 DNA 之交互作用，SaDnaB 本身與 dT42 不易產生作用，當同時加入 SaDnaI 時，隨著 SaDnaI 濃度的上升，則出現螢光共振能量傳遞現象，顯示 DnaI-DnaB complex 會與 DNA 結合，並造成 DNA 構形的改變，並拉扯 DNA 趨於緊密。

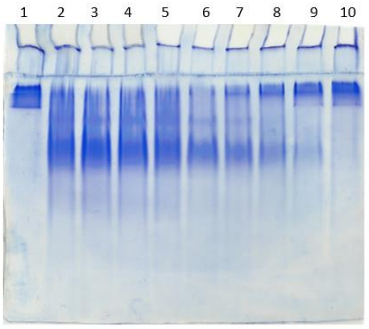


9% Native PAGE, 150V, 150min

| | SaPriA (uM) | SaDnaD 1-204 (uM) |
|---|---|---|
| 1 | 50 | 0 |
| 2 | 0 | 50 |
| 3 | 0.4 | |
| 4 | 0.8 | |
| 5 | 1.6 | |
| 6 | 3.2 | |
| 7 | 6.25 | |
| 8 | 12.5 | |
| 9 | 25 | |
| 10 | 50 | |

A

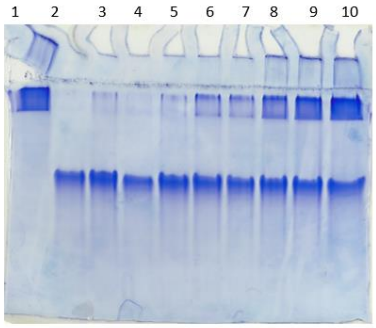


9% Native PAGE, 150V, 150min

| | SaPriA (uM) | SaDnaD 1-195 (uM) |
|---|---|---|
| 1 | 50 | 0 |
| 2 | 0 | 50 |
| 3 | 0.4 | |
| 4 | 0.8 | |
| 5 | 1.6 | |
| 6 | 3.2 | |
| 7 | 6.25 | |
| 8 | 12.5 | |
| 9 | 25 | |
| 10 | 50 | |

B

**圖二十八：**以 Native PAGE 分析 SaPriA 與 SaDnaD 之交互作用，從 Native PAGE 結果可以發現其 a.a 1-204 片段會與 SaPriA 產生交互作用(A)，但其 a.a 1-195 片段則不會與 SaPriA 產生交互作用(B)，顯示 SaDnaD C 端可能為與 PriA 交互作用之位置。

| Residue | Distance shorter than 3 Angstrom (times) |
|---|---|
| E50 | 36 |
| L20 | 25 |
| I44 | 18 |
| V48 | 18 |
| G43 | 16 |
| V45 | 15 |
| D17 | 14 |
| Y18 | 11 |
| L19 | 10 |
| A46 | 10 |
| A47 | 10 |
| E22 | 9 |
| T15 | 7 |
| F16 | 7 |
| V26 | 7 |
| L56 | 7 |
| H88 | 6 |

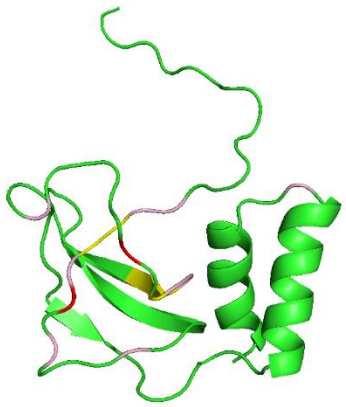

**圖二十九：**上表為每個黃酮醇與三種分子對接方法進行模擬，並取其前三個最佳解，分析並觀察位於黃酮醇分子周圍 3Å 之胺基酸分布狀況，以及預測其氫鍵鍵長，統計 36 個 solution 後之結果：黃酮醇與紅色欄位之 E50 及 L20 兩個胺基酸產生氫鍵的次數最多，平均每個 solution 中黃酮醇均會與此二殘基產生一個氫鍵，另外，黃色欄位中，D17, Y18, I44, V45, V48 殘基也會與黃酮醇中的 OH 產生氫鍵，這些殘基位於 PriA 之 3’ BD (3’ DNA Binding Domain)，此區域負責 PriA 與 DNA 之交互作用，紫色欄位則為黃酮醇偶而會與之產生氫健之殘基，上表之殘基利用 PyMol 於 KpPriA N 端之模型上標出，結果顯示黃酮醇可能藉由抑制 DNA 與 PriA 結合影響 PriA 之 DNA unwinding，及影響 PriA 之構形。

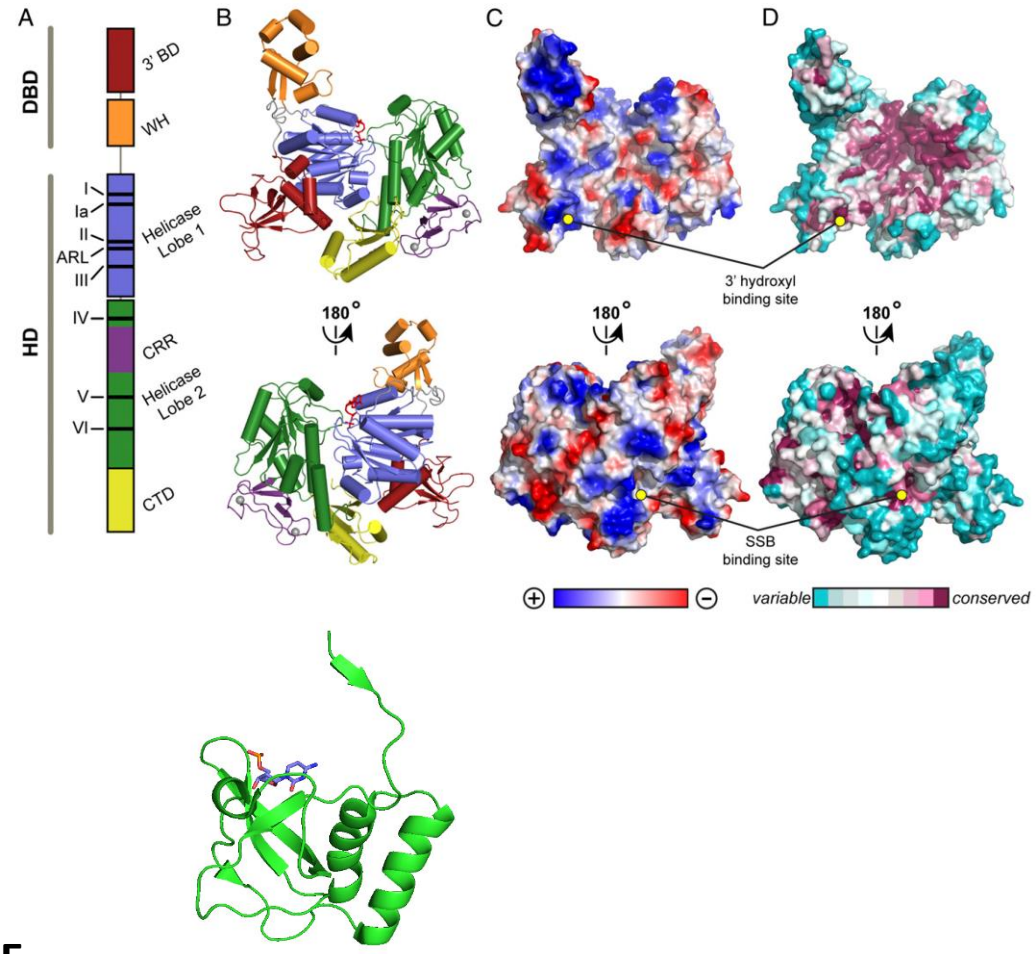


**圖三十：**解旋酶 PriA 之結構：(A)PriA 之 Domian 分佈 (B)KpPriA 之結晶結構，各 domain 之顏色根據圖 A 的分佈繪製，ADP(紅色)結合於 helicase core，兩個 $Zn^{2+}$(灰色點)結合於 CRR domain (C)KpPriA 之靜電分布(藍色代表正電性, electropositive；紅色代表負電性,electronegative；白色為電中性,neutral) (D)KpPriA 演化保留殘基之分布(根據 150PriA sequence 之 sequence alignment) (E)KpPriA N-端結構，對應於 3'BD (3' binding domain)，此結構利用 homology modeling 並基於 PDB:2D7H 建立，ATP (藍色)結合於 3'BD 處。

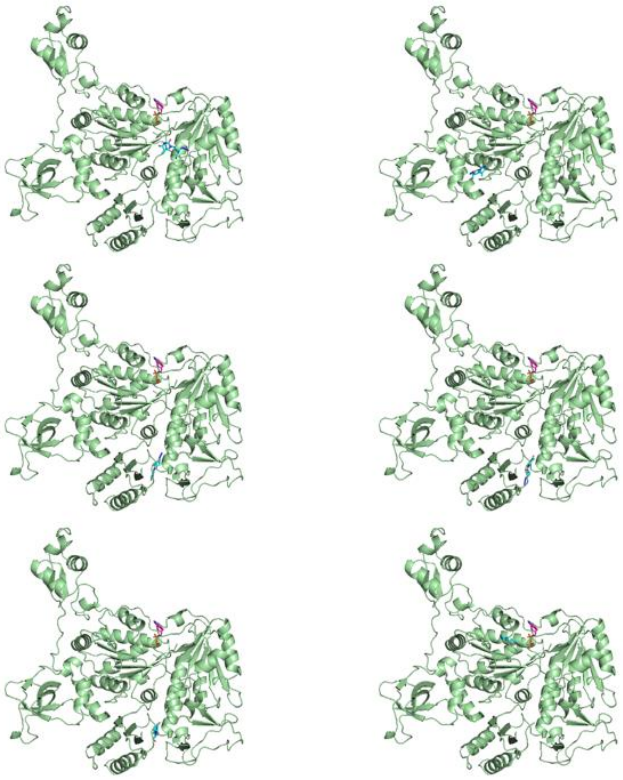

| model | energy |
|---|---|
| 1 | -202.82 |
| 2 | -202.15 |
| 3 | -200.15 |
| 4 | -199.98 |
| 5 | -196.04 |
| 6 | -195.38 |

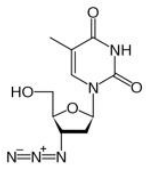


Zidovudine (HEX-S)

**圖三十一：**利用分子對接工具—HEX SERVER (Shape model)模擬 AZT (Zidovudine)與 KpPriA 之結合模式。根據結合能高低順序由左至右，再由上至下，除了 model 1 結合於 Helicase Lobe 2 外，model2-5 結合於 Helicase Lobe 1 及 CRR domain 處，model 6 則結合於靠近 ADP binding site。

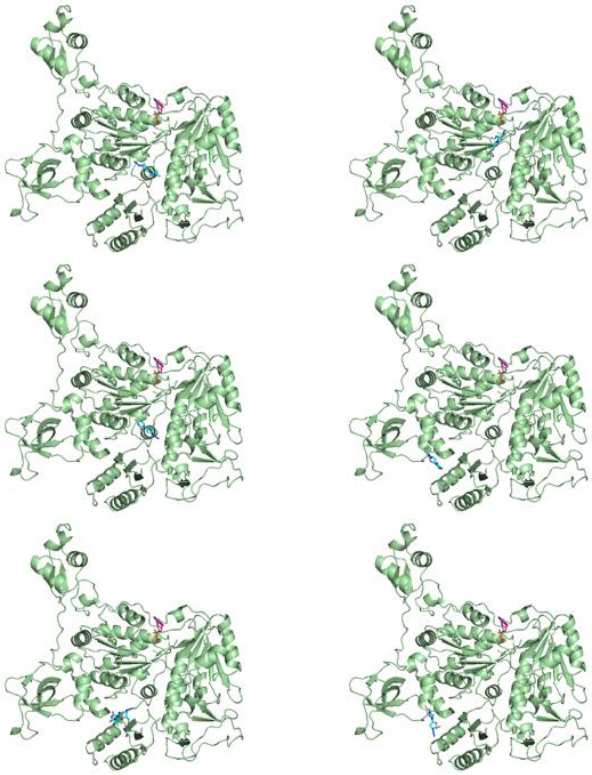

| model | energy |
|---|---|
| 1 | -312.09 |
| 2 | -311.74 |
| 3 | -287.93 |
| 4 | -284.62 |
| 5 | -279.66 |
| 6 | -270.99 |

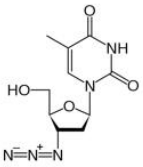

Zidovudine (HEX-S+E)

**圖三十二：**利用分子對接工具—HEX SERVER (Shape + Electrostatic model)模擬 AZT (Zidovudine)與 KpPriA 之結合模式。根據結合能高低順序由左至右，再由上至下，model 1-3 結合於 Helicase Lobe 1，model 4-6 則結合於靠近 CTD 及 3'BD 處。

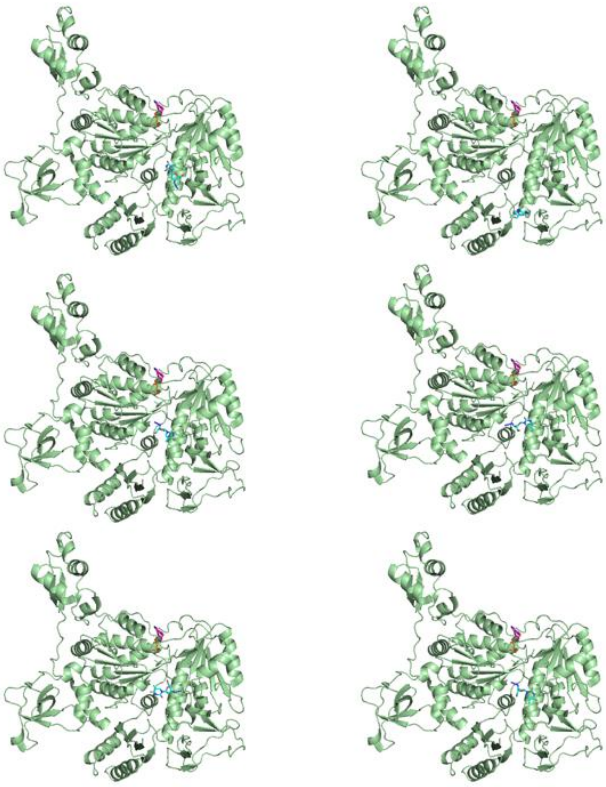

| model | score |
|---|---|
| 1 | 4202 |
| 2 | 4158 |
| 3 | 4156 |
| 4 | 4152 |
| 5 | 4130 |
| 6 | 4128 |

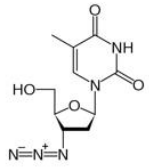


Zidovudine (PD)

**圖三十三：**利用分子對接工具—PATCH DOCK 模擬 AZT (Zidovudine)與 KpPriA 之結合模式。根據結合能高低順序由左至右，再由上至下，model 1-6 均結合於 Helicase Lobe 2 處。

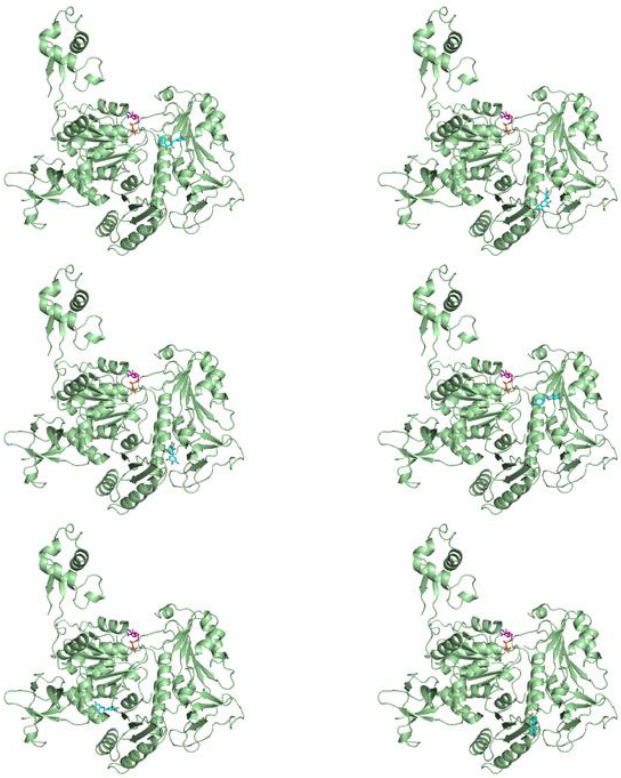

| model | score |
|---|---|
| 1 | -230.74 |
| 2 | -227.91 |
| 3 | -223.67 |
| 4 | -221.67 |
| 5 | -215.13 |
| 6 | -213.29 |

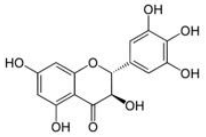


Dihydromyricetin (HEX-S)

**圖三十四：**利用分子對接工具—HEX SERVER (shape model)模擬 Dihydromyricetin 與 KpPriA 之結合模式。根據結合能高低順序由左至右，再由上至下，除了 model 5 外結合於 helicase lobe 1，model 1,4 結合於 helicase lobe 2，model 2,3,6 則結合於 CRR domain 處。

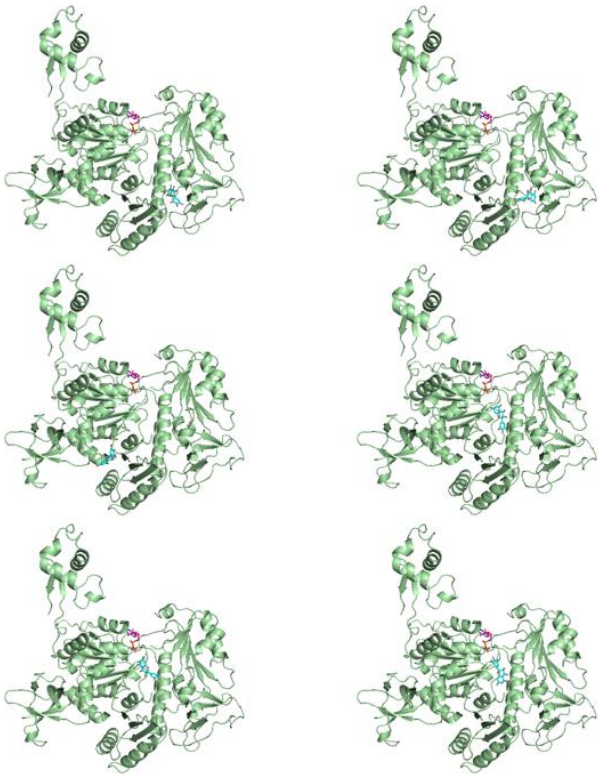

| model | score |
|---|---|
| 1 | -284.64 |
| 2 | -267.75 |
| 3 | -261.36 |
| 4 | -261.11 |
| 5 | -247.27 |
| 6 | -240.23 |

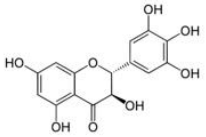


Dihydromyricetin (HEX-S+E)

**圖三十五：**利用分子對接工具—HEX SERVER (shape + electrostatic model)模擬 Dihydromyricetin 與 KpPriA 之結合模式。根據結合能高低順序由左至右，再由上至下，model 1,2 結合於 CRR 處，其餘 model 則結合於 helicase lobe 2。

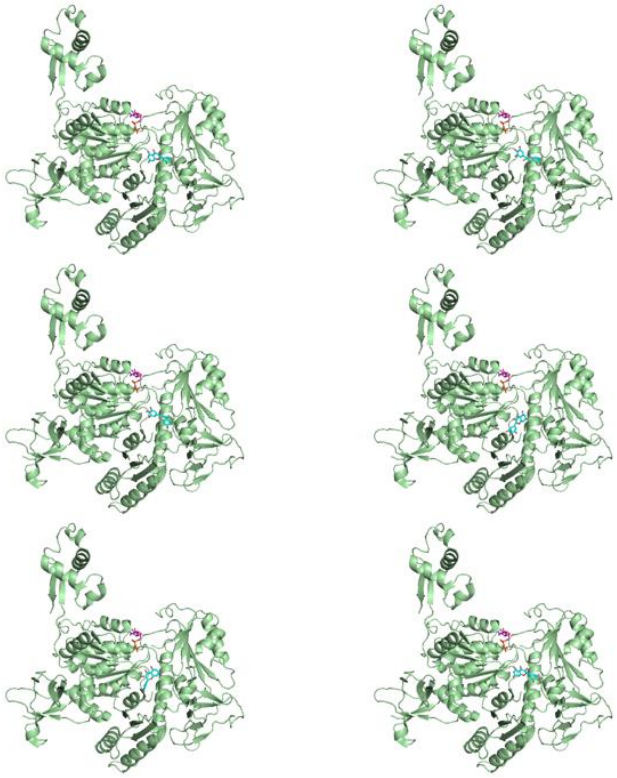

| model | score |
|---|---|
| 1 | 4560 |
| 2 | 4554 |
| 3 | 4494 |
| 4 | 4234 |
| 5 | 4218 |
| 6 | 4182 |

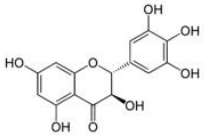


Dihydromyricetin (PD)

**圖三十六：**利用分子對接工具—PATCH DOCK 模擬 Dihydromyricetin 與 KpPriA 之結合模式。根據結合能高低順序由左至右，再由上至下，model 1-6 皆結合於 Helicase lobe 2 。

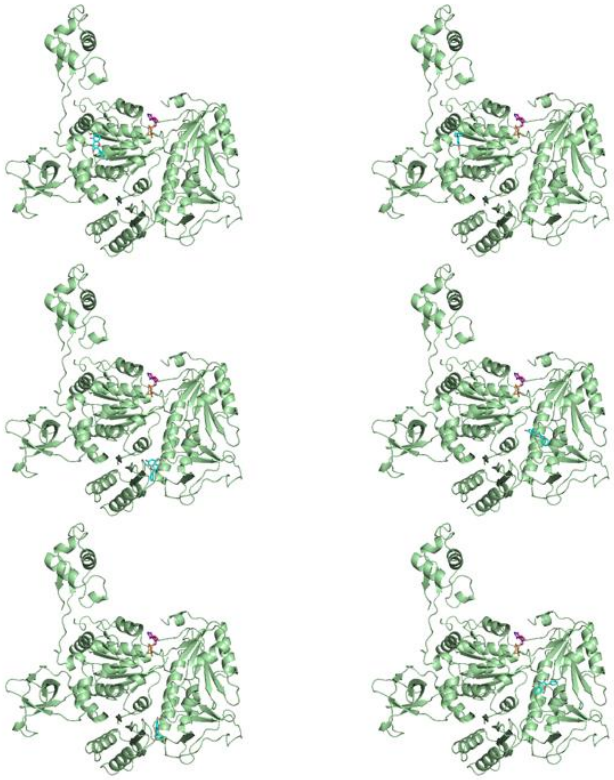

| model | energy |
|---|---|
| 1 | -208.41 |
| 2 | -205.56 |
| 3 | -205.16 |
| 4 | -200.92 |
| 5 | -200.57 |
| 6 | -199.26 |

Galangin (Hex-S)

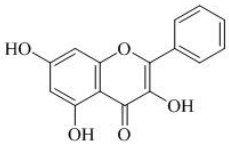


**圖三十七：**利用分子對接工具—HEX SERVER (shape model)模擬 galangin 與 KpPriA 之結合模式。根據結合能高低順序由左至右，再由上至下，model 1,2 結合於 helicase lobe 1，model 3,5 結合於 CRR domain 處，model 4,6 結合於 helicase lobe 2。

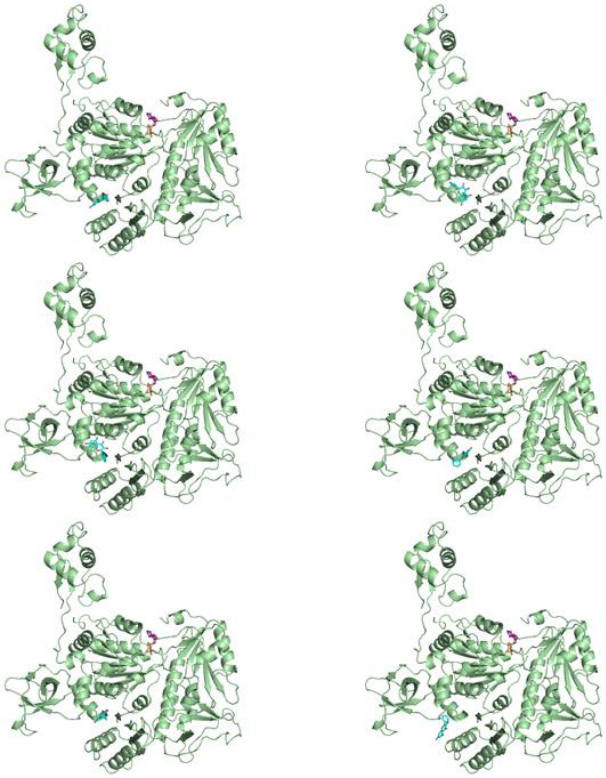

| model | energy |
|---|---|
| 1 | -320.64 |
| 2 | -298.06 |
| 3 | -266.19 |
| 4 | -258.66 |
| 5 | -255.91 |
| 6 | -253.60 |

Galangin (Hex-S+E)

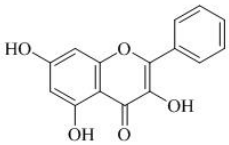


**圖三十八：**利用分子對接工具—HEX SERVER (shape + electrostatic model)模擬 galangin 與 KpPriA 之結合模式。根據結合能高低順序由左至右，再由上至下，model 1-6 均結合於 3’BD 處。

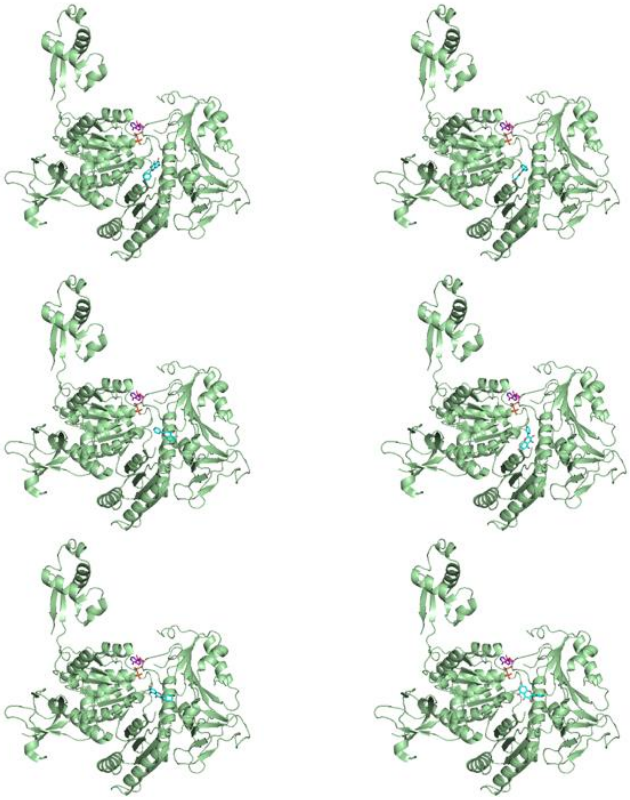

| model | energy |
|---|---|
| 1 | 4432 |
| 2 | 4254 |
| 3 | 4250 |
| 4 | 4234 |
| 5 | 4232 |
| 6 | 4222 |

Galangin (PD)

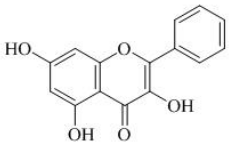


**圖三十九：**利用分子對接工具—PATCH DOCK 模擬 galangin 與 KpPriA 之結合模式。根據結合能高低順序由左至右，再由上至下，model 1-6 均結合於 helicase lobe 2 處。

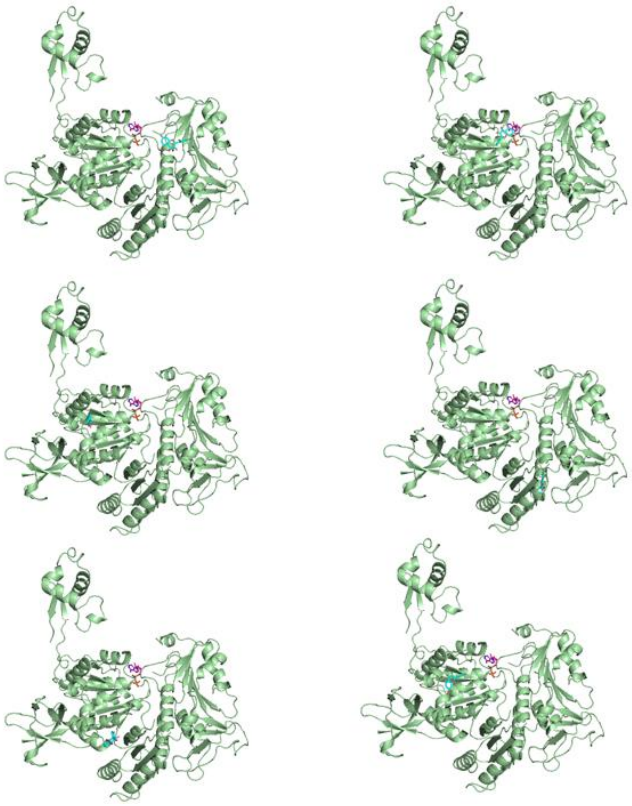

| model | energy |
|---|---|
| 1 | -213.91 |
| 2 | -209.29 |
| 3 | -209.16 |
| 4 | -203.85 |
| 5 | -203.23 |
| 6 | -199.18 |

Kaempferol (Hex-S)

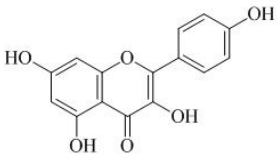


**圖四十：**利用分子對接工具—HEX SERVER (shape model)模擬 Kaempferol 與 KpPriA 之結合模式。根據結合能高低順序由左至右，再由上至下，model 1-6 均結合於 helicase lobe 2 處。

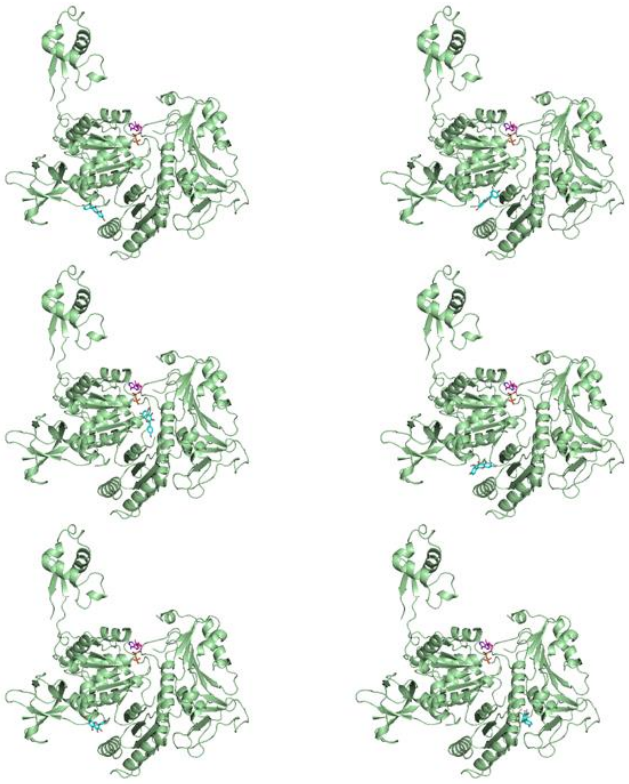

| model | energy |
|---|---|
| 1 | -293.34 |
| 2 | -279.92 |
| 3 | -273.58 |
| 4 | -271.25 |
| 5 | -266.86 |
| 6 | -264.22 |

Kaempferol (Hex-S+E)

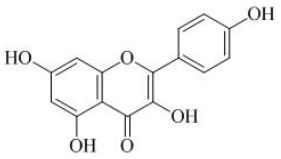


**圖四十一：**利用分子對接工具—HEX SERVER (shape + electrostatic model)模擬 Kaempferol 與 KpPriA 之結合模式。根據結合能高低順序由左至右，再由上至下，model 1,2,4,5 結合於 3'BD，而 model 3,6 則結合於 helicase lobe 2。

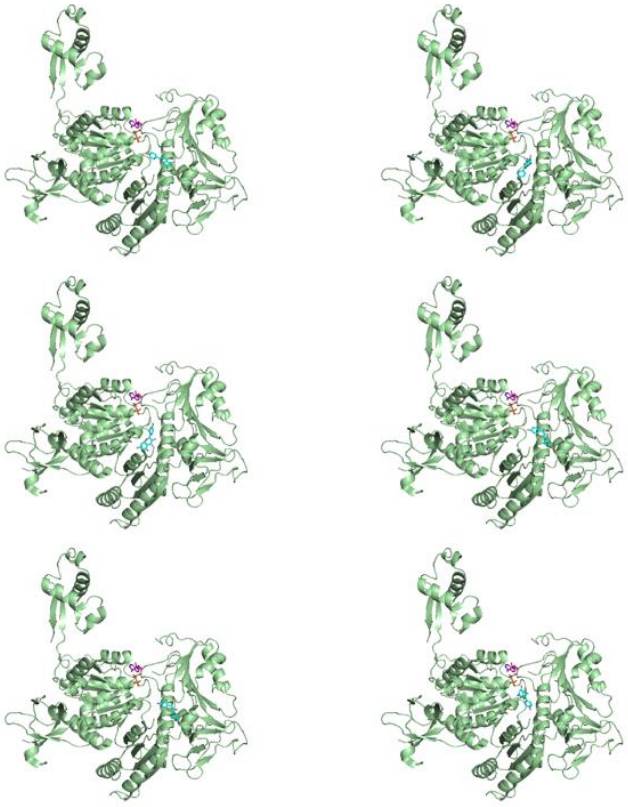

| model | energy |
|---|---|
| 1 | 4500 |
| 2 | 4472 |
| 3 | 4464 |
| 4 | 4438 |
| 5 | 4292 |
| 6 | 4252 |

Kaempferol (PD)

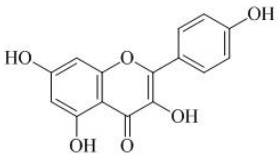


**圖四十二：**利用分子對接工具—PATCH DOCK 模擬 Kaempferol 與 KpPriA 之結合模式。根據結合能高低順序由左至右，再由上至下，model 1-6 均結合於 helicase lobe 2 處。

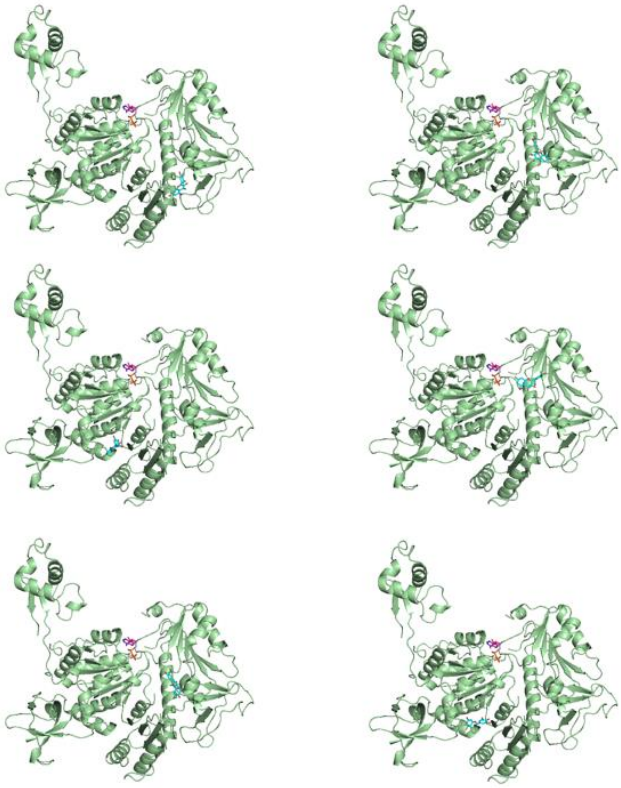

| model | energy |
|---|---|
| 1 | -225.49 |
| 2 | -224.52 |
| 3 | -222.13 |
| 4 | -221.27 |
| 5 | -220.80 |
| 6 | -219.51 |

Myricetin (HEX-S)

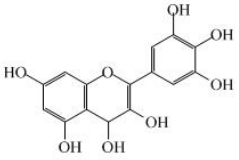


**圖四十三：**利用分子對接工具—HEX SERVER (shape model) 模擬 Myricetin 與 KpPriA 之結合模式。根據結合能高低順序由左至右，再由上至下，model 3,6 結合於 helicase lobe 1 接近 3'BD 處，其餘 model 均結合於 helicase lobe 2 處。

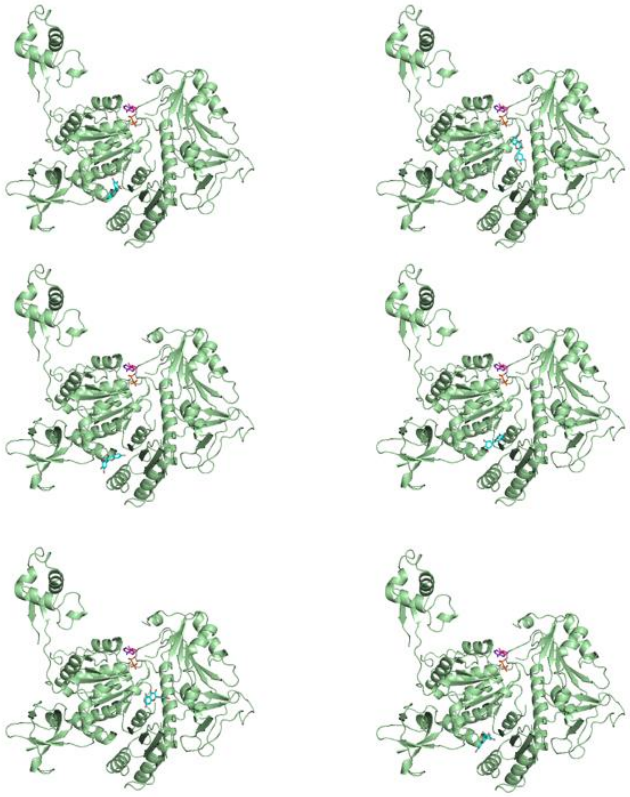

| model | energy |
|---|---|
| 1 | -279.17 |
| 2 | -275.31 |
| 3 | -258.10 |
| 4 | -256.93 |
| 5 | -254.28 |
| 6 | -242.51 |

Myricetin (HEX-S+E)

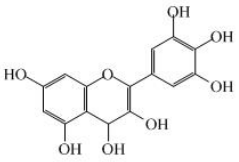


**圖四十四：**利用分子對接工具—HEX SERVER (shape + electrostatic model)模擬 Myricetin 與 KpPriA 之結合模式。根據結合能高低順序由左至右，再由上至下，model 1,3,4,6 結合於 helicase lobe 與 3’BD 之間，其餘 model 結合於 helicase lobe 2 處。

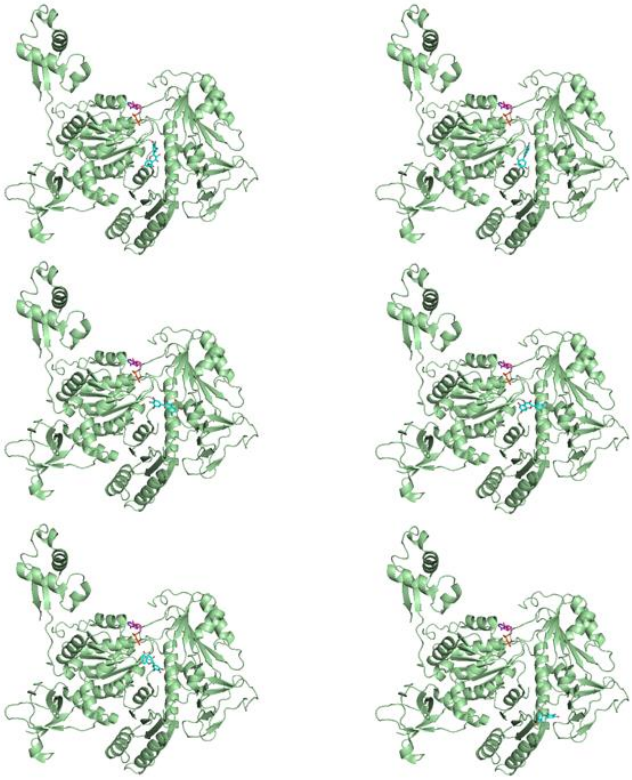

| model | energy |
|---|---|
| 1 | 4760 |
| 2 | 4662 |
| 3 | 4568 |
| 4 | 4496 |
| 5 | 4464 |
| 6 | 4398 |

Myricetin (PD)

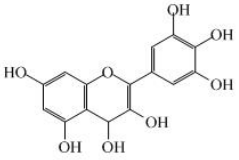


**圖四十五：**利用分子對接工具—PATCH DOCK 模擬 Myricetin 與 KpPriA 之結合模式。根據結合能高低順序由左至右，再由上至下，model 1-6 均結合於 helicase lobe 2 處。

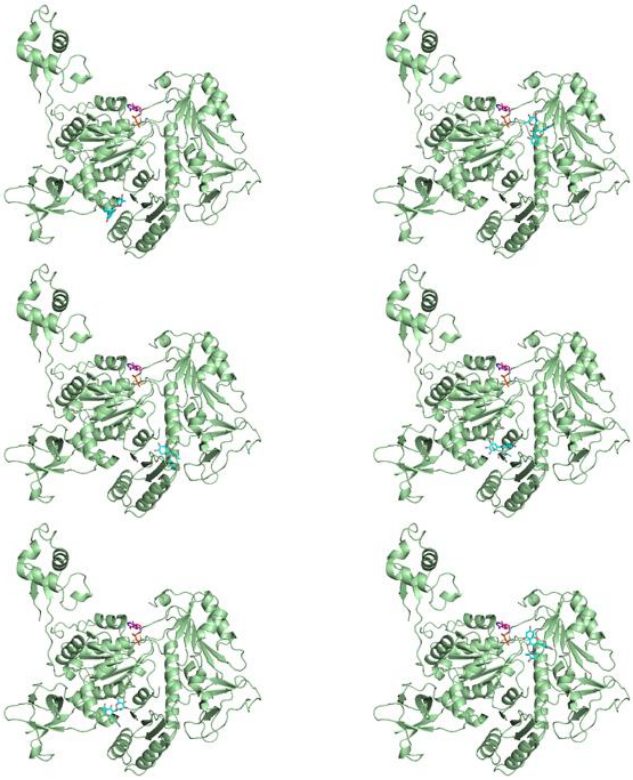

| model | energy |
|---|---|
| 1 | -287.58 |
| 2 | -283.55 |
| 3 | -275.10 |
| 4 | -262.39 |
| 5 | -260.94 |
| 6 | -257.86 |

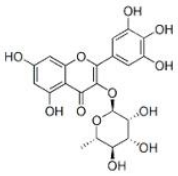


Myricitrin (Hex-S)

**圖四十六：**利用分子對接工具—HEX SERVER (shape model)模擬 Myricitrin 與 KpPriA 之結合模式。根據結合能高低順序由左至右，再由上至下，model 1,4,5 結合於 helicase lobe 1 處，其餘 model 結合於 helicase lobe 2 處。

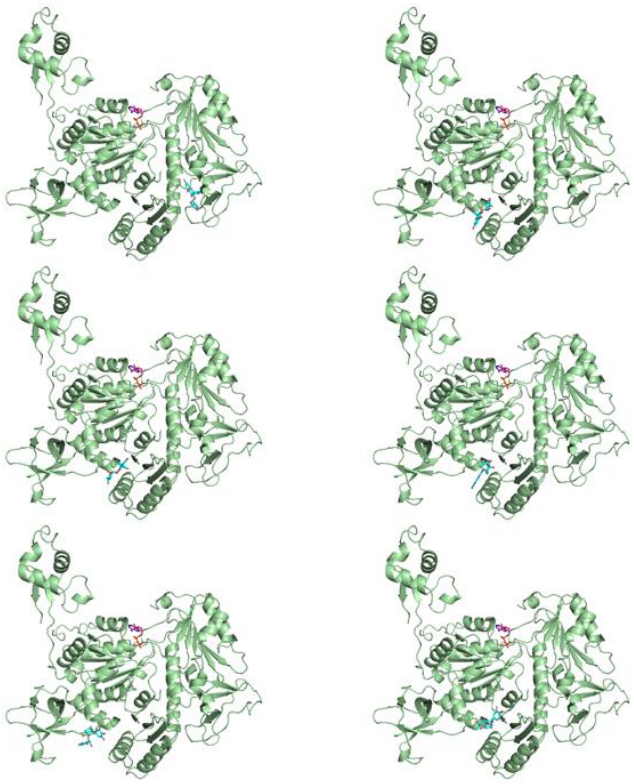

| model | energy |
|---|---|
| 1 | -378.32 |
| 2 | -373.40 |
| 3 | -371.26 |
| 4 | -361.16 |
| 5 | -358.07 |
| 6 | -357.24 |

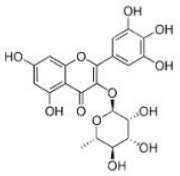


Myricitrin (Hex-S+E)

**圖四十七：**利用分子對接工具—HEX SERVER (shape + electrostatic model)模擬 Myricitrin 與 KpPriA 之結合模式。根據結合能高低順序由左至右，再由上至下，model 1 結合於 CRR domain 處，model 2-6 結合於靠近 3’BD 處。

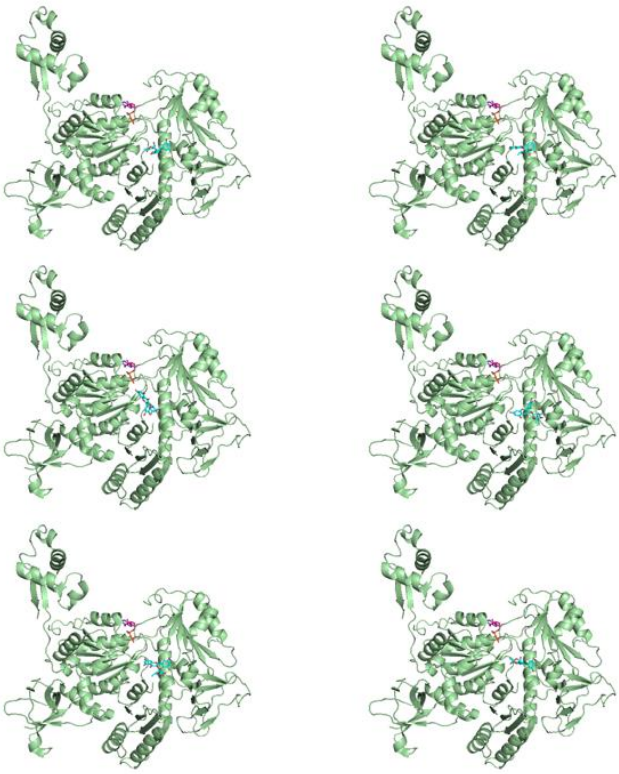

| model | score |
|---|---|
| 1 | 5608 |
| 2 | 5508 |
| 3 | 5460 |
| 4 | 5434 |
| 5 | 5412 |
| 6 | 5404 |

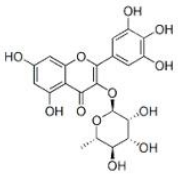

Myricitrin (PD)

**圖四十八：**利用分子對接工具—PATCH DOCK 模擬 Myricitrin 與 KpPriA 之結合模式。根據結合能高低順序由左至右，再由上至下，model 1-6 均結合於 helicase lobe 2 處。

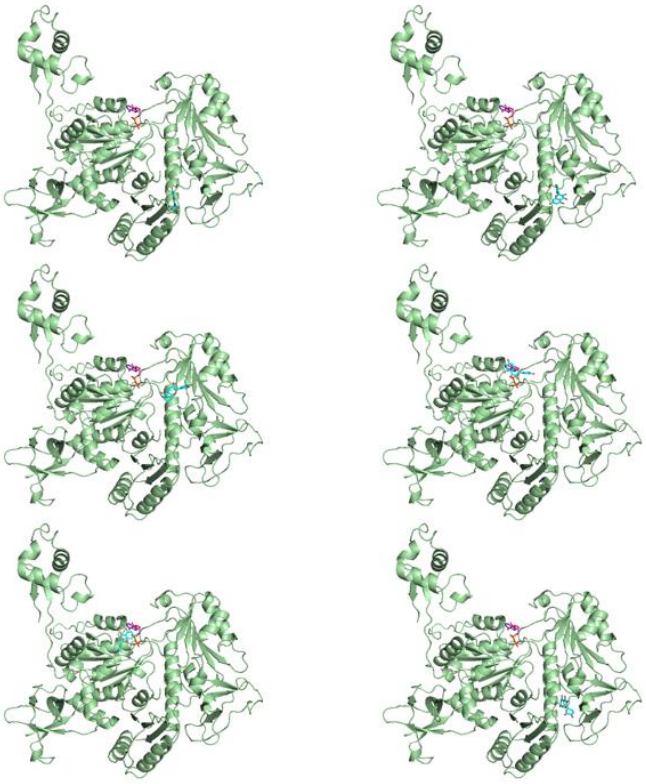

| model | energy |
|---|---|
| 1 | -212.26 |
| 2 | -211.46 |
| 3 | -210.58 |
| 4 | -210.35 |
| 5 | -208.15 |
| 6 | -207.82 |

Quercetin (Hex-S)

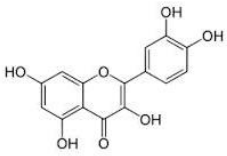


**圖四十九：**利用分子對接工具—HEX SERVER (shape model)模擬 Quercetin 與 KpPriA 之結合模式。根據結合能高低順序由左至右，再由上至下，model 1,2,6 結合於 CRR domain 處，model 3 結合於 helicase lobe 2，model 4,5 結合於 ADP binding site。

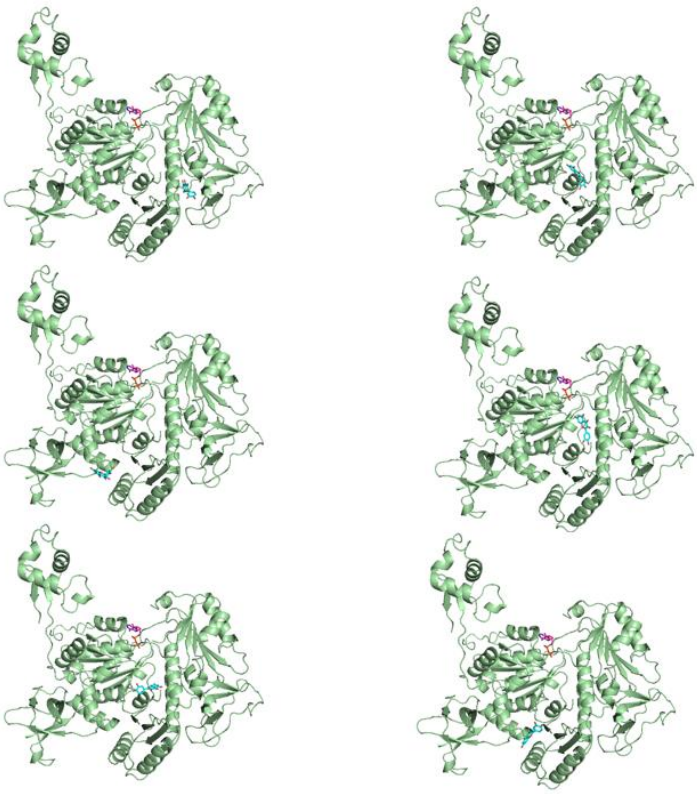

| model | energy |
|---|---|
| 1 | -294.64 |
| 2 | -279.67 |
| 3 | -270.50 |
| 4 | -268.11 |
| 5 | -257.57 |
| 6 | -244.45 |

Quercetin (Hex-S+E)

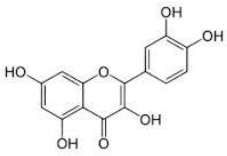


**圖五十：**利用分子對接工具—HEX SERVER (shape + electrostatic model)模擬 Quercetin 與 KpPriA 之結合模式。根據結合能高低順序由左至右，再由上至下，model 1 結合於 CRR domian 處，model 2,4,5 結合於 helicase lobe 2，model 3,6 結合於 3'BD 處。

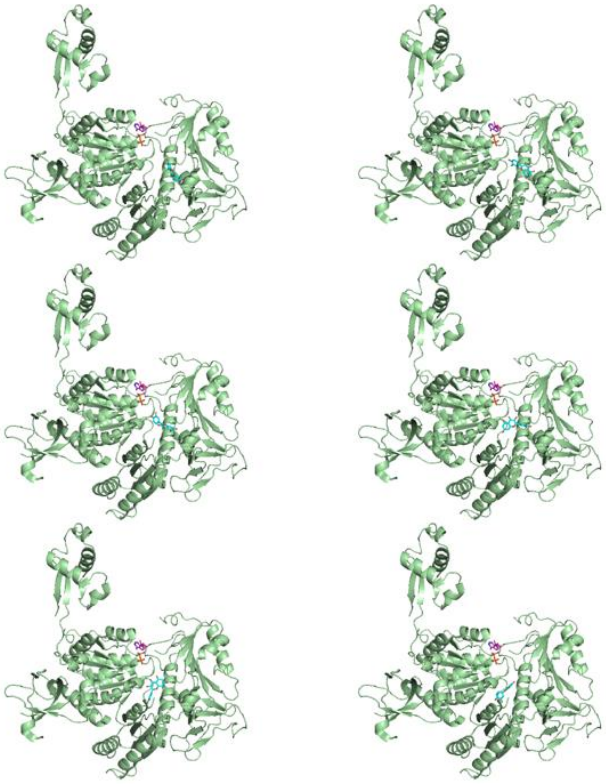

| model | energy |
|---|---|
| 1 | 4278 |
| 2 | 4198 |
| 3 | 4196 |
| 4 | 4182 |
| 5 | 4148 |
| 6 | 4134 |

Quercetin (PD)

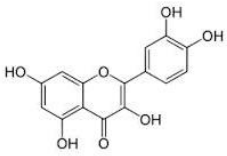


**圖五十一：**利用分子對接工具—PATCH DOCK 模擬 Quercetin 與 KpPriA 之結合模式。根據結合能高低順序由左至右，再由上至下，model 1-6 均結合於 helicase lobe 2 處。

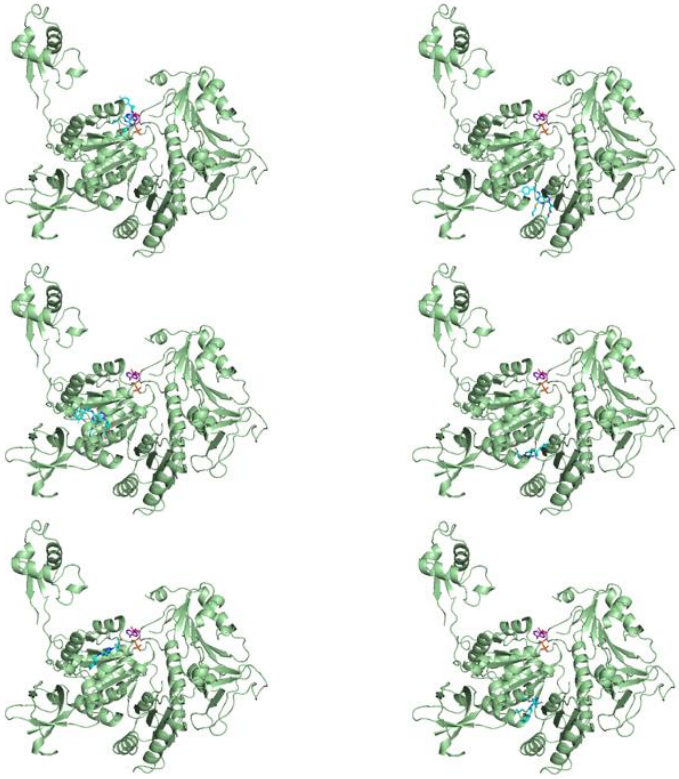

| model | energy |
|---|---|
| 1 | -289.31 |
| 2 | -272.03 |
| 3 | -265.62 |
| 4 | -265.35 |
| 5 | -263.40 |
| 6 | -262.86 |

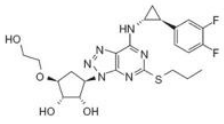

Ticagrelor (HEX-S)

**圖五十二：**利用分子對接工具—HEX SERVER (shape model)模擬 Ticagrelor 與 KpPriA 之結合模式。根據結合能高低順序由左至右，再由上至下，model 1 結合於 ADP binding site，model 3,5 結合於 helicase lobe1，model 4,6 結合於 3’BD 處。

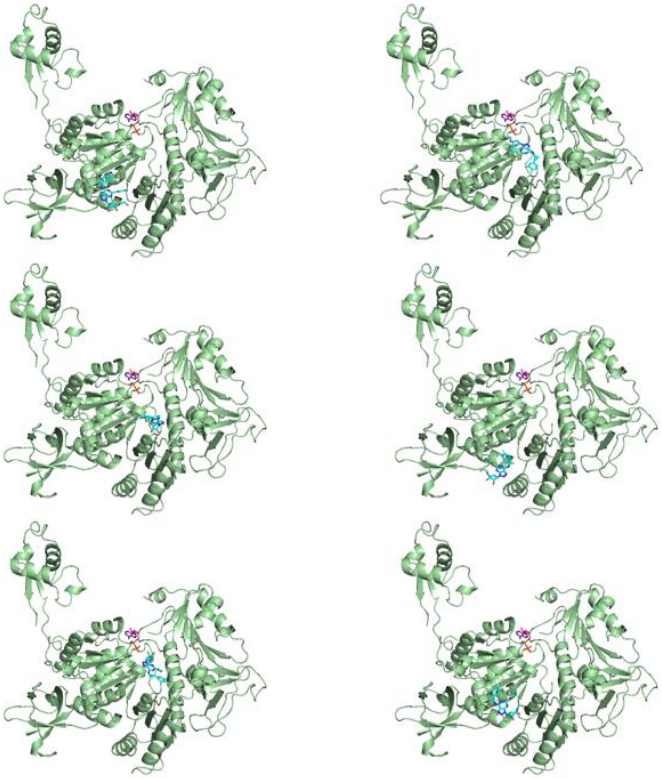

| model | energy |
|---|---|
| 1 | -392.34 |
| 2 | -378.79 |
| 3 | -364.09 |
| 4 | -357.80 |
| 5 | -353.26 |
| 6 | -338.09 |

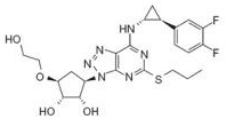

Ticagrelor (HEX-S+E)

**圖五十三：**利用分子對接工具—PATCH DOCK 模擬 Ticagrelor 與 KpPriA 之結合模式。根據結合能高低順序由左至右，再由上至下，model 1,4,6 結合於 3'BD 處，model 2,3,5 均結合於 helicase lobe 2 處。

| model | score |
|---|---|
| 1 | 6922 |
| 2 | 6668 |
| 3 | 6636 |
| 4 | 6586 |
| 5 | 6556 |
| 6 | 6544 |

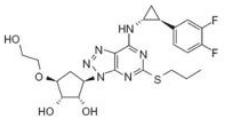

Ticagrelor (PD)

**圖五十四：**利用分子對接工具—PATCH DOCK 模擬 Ticagrelor 與 KpPriA 之結合模式。根據結合能高低順序由左至右，再由上至下，model 1-6 均結合於 helicase lobe 2 處。

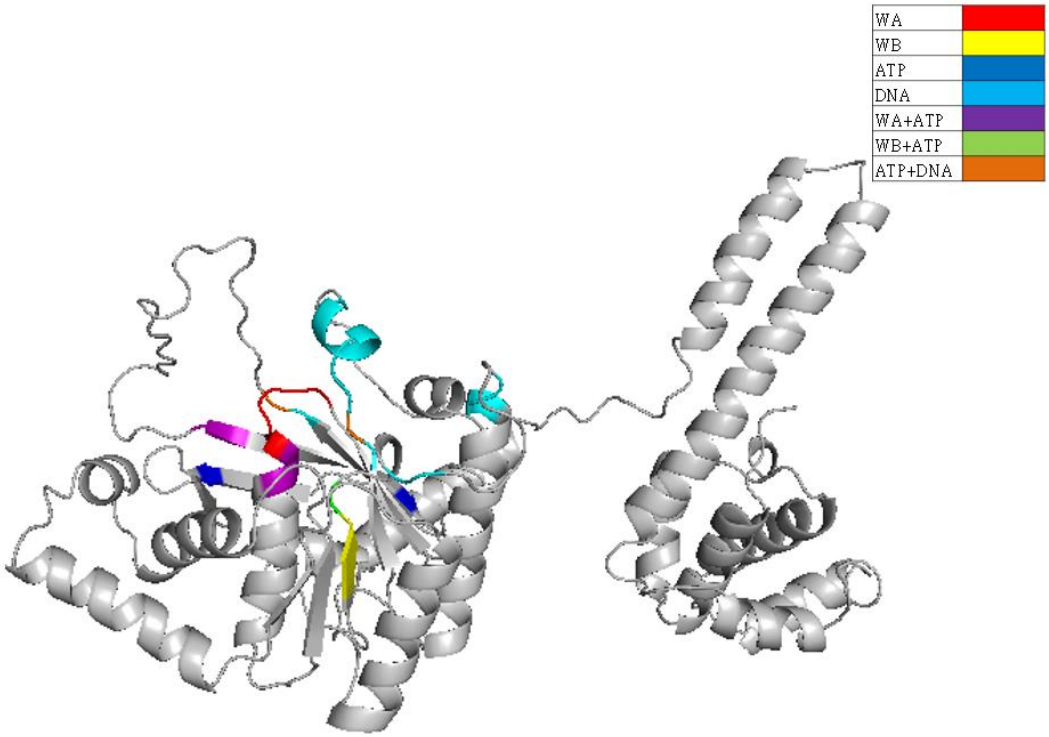


**圖五十五**：利用 SWISS MODEL 以 homology modeling 模擬 SaDnaB 模型，並基於 Geobacillus kaustophilus DnaC (2R6C) 之結構，紅色標示處代表 Walker A，黃色標示處代表 Walker B，ATP binding site 以藍色標註，DNA binding loop 以青色標註，紫色處為 ATP binding site 與 Walker A 疊合處，綠色為 ATP binding site 與 Walker B 疊合處，橘色區則為 ATP binding site 與 DNA binding loop 疊合處。

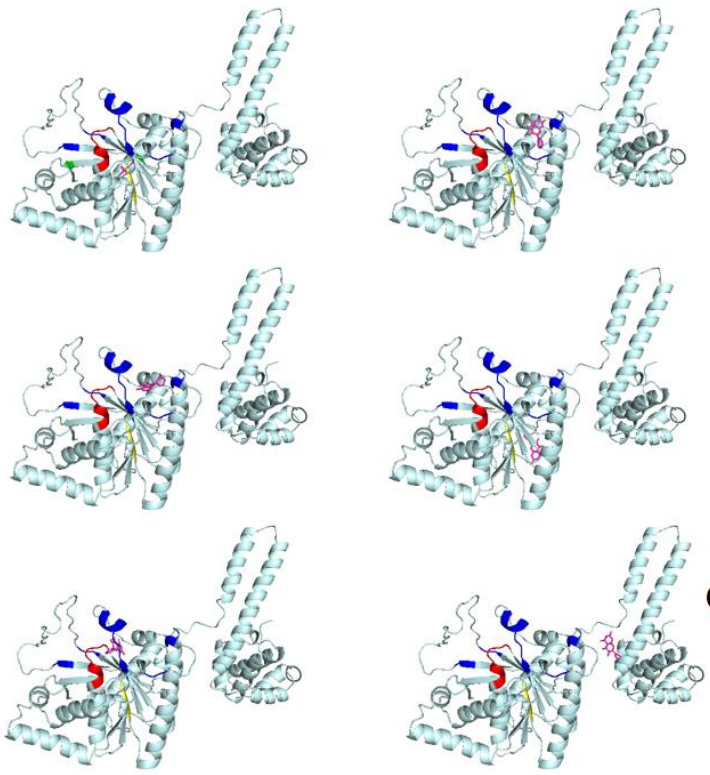

| model | energy |
|---|---|
| 1 | -203.96 |
| 2 | -186.95 |
| 3 | -184.94 |
| 4 | -183.85 |
| 5 | -183.79 |
| 6 | -181.96 |

Galangin (Hex-S)

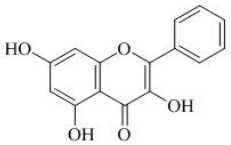


**圖五十六：**利用分子對接工具—HEX SERVER (shape model)模擬 galangin 與 SaDnaB 之結合模式。根據結合能高低順序由左至右，再由上至下，model 1 結合於 walker B 處，model 2,3,5 結合於 DNA binding loop，model 6 結合於靠近 N-terminus 處。

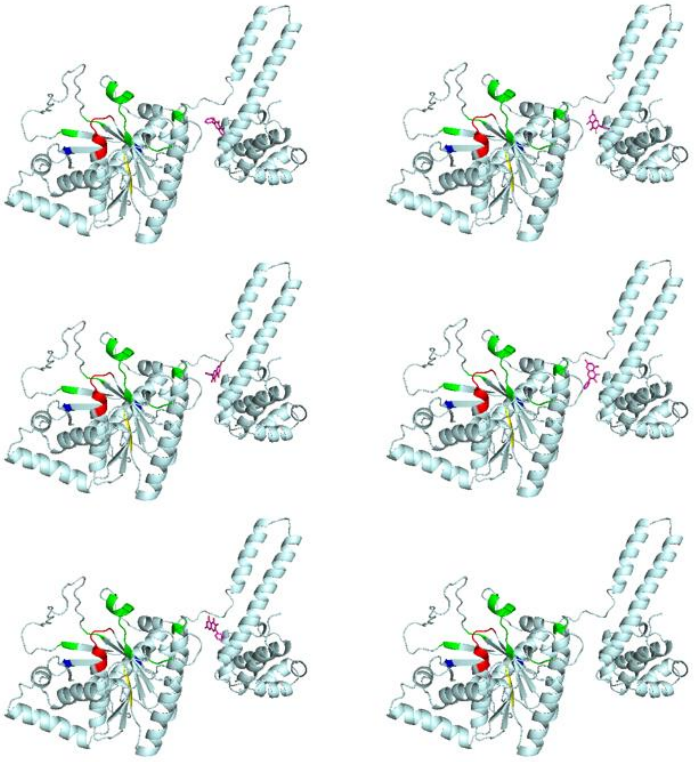

| model | energy |
|---|---|
| 1 | -1443.27 |
| 2 | -1407.87 |
| 3 | -1396.05 |
| 4 | -1349.03 |
| 5 | -1297.65 |
| 6 | -1295.50 |

Galangin (Hex-S+E)

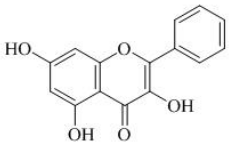


**圖五十七：**利用分子對接工具—HEX SERVER (shape + electrostatic model)模擬 galangin 與 SaDnaB 之結合模式。根據結合能高低順序由左至右，再由上至下，model 1-5 均結合於靠近 N-terminus 處。

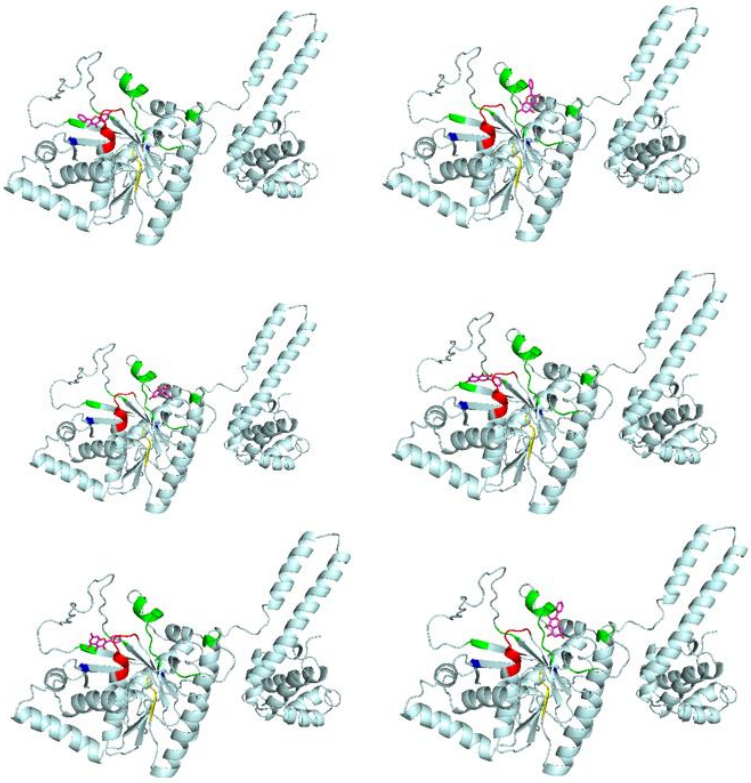

| model | score |
|---|---|
| 1 | 4180 |
| 2 | 4140 |
| 3 | 3962 |
| 4 | 3952 |
| 5 | 3880 |
| 6 | 3880 |

Galangin (PD)

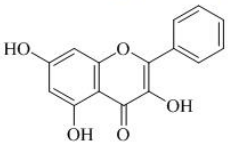


**圖五十八：**利用分子對接工具—PATCH DOCK 模擬 galangin 與 SaDnaB 之結合模式。根據結合能高低順序由左至右，再由上至下，model 1,4,5 結合於靠近 walker A 處，model 2,3,6 則結合於 DNA binding loop 處。

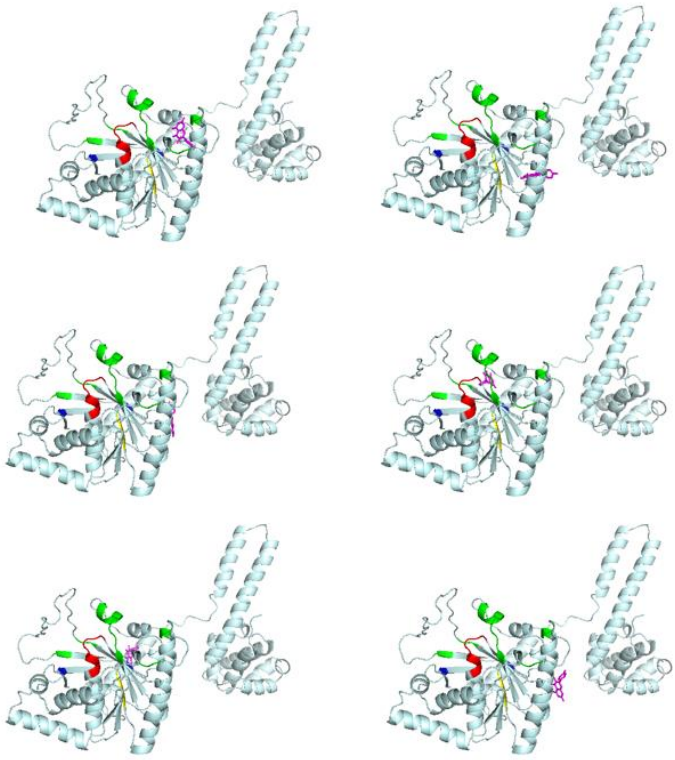

| model | energy |
|---|---|
| 1 | -193.38 |
| 2 | -190.77 |
| 3 | -190.75 |
| 4 | -189.82 |
| 5 | -188.65 |
| 6 | -188.56 |

Kaempherol (Hex-S)

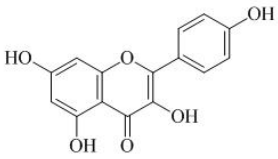


**圖五十九：**利用分子對接工具—HEX SERVER (shape model)模擬 kaempferol 與 SaDnaB 之結合模式。根據結合能高低順序由左至右，再由上至下，model 1,5 結合於 DNA binding loop 處，model 4 結合於 walker A 與 DNA binding loop 交接處。

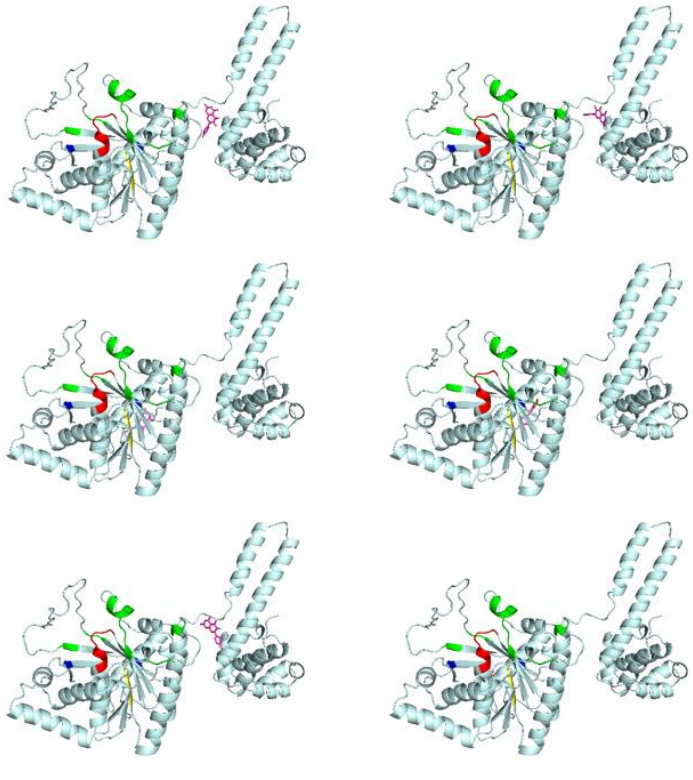

| model | energy |
|---|---|
| 1 | -1275.21 |
| 2 | -1261.99 |
| 3 | -1217.74 |
| 4 | -1215.98 |
| 5 | -1209.94 |
| 6 | -1202.07 |

Kaempherol (Hex-S+E)

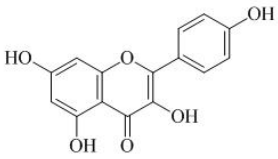


**圖六十：**利用分子對接工具—HEX SERVER (shape + electrostatic model)模擬與 SaDnaB 之結合模式。根據結合能高低順序由左至右，再由上至下，model 1,2,5 結合於靠近 N-terminus 處。

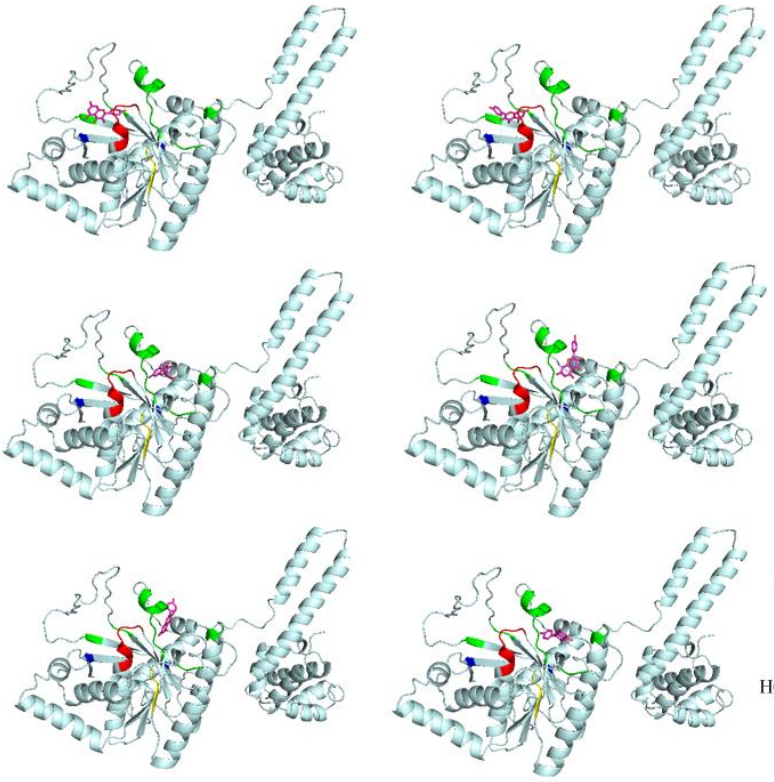

| model | score |
|---|---|
| 1 | 4142 |
| 2 | 3980 |
| 3 | 3956 |
| 4 | 3914 |
| 5 | 3814 |
| 6 | 3810 |

Kaempherol (PD)

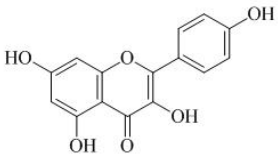


**圖六十一：**利用分子對接工具—PATCH DOCK 模擬 kaempferol 與 SaDnaB 之結合模式。根據結合能高低順序由左至右，再由上至下，model 1,2 結合於靠近 walker A 處，其餘 model 結合於 DNA binding loop 處。

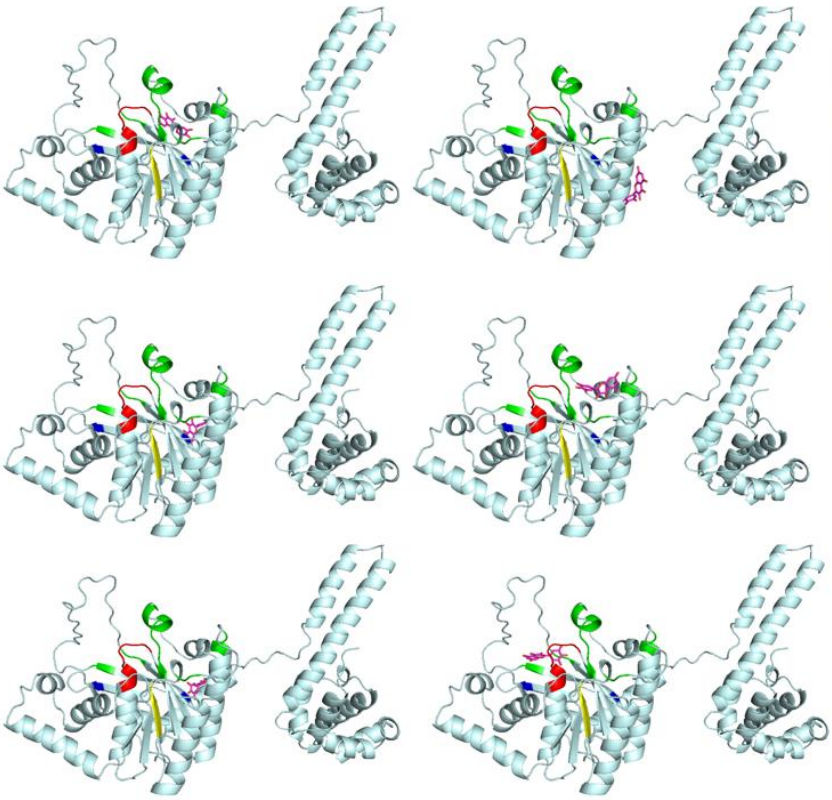

| model | energy |
|---|---|
| 1 | -203.45 |
| 2 | -199.61 |
| 3 | -197.61 |
| 4 | -195.63 |
| 5 | -195.20 |
| 6 | -193.40 |

Myricetin (HEX-S)

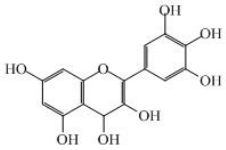


**圖六十二：**利用分子對接工具—HEX SERVER (shape model)模擬 myricetin 與 SaDnaB 之結合模式。根據結合能高低順序由左至右，再由上至下，model 1,4 結合於 DNA binding loop 處，model 6 結合於 walker A 處。

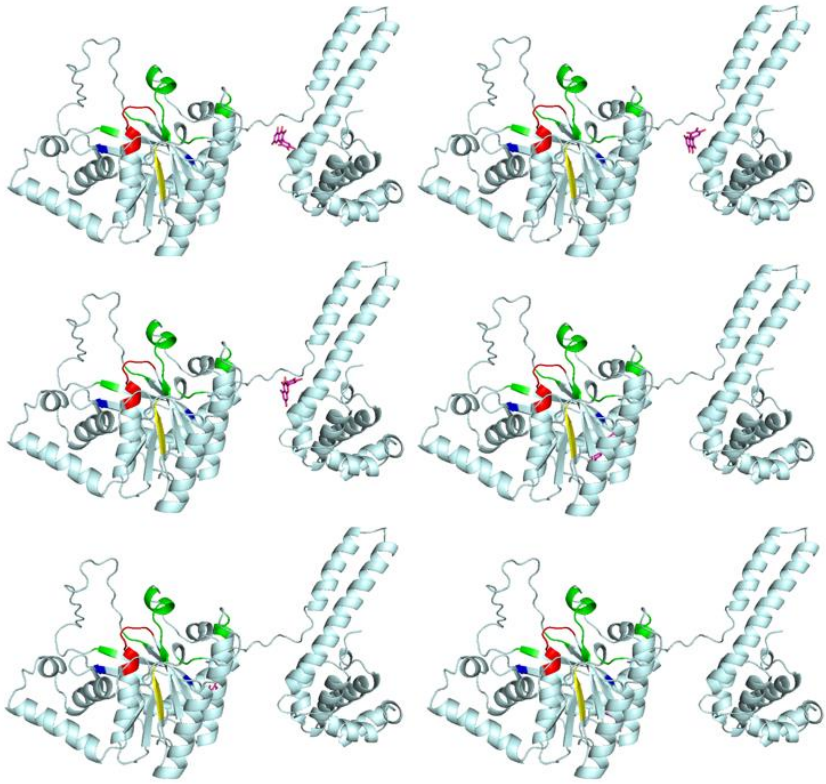

| model | energy |
|---|---|
| 1 | -1146.19 |
| 2 | -1131.86 |
| 3 | -1125.02 |
| 4 | -1112.49 |
| 5 | -1086.10 |
| 6 | -1071.69 |

Myricetin (HEX-S+E)

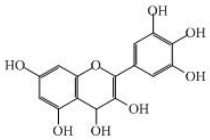


**圖六十三：**利用分子對接工具—HEX SERVER (Shape + electrostatic model)模擬 myricetin 與 SaDnaB 之結合模式。根據結合能高低順序由左至右，再由上至下，model 1,2,3 結合於靠近 N-terminus 處。

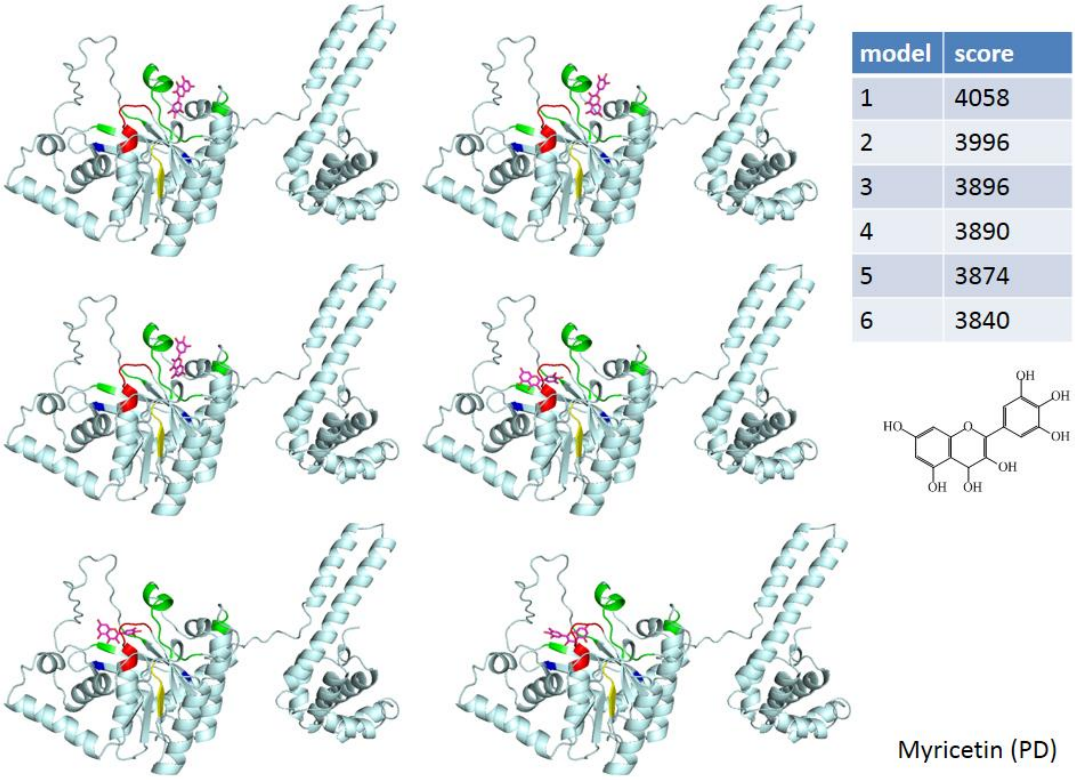

| model | score |
|---|---|
| 1 | 4058 |
| 2 | 3996 |
| 3 | 3896 |
| 4 | 3890 |
| 5 | 3874 |
| 6 | 3840 |




Myricetin (PD)

**圖六十四：**利用分子對接工具—PATCH DOCK 模擬 myricetin 與 SaDnaB 之結合模式。根據結合能高低順序由左至右，再由上至下，model 1,2,3 結合於 DNA binding model 處，model 4,5,6 則結合於 walker A 處。

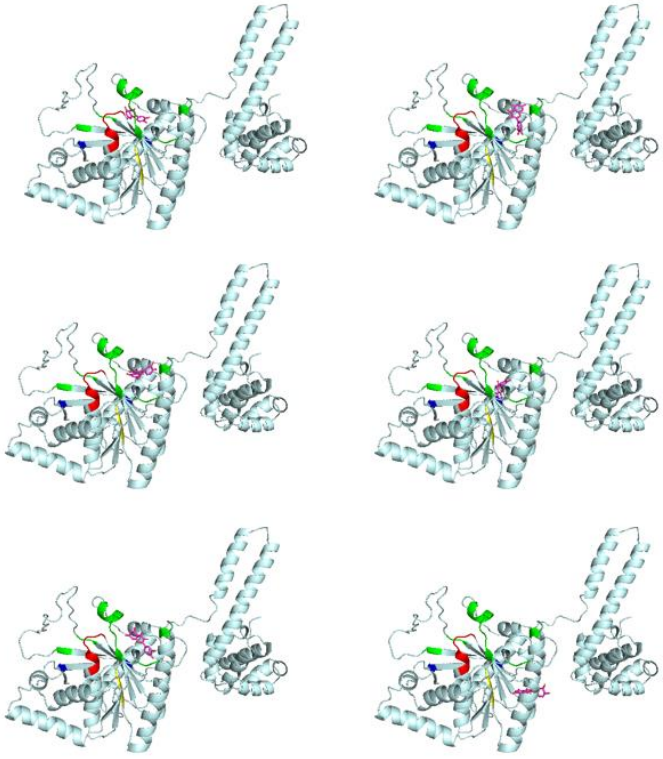

| model | energy |
|---|---|
| 1 | -202.15 |
| 2 | -200.00 |
| 3 | -198.96 |
| 4 | -198.30 |
| 5 | -194.84 |
| 6 | -192.98 |

Quercetin (Hex-S)

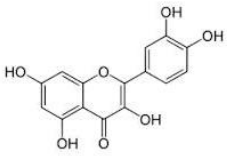


**圖六十五：**利用分子對接工具—HEX SERVER (shape model)模擬 quercetin 與 SaDnaB 之結合模式。根據結合能高低順序由左至右，再由上至下，model 1 結合於 walker A 與 DNA binding loop 之間，model 2,3,4,5 結合於 DNA binding loop 處。

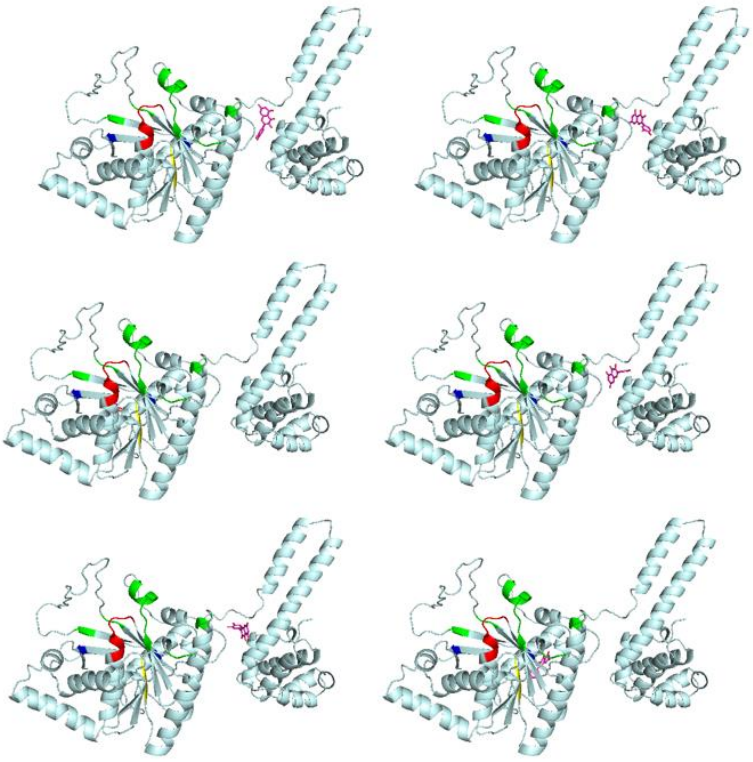

| model | energy |
|---|---|
| 1 | -1223.70 |
| 2 | -1220.14 |
| 3 | -1146.89 |
| 4 | -1145.75 |
| 5 | -1138.65 |
| 6 | -1135.99 |

Quercetin

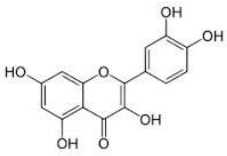


**圖六十六：**利用分子對接工具—HEX SERVER (shape + electrostatic model)模擬 quercetin 與 SaDnaB 之結合模式。根據結合能高低順序由左至右，再由上至下，model 1,2,4,5 結合於靠近 N-terminus 處。

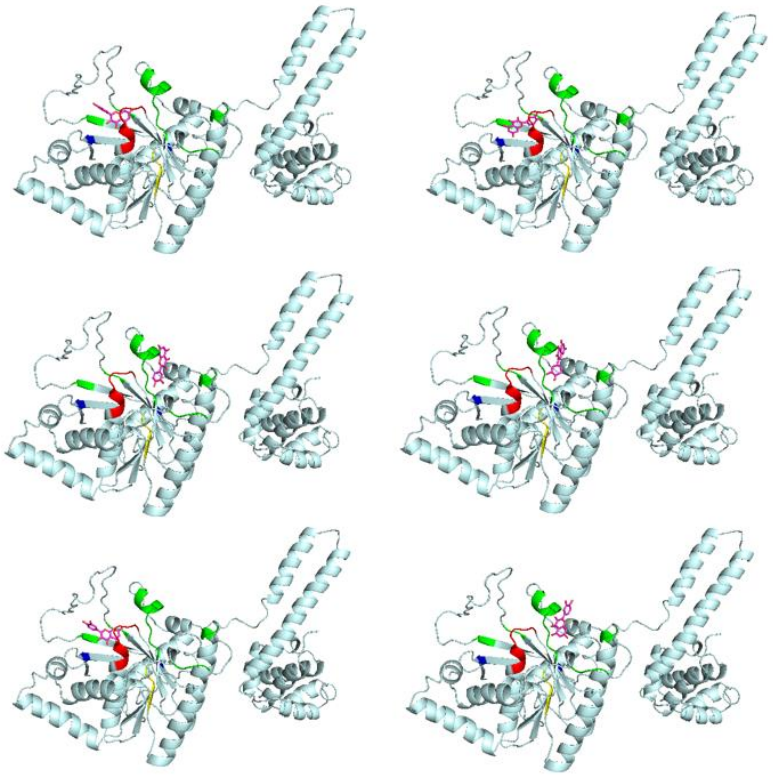

| model | score |
|---|---|
| 1 | 4026 |
| 2 | 3976 |
| 3 | 3956 |
| 4 | 3880 |
| 5 | 3856 |
| 6 | 3842 |

Quercetin (PD)

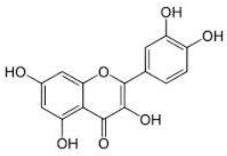


**圖六十七：**利用分子對接工具—模擬與 SaDnaB 之結合模式。根據結合能高低順序由左至右，再由上至下，model 1,2,5 結合於 walker A 處，model 3,4,6 結合於 DNA binding loop 處。

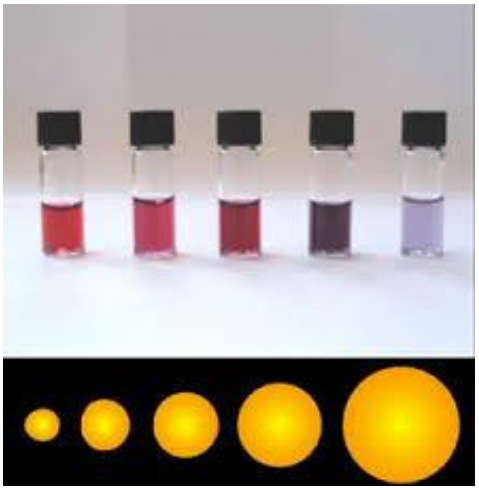

A

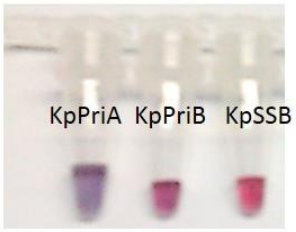



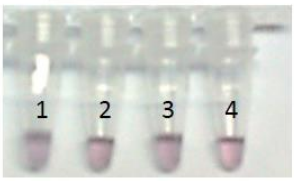


1. KpPriA+KpPriB
2. KpPriA+KpSSB
3. KpPriA+KpPriB+33 μM Myricetin
4. KpPriA+KpSSB+33 μM Myricetin

B

**圖六十八：**以奈米金粒子分析 KpPriA 與 KpPriB 及 KpSSB 之交互作用，(A)奈米金粒子隨著顆粒直徑的上昇而改變顏色，由桃紅色轉為淺紫色 (B)KpPriA 與金粒子混和後為深紫色，顯示其 PriA 與奈米金粒子結合後粒徑上昇，KpPriB 及 KpSSB 與奈米金粒子結合後則未明顯改變金粒子之粒徑；將 KpPriA 與 KpPriB 及 KpSSB 混和後，奈米金粒子顏色均轉為淺紫色，顯示 KpPriA 與 KpPriB 及 KpSSB 之交互作用；加入 myricetin 後發現顏色與控制組未有明顯差異，顯示 myricetin 對於 KpPriA 之抑制標的並非 KpPriA 與其他 primosomal protein 之結合。

# 第四章：參考文獻

# （References）


[1] H.F. Chambers, F.R. Deleo, Waves of resistance: Staphylococcus aureus in the antibiotic era, Nat Rev Microbiol 7 (2009) 629-641.

[2] M. Otto, Basis of virulence in community-associated methicillin-resistant Staphylococcus aureus, Annu Rev Microbiol 64 (2010) 143-162.

[3] S.D. Kobayashi, F.R. DeLeo, An update on community-associated MRSA virulence, Curr Opin Pharmacol 9 (2009) 545-551.

[4] M.A. Fischbach, C.T. Walsh, Antibiotics for emerging pathogens, Science 325 (2009) 1089-1093.

[5] H.J. Wu, A.H. Wang, M.P. Jennings, Discovery of virulence factors of pathogenic bacteria, Curr Opin Chem Biol 12 (2008) 93-101.

[6] N. Koyama, J. Inokoshi, H. Tomoda, Anti-infectious agents against MRSA, Molecules 18 (2012) 204-224.

[7] G.M. Rossolini, E. Mantengoli, F. Montagnani, S. Pollini, Epidemiology and clinical relevance of microbial resistance determinants versus anti-Gram-positive agents, Curr Opin Microbiol 13 (2010) 582-588.

[8] R. Podschun, U. Ullmann, Klebsiella spp. as nosocomial pathogens: epidemiology, taxonomy, typing methods, and pathogenicity factors, Clin Microbiol Rev 11 (1998) 589-603.

[9] K.K. Kumarasamy, M.A. Toleman, T.R. Walsh, J. Bagaria, F. Butt, R. Balakrishnan, U. Chaudhary, M. Doumith, C.G. Giske, S. Irfan, P. Krishnan, A.V. Kumar, S. Maharjan, S. Mushtaq, T. Noorie, D.L. Paterson, A. Pearson, C. Perry, R. Pike, B. Rao, U. Ray, J.B. Sarma, M. Sharma, E. Sheridan, M.A. Thirunarayan, J. Turton, S. Upadhyay, M. Warner, W. Welfare, D.M. Livermore, N. Woodford, Emergence of a new antibiotic resistance mechanism in India, Pakistan, and the UK: a molecular, biological, and epidemiological study, Lancet Infect Dis 10 (2010) 597-602.

[10] W.L. Yu, Y.C. Chuang, J. Walther-Rasmussen, Extended-spectrum beta-lactamases in Taiwan: epidemiology, detection, treatment and infection control, J Microbiol Immunol Infect 39 (2006) 264-277.

[11] A. Gupta, K. Ampofo, D. Rubenstein, L. Saiman, Extended spectrum beta lactamase-producing Klebsiella pneumoniae infections: a review of the literature, J Perinatol 23 (2003) 439-443.

[12] E. Arias-Palomo, V.L. O'Shea, I.V. Hood, J.M. Berger, The bacterial DnaC helicase loader is a DnaB ring breaker, Cell 153 (2013) 438-448.

[13] M. Schlierf, T. Ha, A helicase with an extra spring in its step, Cell 151 (2012) 244-246.

[14] O. Itsathitphaisarn, R.A. Wing, W.K. Eliason, J. Wang, T.A. Steitz, The hexameric helicase DnaB adopts a nonplanar conformation during translocation, Cell 151 (2012) 267-277.

[15] M.R. Singleton, M.S. Dillingham, D.B. Wigley, Structure and mechanism of helicases and nucleic acid translocases, Annu Rev Biochem 76 (2007) 23-50.

[16] H.H. Lin, C.Y. Huang, Characterization of Flavonol Inhibition of DnaB Helicase: Real-Time Monitoring, Structural Modeling, and Proposed Mechanism, J Biomed Biotechnol 2012 (2012) 735368.

[17] G. Wang, M.G. Klein, E. Tokonzaba, Y. Zhang, L.G. Holden, X.S. Chen, The structure of a DnaB-family replicative helicase and its interactions with primase, Nat Struct Mol Biol 15 (2008) 94-100.

[18] B. Bhattacharyya, N.P. George, T.M. Thurmes, R. Zhou, N. Jani, S.R. Wessel, S.J. Sandler, T. Ha, J.L. Keck, Structural mechanisms of PriA-mediated DNA replication

restart, Proc Natl Acad Sci U S A 111 (2014) 1373-1378.
[19] K. Sasaki, T. Ose, N. Okamoto, K. Maenaka, T. Tanaka, H. Masai, M. Saito, T. Shirai, D. Kohda, Structural basis of the 3'-end recognition of a leading strand in stalled replication forks by PriA, EMBO J 26 (2007) 2584-2593.
[20] H. Merrikh, C. Machon, W.H. Grainger, A.D. Grossman, P. Soultanas, Co-directional replication-transcription conflicts lead to replication restart, Nature 470 (2011) 554-557.
[21] S.S. Patel, M. Pandey, D. Nandakumar, Dynamic coupling between the motors of DNA replication: hexameric helicase, DNA polymerase, and primase, Curr Opin Chem Biol 15 (2011) 595-605.
[22] R.L. Maher, A.M. Branagan, S.W. Morrical, Coordination of DNA replication and recombination activities in the maintenance of genome stability, J Cell Biochem 112 (2011) 2672-2682.
[23] T.M. Lohman, E.J. Tomko, C.G. Wu, Non-hexameric DNA helicases and translocases: mechanisms and regulation, Nat Rev Mol Cell Biol 9 (2008) 391-401.
[24] K.J. Marians, PriA: at the crossroads of DNA replication and recombination, Prog Nucleic Acid Res Mol Biol 63 (1999) 39-67.
[25] R. Boonsombat, S.P. Yeh, A. Milne, S.J. Sandler, A novel dnaC mutation that suppresses priB rep mutant phenotypes in Escherichia coli K-12, Mol Microbiol 60 (2006) 973-983.
[26] S.J. Sandler, Requirements for replication restart proteins during constitutive stable DNA replication in Escherichia coli K-12, Genetics 169 (2005) 1799-1806.
[27] S.H. North, H. Nakai, Host factors that promote transpososome disassembly and the PriA-PriC pathway for restart primosome assembly, Mol Microbiol 56 (2005) 1601-1616.
[28] J.D. McCool, C.C. Ford, S.J. Sandler, A dnaT mutant with phenotypes similar to those of a priA2::kan mutant in Escherichia coli K-12, Genetics 167 (2004) 569-578.
[29] T. Hinds, S.J. Sandler, Allele specific synthetic lethality between priC and dnaAts alleles at the permissive temperature of 30 degrees C in E. coli K-12, BMC Microbiol 4 (2004) 47.
[30] S.J. Sandler, Multiple genetic pathways for restarting DNA replication forks in *Escherichia coli* K-12, Genetics 155 (2000) 487-497.
[31] S.J. Sandler, K.J. Marians, K.H. Zavitz, J. Coutu, M.A. Parent, A.J. Clark, dnaC mutations suppress defects in DNA replication- and recombination-associated functions in priB and priC double mutants in Escherichia coli K-12, Mol Microbiol 34 (1999) 91-101.
[32] H. Masai, T. Asai, Y. Kubota, K. Arai, T. Kogoma, Escherichia coli PriA protein is essential for inducible and constitutive stable DNA replication, EMBO J 13 (1994) 5338-5345.
[33] H. Masai, T. Tanaka, D. Kohda, Stalled replication forks: making ends meet for recognition and stabilization, Bioessays 32 (2010) 687-697.
[34] M.R. Szymanski, P.J. Bujalowski, M.J. Jezewska, A.M. Gmyrek, W. Bujalowski, The N-terminal domain of the Escherichia coli PriA helicase contains both the DNA- and nucleotide-binding sites. Energetics of domain--DNA interactions and allosteric effect of the nucleotide cofactors, Biochemistry 50 (2011) 9167-9183.
[35] K.J. Marians, Prokaryotic DNA replication, Annu. Rev. Biochem. 61 (1992) 673-719.
[36] A. Kornberg, DNA replication, J Biol Chem 263 (1988) 1-4.
[37] D. Bramhill, A. Kornberg, A model for initiation at origins of DNA replication, Cell 54 (1988) 915-918.
[38] K. Arai, A. Kornberg, Unique primed start of phage phi X174 DNA replication and mobility of the primosome in a direction opposite chain synthesis, Proc Natl Acad Sci U S A 78 (1981) 69-73.
[39] R. Schekman, A. Weiner, A. Kornberg, Multienzyme systems of DNA replication,

Science 186 (1974) 987-993.
[40] L. Xu, K.J. Marians, PriA mediates DNA replication pathway choice at recombination intermediates, Mol Cell 11 (2003) 817-826.
[41] J. Liu, L. Xu, S.J. Sandler, K.J. Marians, Replication fork assembly at recombination intermediates is required for bacterial growth, Proc Natl Acad Sci U S A 96 (1999) 3552-3555.
[42] C.B. Gabbai, K.J. Marians, Recruitment to stalled replication forks of the PriA DNA helicase and replisome-loading activities is essential for survival, DNA Repair (Amst) 9 (2010) 202-209.
[43] R.C. Heller, K.J. Marians, Replication fork reactivation downstream of a blocked nascent leading strand, Nature 439 (2006) 557-562.
[44] R.C. Heller, K.J. Marians, Replisome assembly and the direct restart of stalled replication forks, Nat Rev Mol Cell Biol 7 (2006) 932-943.
[45] R.C. Heller, K.J. Marians, The disposition of nascent strands at stalled replication forks dictates the pathway of replisome loading during restart, Mol Cell 17 (2005) 733-743.
[46] S.J. Sandler, K.J. Marians, Role of PriA in replication fork reactivation in Escherichia coli, J Bacteriol 182 (2000) 9-13.
[47] K.J. Marians, PriA-directed replication fork restart in *Escherichia coli*, Trends Biochem. Sci. 25 (2000) 185-189.
[48] M.M. Cox, M.F. Goodman, K.N. Kreuzer, D.J. Sherratt, S.J. Sandler, K.J. Marians, The importance of repairing stalled replication forks, Nature 404 (2000) 37-41.
[49] C. Bruand, S.D. Ehrlich, L. Janniere, Primosome assembly site in Bacillus subtilis, Embo J 14 (1995) 2642-2650.
[50] M. Velten, S. McGovern, S. Marsin, S.D. Ehrlich, P. Noirot, P. Polard, A two-protein strategy for the functional loading of a cellular replicative DNA helicase, Mol Cell 11 (2003) 1009-1020.
[51] W.K. Smits, H. Merrikh, C.Y. Bonilla, A.D. Grossman, Primosomal proteins DnaD and DnaB are recruited to chromosomal regions bound by DnaA in Bacillus subtilis, J Bacteriol 193 (2011) 640-648.
[52] W.K. Smits, A.I. Goranov, A.D. Grossman, Ordered association of helicase loader proteins with the Bacillus subtilis origin of replication in vivo, Mol Microbiol 75 (2010) 452-461.
[53] W.H. Grainger, C. Machon, D.J. Scott, P. Soultanas, DnaB proteolysis in vivo regulates oligomerization and its localization at oriC in Bacillus subtilis, Nucleic Acids Res 38 (2010) 2851-2864.
[54] C. Ioannou, P.M. Schaeffer, N.E. Dixon, P. Soultanas, Helicase binding to DnaI exposes a cryptic DNA-binding site during helicase loading in Bacillus subtilis, Nucleic Acids Res 34 (2006) 5247-5258.
[55] W. Zhang, M.J. Carneiro, I.J. Turner, S. Allen, C.J. Roberts, P. Soultanas, The Bacillus subtilis DnaD and DnaB proteins exhibit different DNA remodelling activities, J Mol Biol 351 (2005) 66-75.
[56] P. Soultanas, A functional interaction between the putative primosomal protein DnaI and the main replicative DNA helicase DnaB in Bacillus, Nucleic Acids Res 30 (2002) 966-974.
[57] S. Marsin, S. McGovern, S.D. Ehrlich, C. Bruand, P. Polard, Early steps of Bacillus subtilis primosome assembly, J Biol Chem 276 (2001) 45818-45825.
[58] C. Bruand, M. Farache, S. McGovern, S.D. Ehrlich, P. Polard, DnaB, DnaD and DnaI proteins are components of the Bacillus subtilis replication restart primosome, Mol Microbiol 42 (2001) 245-255.
[59] S. Chirumbolo, Plant polyphenolic compounds as potential antimicrobial drugs, J Med Microbiol 60 (2011) 1562-1563.
[60] M.K. Chahar, N. Sharma, M.P. Dobhal, Y.C. Joshi, Flavonoids: A versatile source of

anticancer drugs, Pharmacogn Rev 5 (2011) 1-12.
[61] L. Zhang, Y. Kong, D. Wu, H. Zhang, J. Wu, J. Chen, J. Ding, L. Hu, H. Jiang, X. Shen, Three flavonoids targeting the beta-hydroxyacyl-acyl carrier protein dehydratase from Helicobacter pylori: crystal structure characterization with enzymatic inhibition assay, Protein Sci 17 (2008) 1971-1978.
[62] F. Teillet, A. Boumendjel, J. Boutonnat, X. Ronot, Flavonoids as RTK inhibitors and potential anticancer agents, Med Res Rev 28 (2008) 715-745.
[63] J.A. Ross, C.M. Kasum, Dietary flavonoids: bioavailability, metabolic effects, and safety, Annu Rev Nutr 22 (2002) 19-34.
[64] S. Burda, W. Oleszek, Antioxidant and antiradical activities of flavonoids, J Agric Food Chem 49 (2001) 2774-2779.
[65] S.H. Hakkinen, S.O. Karenlampi, I.M. Heinonen, H.M. Mykkanen, A.R. Torronen, Content of the flavonols quercetin, myricetin, and kaempferol in 25 edible berries, J Agric Food Chem 47 (1999) 2274-2279.
[66] B.M. Fahlman, E.S. Krol, Inhibition of UVA and UVB radiation-induced lipid oxidation by quercetin, J Agric Food Chem 57 (2009) 5301-5305.
[67] O. Kwon, P. Eck, S. Chen, C.P. Corpe, J.H. Lee, M. Kruhlak, M. Levine, Inhibition of the intestinal glucose transporter GLUT2 by flavonoids, Faseb J 21 (2007) 366-377.
[68] S. Holder, M. Zemskova, C. Zhang, M. Tabrizizad, R. Bremer, J.W. Neidigh, M.B. Lilly, Characterization of a potent and selective small-molecule inhibitor of the PIM1 kinase, Mol Cancer Ther 6 (2007) 163-172.
[69] J. Lu, L.V. Papp, J. Fang, S. Rodriguez-Nieto, B. Zhivotovsky, A. Holmgren, Inhibition of Mammalian thioredoxin reductase by some flavonoids: implications for myricetin and quercetin anticancer activity, Cancer Res 66 (2006) 4410-4418.
[70] S.C. Chu, Y.S. Hsieh, J.Y. Lin, Inhibitory effects of flavonoids on Moloney murine leukemia virus reverse transcriptase activity, J Nat Prod 55 (1992) 179-183.
[71] S. Li, T. Hattori, E.N. Kodama, Epigallocatechin gallate inhibits the HIV reverse transcription step, Antivir Chem Chemother 21 (2011) 239-243.
[72] G.L. Plosker, Rivaroxaban: A Review of Its Use in Acute Coronary Syndromes, Drugs (2014).
[73] G. Gouya, J. Arrich, M. Wolzt, K. Huber, F.W. Verheugt, P.A. Gurbel, A. Pirker-Kees, J.M. Siller-Matula, Antiplatelet treatment for prevention of cerebrovascular events in patients with vascular diseases: a systematic review and meta-analysis, Stroke 45 (2014) 492-503.
[74] J.A. Gerlt, K.N. Allen, S.C. Almo, R.N. Armstrong, P.C. Babbitt, J.E. Cronan, D. Dunaway-Mariano, H.J. Imker, M.P. Jacobson, W. Minor, C.D. Poulter, F.M. Raushel, A. Sali, B.K. Shoichet, J.V. Sweedler, The enzyme function initiative, Biochemistry 50 (2011) 9950-9962.
[75] C.M. Seibert, F.M. Raushel, Structural and catalytic diversity within the amidohydrolase superfamily, Biochemistry 44 (2005) 6383-6391.
[76] J.A. Gerlt, P.C. Babbitt, Divergent evolution of enzymatic function: mechanistically diverse superfamilies and functionally distinct suprafamilies, Annu Rev Biochem 70 (2001) 209-246.
[77] L. Holm, C. Sander, An evolutionary treasure: unification of a broad set of amidohydrolases related to urease, Proteins 28 (1997) 72-82.
[78] Y.Y. Ho, Y.H. Huang, C.Y. Huang, Chemical rescue of the post-translationally carboxylated lysine mutant of allantoinase and dihydroorotase by metal ions and short-chain carboxylic acids, Amino Acids 44 (2013) 1181-1191.
[79] Y.Y. Ho, H.C. Hsieh, C.Y. Huang, Biochemical characterization of allantoinase from *Escherichia coli* BL21, Protein J 30 (2011) 384-394.
[80] K. Kim, M.I. Kim, J. Chung, J.H. Ahn, S. Rhee, Crystal structure of metal-dependent allantoinase from Escherichia coli, J Mol Biol 387 (2009) 1067-1074.
[81] I. Ramazzina, L. Cendron, C. Folli, R. Berni, D. Monteverdi, G. Zanotti, R. Percudani,

Logical identification of an allantoinase analog (puuE) recruited from polysaccharide deacetylases, J Biol Chem 283 (2008) 23295-23304.
[82] G.J. Kim, D.E. Lee, H.S. Kim, Functional expression and characterization of the two cyclic amidohydrolase enzymes, allantoinase and a novel phenylhydantoinase, from Escherichia coli, J Bacteriol 182 (2000) 7021-7028.
[83] C.C. Wang, H.W. Tsau, W.T. Chen, C.Y. Huang, Identification and characterization of a putative dihydroorotase, KPN01074, from *Klebsiella pneumoniae*, Protein J 29 (2010) 445-452.
[84] P.D. Martin, C. Purcarea, P. Zhang, A. Vaishnav, S. Sadecki, H.I. Guy-Evans, D.R. Evans, B.F. Edwards, The crystal structure of a novel, latent dihydroorotase from Aquifex aeolicus at 1.7A resolution, J Mol Biol 348 (2005) 535-547.
[85] Z. Gojkovic, L. Rislund, B. Andersen, M.P. Sandrini, P.F. Cook, K.D. Schnackerz, J. Piskur, Dihydropyrimidine amidohydrolases and dihydroorotases share the same origin and several enzymatic properties, Nucleic Acids Res 31 (2003) 1683-1692.
[86] J.B. Thoden, G.N. Phillips, Jr., T.M. Neal, F.M. Raushel, H.M. Holden, Molecular structure of dihydroorotase: a paradigm for catalysis through the use of a binuclear metal center, Biochemistry 40 (2001) 6989-6997.
[87] D.T. Huang, M.A. Thomas, R.I. Christopherson, Divalent metal derivatives of the hamster dihydroorotase domain, Biochemistry 38 (1999) 9964-9970.
[88] U. Engel, C. Syldatk, J. Rudat, Stereoselective hydrolysis of aryl-substituted dihydropyrimidines by hydantoinases, Appl Microbiol Biotechnol 94 (2012) 1221-1231.
[89] V. Kumar, N. Saxena, M. Sarma, K.V. Radha Kishan, Carboxylated lysine is required for higher activities in Hydantoinases, Protein Pept Lett 18 (2011) 663-669.
[90] S. Martinez-Rodriguez, A.I. Martinez-Gomez, F. Rodriguez-Vico, J.M. Clemente-Jimenez, F.J. Las Heras-Vazquez, Carbamoylases: characteristics and applications in biotechnological processes, Appl Microbiol Biotechnol 85 (2010) 441-458.
[91] C.Y. Huang, Y.P. Chao, Y.S. Yang, Purification of industrial hydantoinase in one chromatographic step without affinity tag, Protein Expr Purif 30 (2003) 134-139.
[92] Y.H. Cheon, H.S. Kim, K.H. Han, J. Abendroth, K. Niefind, D. Schomburg, J. Wang, Y. Kim, Crystal structure of D-hydantoinase from Bacillus stearothermophilus: insight into the stereochemistry of enantioselectivity, Biochemistry 41 (2002) 9410-9417.
[93] J. Altenbuchner, M. Siemann-Herzberg, C. Syldatk, Hydantoinases and related enzymes as biocatalysts for the synthesis of unnatural chiral amino acids, Curr Opin Biotechnol 12 (2001) 559-563.
[94] G.J. Kim, H.S. Kim, Identification of the structural similarity in the functionally related amidohydrolases acting on the cyclic amide ring, Biochem J 330 ( Pt 1) (1998) 295-302.
[95] Y.S. Yang, S. Ramaswamy, W.B. Jakoby, Rat liver imidase, J Biol Chem 268 (1993) 10870-10875.
[96] Y.C. Hsieh, M.C. Chen, C.C. Hsu, S.I. Chan, Y.S. Yang, C.J. Chen, Crystal Structures of Vertebrate Dihydropyrimidinase and Complexes from Tetraodon Nigroviridis with Lysine Carbamylation: Metal and Structural Requirements for Post-Translational Modification and Function, J Biol Chem (2013).
[97] S. Martinez-Rodriguez, A.I. Martinez-Gomez, J.M. Clemente-Jimenez, F. Rodriguez-Vico, J.M. Garcia-Ruiz, F.J. Las Heras-Vazquez, J.A. Gavira, Structure of dihydropyrimidinase from Sinorhizobium meliloti CECT4114: new features in an amidohydrolase family member, J Struct Biol 169 (2010) 200-208.
[98] B. Lohkamp, B. Andersen, J. Piskur, D. Dobritzsch, The crystal structures of dihydropyrimidinases reaffirm the close relationship between cyclic amidohydrolases and explain their substrate specificity, J Biol Chem 281 (2006) 13762-13776.

[99] C.Y. Huang, S.K. Chiang, Y.S. Yang, Y.J. Sun, Crystallization and preliminary X-ray diffraction analysis of thermophilic imidase from pig liver, Acta Crystallogr D Biol Crystallogr 59 (2003) 943-945.
[100] J. Abendroth, K. Niefind, D. Schomburg, X-ray structure of a dihydropyrimidinase from Thermus sp. at 1.3 A resolution, J Mol Biol 320 (2002) 143-156.
[101] J. Ogawa, C.L. Soong, M. Honda, S. Shimizu, Imidase, a dihydropyrimidinase-like enzyme involved in the metabolism of cyclic imides, Eur J Biochem 243 (1997) 322-327.
[102] Y.W. Shi, X.Q. Liu, P. Shi, X.Y. Zhang, Characterization of zinc-binding properties of a novel imidase from Pseudomonas putida YZ-26, Arch Biochem Biophys 494 (2009) 1-6.
[103] C.Y. Huang, Y.S. Yang, Discovery of a novel N-iminylamidase activity: substrate specificity, chemicoselectivity and catalytic mechanism, Protein Expr Purif 40 (2005) 203-211.
[104] C.Y. Huang, Y.S. Yang, A novel cold-adapted imidase from fish Oreochromis niloticus that catalyzes hydrolysis of maleimide, Biochem Biophys Res Commun 312 (2003) 467-472.
[105] C.Y. Huang, Y.S. Yang, The role of metal on imide hydrolysis: metal content and pH profiles of metal ion-replaced mammalian imidase, Biochem Biophys Res Commun 297 (2002) 1027-1032.
[106] M.J. Raso, M. Pineda, P. Piedras, Tissue abundance and characterization of two purified proteins with allantoinase activity from French bean (Phaseolus vulgaris), Physiol Plant 131 (2007) 355-366.
[107] P.J. Gaines, L. Tang, N. Wisnewski, Insect allantoinase: cDNA cloning, purification, and characterization of the native protein from the cat flea, Ctenocephalides felis, Insect Biochem Mol Biol 34 (2004) 203-214.
[108] S. Hayashi, S. Fujiwara, T. Noguchi, Evolution of urate-degrading enzymes in animal peroxisomes, Cell Biochem Biophys 32 Spring (2000) 123-129.
[109] S. Hayashi, S. Fujiwara, T. Noguchi, Degradation of uric acid in fish liver peroxisomes. Intraperoxisomal localization of hepatic allantoicase and purification of its peroxisomal membrane-bound form, J Biol Chem 264 (1989) 3211-3215.
[110] T. Noguchi, S. Fujiwara, S. Hayashi, Evolution of allantoinase and allantoicase involved in urate degradation in liver peroxisomes. A rapid purification of amphibian allantoinase and allantoicase complex, its subunit locations of the two enzymes, and its comparison with fish allantoinase and allantoicase, J Biol Chem 261 (1986) 4221-4223.
[111] Y. Takada, T. Noguchi, The degradation of urate in liver peroxisomes. Association of allantoinase with allantoicase in amphibian liver but not in fish and invertebrate liver, J Biol Chem 258 (1983) 4762-4764.
[112] D.B. Janssen, R.A. Smits, C. van der Drift, Allantoinase from Pseudomonas aeruginosa. Purification, properties and immunochemical characterization of its in vivo inactivation, Biochim Biophys Acta 718 (1982) 212-219.
[113] T. Nara, M. Hashimoto, H. Hirawake, C.W. Liao, Y. Fukai, S. Suzuki, A. Tsubouchi, J. Morales, S. Takamiya, T. Fujimura, H. Taka, R. Mineki, C.K. Fan, D.K. Inaoka, M. Inoue, A. Tanaka, S. Harada, K. Kita, T. Aoki, Molecular interaction of the first 3 enzymes of the de novo pyrimidine biosynthetic pathway of Trypanosoma cruzi, Biochem Biophys Res Commun 418 (2012) 140-143.
[114] D.C. Brown, K.D. Collins, Dihydroorotase from Escherichia coli. Substitution of Co(II) for the active site Zn(II), J Biol Chem 266 (1991) 1597-1604.
[115] M.I. Mally, D.R. Grayson, D.R. Evans, Catalytic synergy in the multifunctional protein that initiates pyrimidine biosynthesis in Syrian hamster cells, J Biol Chem 255 (1980) 11372-11380.
[116] R.I. Christopherson, M.E. Jones, The overall synthesis of L-5,6-dihydroorotate by

multienzymatic protein pyr1-3 from hamster cells. Kinetic studies, substrate channeling, and the effects of inhibitors, J Biol Chem 255 (1980) 11381-11395.
[117] D.R. Evans, H.I. Guy, Mammalian pyrimidine biosynthesis: fresh insights into an ancient pathway, J Biol Chem 279 (2004) 33035-33038.
[118] A. Ahuja, C. Purcarea, R. Ebert, S. Sadecki, H.I. Guy, D.R. Evans, Aquifex aeolicus dihydroorotase: association with aspartate transcarbamoylase switches on catalytic activity, J Biol Chem 279 (2004) 53136-53144.
[119] C.C. Chen, C.Y. Huang, Inhibition of *Klebsiella pneumoniae* DnaB helicase by the flavonol galangin, Protein J 30 (2011) 59-65.

Biochimie xxx (2014) 1–10

Contents lists available at ScienceDirect

Biochimie

journal homepage: www.elsevier.com/locate/biochi

Research paper

# Allantoinase and dihydroorotase binding and inhibition by flavonols and the substrates of cyclic amidohydrolases

Wei-Feng Peng [a,b], Cheng-Yang Huang [a,c,*]

[a] School of Biomedical Sciences, Chung Shan Medical University, No. 110, Sec. 1, Chien-Kuo N. Rd., Taichung City, Taiwan
[b] School of Medicine, College of Medicine, Chung Shan Medical University, No. 110, Sec. 1, Chien-Kuo N. Rd., Taichung City, Taiwan
[c] Department of Medical Research, Chung Shan Medical University Hospital, No. 110, Sec. 1, Chien-Kuo N. Rd., Taichung City, Taiwan

ARTICLE INFO

*Article history:*
Received 14 October 2013
Accepted 2 January 2014
Available online xxx

*Keywords:*
Allantoinase
Dihydroorotase
Hydantoinase
Imidase
Amidohydrolase

ABSTRACT

Allantoinase and dihydroorotase are members of the cyclic amidohydrolases family. Allantoinase and dihydroorotase possess very similar binuclear metal centers in the active site and may use a similar mechanism for catalysis. However, whether the substrate specificities of allantoinase and dihydroorotase overlap and whether the substrates of other cyclic amidohydrolases inhibit allantoinase and dihydroorotase remain unknown. In this study, the binding and inhibition of allantoinase (*Salmonella enterica* serovar Typhimurium LT2) and dihydroorotase (*Klebsiella pneumoniae*) by flavonols and the substrates of other cyclic amidohydrolases were investigated. Hydantoin and phthalimide, substrates of hydantoinase and imidase, were not hydrolyzed by allantoinase and dihydroorotase. Hydantoin and dihydroorotate competitively inhibited allantoinase, whereas hydantoin and allantoin bind to dihydroorotase, but do not affect its activity. We further investigated the effects of the flavonols myricetin, quercetin, kaempferol, and galangin, on the inhibition of allantoinase and dihydroorotase. Allantoinase and dihydroorotase were both significantly inhibited by kaempferol, with $IC_{50}$ values of 35 ± 3 μM and 31 ± 2 μM, respectively. Myricetin strongly inhibited dihydroorotase, with an $IC_{50}$ of 40 ± 1 μM. The double reciprocal of the Lineweaver–Burk plot indicated that kaempferol was a competitive inhibitor for allantoinase but an uncompetitive inhibitor for dihydroorotase. A structural study using PatchDock showed that kaempferol was docked in the active site pocket of allantoinase but outside the active site pocket of dihydroorotase. These results constituted a first study that naturally occurring product flavonols inhibit the cyclic amidohydrolases, allantoinase, and dihydroorotase, even more than the substrate analogs (>3 orders of magnitude). Thus, flavonols may serve as drug leads for designing compounds that target several cyclic amidohydrolases.



## 1. Introduction

The amidohydrolase superfamily comprises a remarkable set of enzymes that catalyze the hydrolysis of a wide range of substrates with amide or ester functional groups at their carbon and phosphorus centers [1–3]. Based on their functional and structural similarities to related enzymes, hydantoinase, allantoinase, dihydropyrimidinase, and dihydroorotase belong to the cyclic amidohydrolase family [4,5]. Hydantoinase is also known as dihydro pyrimidinase because of an overlap in substrate specificity [6]. Enzymes in this family [7–11], including imidase, are imide-hydrolyzing enzymes. Even though they are functionally similar, these enzymes have a relatively low amino acid sequence identity. These metal-dependent enzymes catalyze the ring-opening hydrolysis of the cyclic amide bond of each substrate in either five- or six-member rings in the metabolism of purines, pyrimidines, and many xenobiotics (Fig. 1A).

Allantoinase occurs in a wide variety of organisms, including bacteria, fungi, and plants, and a few animals. Allantoinase catalyzes the reversible hydrolysis of allantoin to allantoic acid, which is a key reaction in the biosynthesis and degradation of ureide required for the utilization of nitrogen in purine-derived compounds [12]. Allantoinase is a homotetrameric dinuclear metalloenzyme [13,14], but some allantoinases initially annotated as polysaccharide deacetylases [15] are metal independent. Thus, even without the allantoinase gene, some bacteria use allantoin to utilize nitrogen.

* Corresponding author. School of Biomedical Sciences, Chung Shan Medical University, No. 110, Sec. 1, Chien-Kuo N. Rd., Taichung City, Taiwan. Tel.: +886 4 24730022x11472; fax: +886 4 23248187.
*E-mail address:* cyhuang@csmu.edu.tw (C.-Y. Huang).

0300-9084/$ – see front matter © 2014 Elsevier Masson SAS. All rights reserved.
http://dx.doi.org/10.1016/j.biochi.2014.01.001

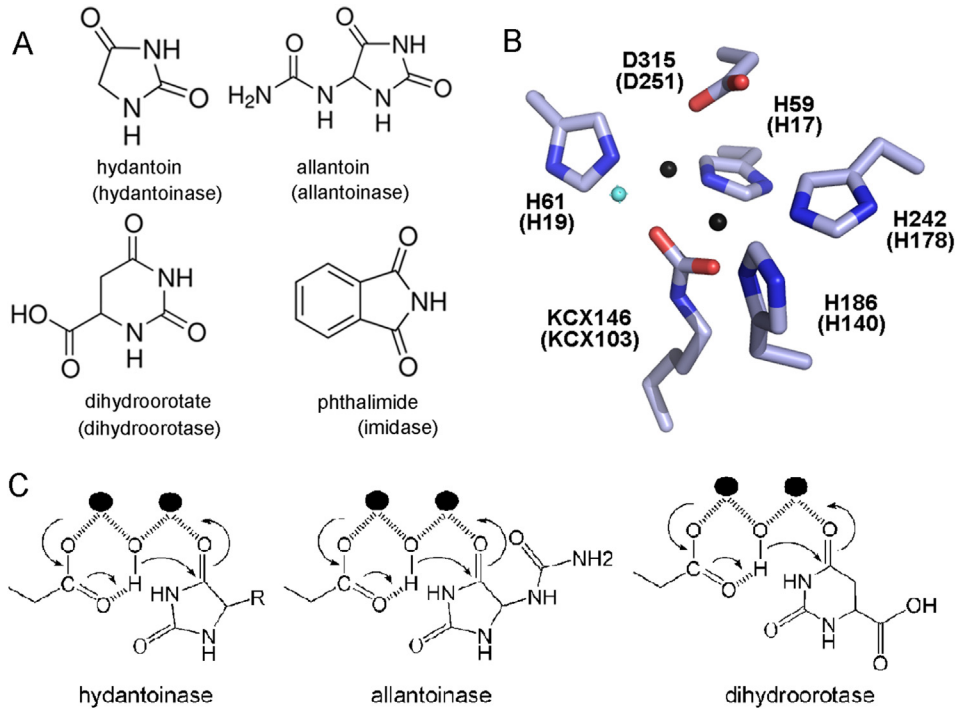


**Fig. 1.** Properties of the cyclic amidohydrolase family. (A) Substrate of hydantoinase/dihydropyrimidinase, allantoinase, dihydroorotase, and imidase. (B) The binuclear metal center within the active site of allantoinase and dihydroorotase (in parentheses). Allantoinase and dihydroorotase contains four histidine, one aspartate, and one post-carboxylated lysine residue, which are required for metal binding and catalytic activity, as revealed by their crystal structures. The coordinate was obtained from the Protein Data Bank (entry 3E74). KCX, a post-carboxylated lysine. The metal ions (in black) and a metal-bound water molecule (in light blue) are also shown. (C) The chemical mechanisms of hydantoinase, allantoinase and dihydroorotase. The hydrolysis of the substrates likely undergoes three steps: the hydrolytic water molecule must be activated for nucleophilic attack, and then the amide bond of the substrate must be made more electrophilic by polarization of the carbonyl-oxygen bond, and the leaving-group nitrogen must be protonated as the carbon–nitrogen bond is cleaved. The metal ions are shown as black circles.

Dihydroorotase catalyzes the reversible cyclization of carbamoyl aspartate into dihydroorotate in the third step of the de novo pyrimidine nucleotide biosynthetic pathway [16]. In mammals, this enzyme is part of the large multifunctional protein carbamoyl phosphate synthetase/aspartate transcarbamoylase/dihydroorotase (CAD) [16–19]. However, in prokaryotic organisms, CADs are usually expressed separately and function independently [20] or form multifunctional complexes [17,21,22]. Similar to allantoinase, dihydroorotase is a metalloenzyme [21,23]. The active site of allantoinase [14] and dihydroorotase [23] contains four histidine, one aspartate, and one post-carboxylated lysine residue or a second aspartate residue, which are required for metal binding and catalytic activity, as revealed by their crystal structures (Fig. 1B) [13,24]. The presence of a post-carboxylated lysine in hydantoinase is also involved in binuclear metal center self-assembly [25] and increases the nucleophilicity of the hydroxide for catalysis [26]. Nevertheless, the substrate specificities of allantoinase, hydantoinase, and dihydroorotase may differ. However, whether the substrate of each enzyme competitively inhibits other enzymes in this family remains unclear.

Infections that are resistant to all antibacterial options have recently developed. Few therapies are effective against the six antibiotic-resistant ESKAPE pathogens (*Enterococcus faecium*, *Staphylococcus aureus*, *Klebsiella pneumoniae*, *Acinetobacter baumannii*, *Pseudomonas aeruginosa*, and *Enterobacter species*) [27]. Considering allantoinase and dihydroorotase are required for metabolizing purines and pyrimidines, blocking their activities would be detrimental to bacterial survival. In addition, allantoinase is not found in humans, and mammalian and prokaryotic dihydroorotases exhibit distinct differences. Thus, these enzymes may be promising therapeutic targets for developing antibiotics. Although some chelators inhibit allantoinase and dihydroorotase, they may be harmful to human health.

Flavonoids are the most common group of plant polyphenols and are responsible for much of the flavor and color of fruits and vegetables [28]. Over 5000 different flavonoids have been described, many which display structure-dependent biological and pharmacologic activities [29]. The six major subclasses of flavonoids are flavonols, flavones, flavanones, flavanols, anthocyanidins, and isoflavones [28]. Flavonols, which are composed of two aromatic rings linked by a heterocyclic pyran-4-one ring, are known to have antioxidant [30], antiradical [31], antiviral [32,33], and antibacterial activities [34,35]. In this study, we investigated the effects of the substrates of cyclic amidohydrolase and the flavonols myricetin, quercetin, kaempferol, and galangin on inhibiting the catalytic activity of allantoinase and dihydroorotase.

## 2. Materials and methods

### 2.1. Materials

All restriction enzymes and DNA-modifying enzymes were purchased from New England Biolabs (Ipswich, MA, USA), unless otherwise stated. All custom oligonucleotide primers were obtained from Invitrogen Corporation (Carlsbad, CA, USA). All chemicals were purchased from Sigma–Aldrich (St. Louis, MO, USA) unless otherwise stated.

### 2.2. Protein expression and purification

The construction of pET21e-*Kp*DHO expression vector for *Klebsiella pneumoniae* dihydroorotase expression has been previously

Please cite this article in press as: W.-F. Peng, C.-Y. Huang, Allantoinase and dihydroorotase binding and inhibition by flavonols and the substrates of cyclic amidohydrolases, Biochimie (2014), http://dx.doi.org/10.1016/j.biochi.2014.01.001

described [36]. The construction of pET21b-*St*ALL expression vector for *Salmonella enterica* serovar Typhimurium LT2 allantoinase expression has been previously described [13]. Recombinant proteins were expressed and purified using a previously described protocol [13,25,37–40]. In a typical procedure, *Escherichia coli* BL21(DE3) cells were individually transformed with the plasmid by the heat shock method, and then grown to 0.9 $OD_{600}$ at 37 °C in Luria–Bertani medium containing 250 μg/mL ampicillin and 1 mM $MnCl_2$ with rapid shaking. Overexpression of the construct was induced by incubating with 1 mM isopropyl thiogalactoside (IPTG) for 3 h at 37 °C. The cells overexpressing the protein were chilled on ice, harvested by centrifugation, resuspended in buffer A (20 mM Tris–HCl, 5 mM imidazole, and 0.5 M NaCl, pH 7.9) and disrupted by sonication with ice cooling. The protein purified from the soluble supernatant by $Ni^{2+}$-affinity chromatography (HiTrap HP; GE Healthcare Bio-Sciences, Piscataway, NJ, USA) was eluted with buffer B (20 mM Tris–HCl, 250 mM imidazole, and 0.5 M NaCl, pH 7.9) and dialyzed against a dialysis buffer (50 mM HEPES and 50 mM NaCl, pH 7.0). Protein purity remained greater than 95% as determined by Coomassie-stained SDS-PAGE (Mini-PROTEAN Tetra System; Bio-Rad, CA, USA).

### 2.3. Protein concentration

The protein concentrations of enzyme solution were determined by the bicinchoninic acid protein assay using bovine serum albumin as a standard [41].

### 2.4. Enzyme assay

A rapid spectrophotometric assay was used to determine the enzymatic activity according to a previously described protocol for allantoinase [42], dihydroorotase [36], imidase [8,9], and hydantoinase [25]. In a typical procedure, the hydrolysis of allantoin and dihydroorotate was measured at 25 °C as the decrease in absorbance at 258 and 230 nm, respectively. To start the reaction, the protein solution (1–30 μg) was added to a 2 mL solution containing the substrate and 100 mM Tris–HCl (pH 8.0). The extinction coefficients of allantoin and dihydroorotate were 0.0261 $mM^{-1}$ $cm^{-1}$ at 258 nm and 0.92 $mM^{-1}$ $cm^{-1}$ at 230 nm, respectively. Substrate hydrolysis was monitored with a UV/vis spectrophotometer (Hitachi U 3300, Hitachi High-Technologies, Tokyo, Japan). The initial rates of change were a function of enzyme concentration within the absorbance range of 0.01–0.3 $min^{-1}$. A unit of activity was defined as the amount of enzyme catalyzing the hydrolysis of 1 μmol substrate/min, and the specific activity was expressed in terms of units of activity per milligram of enzyme. The kinetic parameters $K_m$ and $V_{max}$ were determined by fitting the hydrolyzing rate from individual experiments to the Michaelis–Menten equation.

### 2.5. Dissociation constants determined by fluorescence spectrophotometer

Determination of the dissociation constants ($K_d$) for allantoinase and dihydroorotase was using the fluorescence quenching method as previously described for DnaB helicase [34,37]. An aliquot of each compound was added into the solution containing allantoinase or dihydroorotase (0.8 μM), 50 mM HEPES at pH 7.0 with a final volume of 2 mL in a quartz cuvettes of 1 cm square cross-section. The decrease in intrinsic fluorescence of protein was measured at 330 nm upon excitation at 280 nm and 25 °C with a spectrofluorimeter (Hitachi F-2700; Hitachi High-Technologies, Tokyo, Japan). At least seven data points were used to calculate each $K_d$. Each data point was an average of 2–3 determinants, and the difference of the determinants was within 10%. The $K_d$ was obtained by the equation: $\Delta F = \Delta F_{max} - K_d(\Delta F/[\text{compound}])$ (Enzyme Kinetics module of Sigma-Plot; Systat Software, Chicago, IL, USA).

### 2.6. Determination of $IC_{50}$

Dose-response curves were generated by titrating compound into the enzyme assay solution. The concentration of the compound required for 50% inhibition ($IC_{50}$) was determined directly from the graphic analysis. Due to solubility, $IC_{50}$ of some compounds for allantoinase and dihydroorotase were not determined.

### 2.7. Bioinformatics

The model of *S. enterica* allantoinase was built from the coordinates of *Bacillus halodurans* allantoinase (3HM7; 42% identity) using SWISS-MODEL, (http://swissmodel.expasy.org) [43]. Similarly, the model of *K. pneumoniae* dihydroorotase was built from the coordinates of *S. enterica* dihydroorotase (3JZE; 93% identity). The coordinate and topology file of the flavonols, myricetin, quercetin, kaempferol, and galangin, was found in DrugBank, http://www.drugbank.ca/ [44]. Kaempferol was computationally docked into the three-dimensional models of allantoinase and dihydroorotase by using PatchDock, http://bioinfo3d.cs.tau.ac.il/PatchDock/ [45]. The hydantoin-complexed structure models of allantoinase and dihydroorotase were directly constructed by superimposing the structure of the apo form with the crystal structure of the hydantoin-dihydropyrimidinase complex (the coordinate of 4LCS). The structures were visualized by using the program PyMol.

## 3. Results

### 3.1. Hydantoin is not a substrate for allantoinase and dihydroorotase

Bacterial allantoinase and dihydroorotase are members of the cyclic amidohydrolase family. This family includes hydantoinase/dihydropyrimidinase, dihydroorotase, allantoinase, and imidase, which use hydantoin, dihydroorotate, allantoin, and phthalimide as a substrate, respectively (Fig. 1A). Members of this family have very similar active sites (Fig. 1B) and may use the same catalytic mechanism for substrate hydrolysis (Fig. 1C). This condition raises an interesting question as to whether the substrate specificities of allantoinase and dihydroorotase partially overlap with those of the other cyclic amidohydrolases. Hydantoinase/dihydropyrimidinase [6,46,47] and imidase [7,8,11] have broad and overlapping substrate specificities. However, the standard assays showed no reaction over 2 h when allantoinase was incubated with hydantoin (10 and 100 mM), dihydroorotate (1 and 10 mM), or pthalimide (0.1 and 1 mM) (data not shown). Similarly, dihydroorotase showed no reaction when tested with allantoin (4 and 40 mM), hydantoin (10 and 100 mM), or pthalimide (0.1 and 1 mM) (data not shown). The maximal concentration of phthalimide was limited to 1 mM due to its minimal solubility. Thus, unlike hydantoinase and imidase, allantoinase and dihydroorotase have absolute substrate specificities toward their own substrates, namely, allantoin and dihydroorotate, respectively. Although these cyclic amidohydrolases may use a similar active site and mechanism for catalysis, no substrate overlapping was observed for allantoinase and dihydroorotase.

### 3.2. Hydantoin and dihydroorotate are potential competitive inhibitors of allantoinase

Based on the catalytic mechanism of the cyclic amidohydrolases (Fig. 1C), hydantoin should be, but is actually not, a substrate of

Please cite this article in press as: W.-F. Peng, C.-Y. Huang, Allantoinase and dihydroorotase binding and inhibition by flavonols and the substrates of cyclic amidohydrolases, Biochimie (2014), http://dx.doi.org/10.1016/j.biochi.2014.01.001

**Table 1**
Apparent Michaelis–Menten constants for allantoinase in the presence of kaempferol and the substrate of other cyclic amidohydrolases.

| Compound | Allantoinase | | | |
|---|---|---|---|---|
| | $V_{max}$ | $K_m$ | $V_{max}/K_m$ | Fold |
| Non | 130.5 ± 21.5 | 85.9 ± 20.0 | 1.52 | 1.00 |
| Dihydroorotate | 125.2 ± 21.9 | 129.6 ± 27.1 | 0.97 | 0.64 |
| Phthalimide | 130.0 ± 22.0 | 86.0 ± 20.4 | 1.51 | 0.99 |
| Hydantoin | 120.9 ± 18.4 | 108.3 ± 20.7 | 1.12 | 0.74 |
| Kaempferol | 118.8 ± 18.3 | 231.6 ± 29.2 | 0.51 | 0.34 |

At least seven data points were used to calculate each $V_{max}$ and $K_m$. Each data point was an average of 2–3 determinants, and the difference of the determinants was within 10%. The kinetic parameters *K*m and *V*max were determined by fitting the hydrolyzing rate from individual experiments to the Michaelis–Menten equation, and then the standard errors were given.

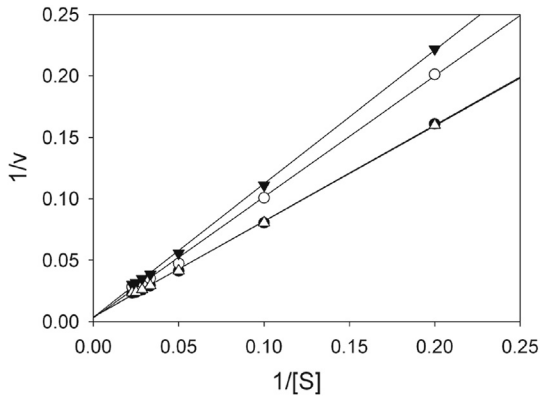


**Fig. 2.** Inhibition of allantoinase by substrate analogs. Inhibition of allantoinase by some substrates of other cyclic amidohydrolase. To determine which type of inhibitor is, the double reciprocal of the Lineweaver–Burk plots was used. The standard assay solution was conducted with hydantoin (open circle), dihydroorotate (inverted filled triangle), phthalimide (open triangle), or without any supplement (filled circle). The inhibitions of allantoinase by these compounds resulted in the Lineweaver–Burk plots where the lines are cross the *y*-axis at the very similar point, indicating that these compounds are competitive inhibitors for allantoinase. Data points are an average of 2–3 determinations within 10% error.

allantoinase and dihydroorotase. Hydantoin has a structure similar to that of allantoin, except for the 5′ side chain (Fig. 1A). Thus, hydantoin may be a potential allantoinase inhibitor. To assess whether hydantoin inhibits the activity of allantoinase, hydantoin (50 mM) was included in the standard allantoinase assay. In addition, dihydroorotate (2 mM) and phthalimide (1 mM) were also individually used for allantoinase inhibition studies (Table 1). The kinetic parameters of allantoinase were calculated from the double reciprocal of the Lineweaver–Burk plot with and without the substrate analog as a potential inhibitor. As shown in Fig. 2, inhibition of allantoinase by hydantoin and dihydroorotate resulted in Lineweaver–Burk plots where the lines intersect the *y*-axis at a similar point, which indicates that these compounds are competitive inhibitors of allantoinase. The inclusion of phthalimide into the assay at 1 mM did not affect the allantoinase activity. Thus, substrates of the cyclic amidohydrolase, at least hydantoin and dihydroorotate competed with allantoin for allantoinase active sites.

### 3.3. $IC_{50}$ of dihydroorotate, phthalimide, and hydantoin for allantoinase

To compare the inhibitory capability of dihydroorotate, phthalimide, and hydantoin on allantoinase, their $IC_{50}$ values, that is, the inhibitor concentration required to reduce the activity of the enzyme by 50%, were determined and compared. As shown in Fig. 3, dihydroorotate, phthalimide, and hydantoin at different concentrations were used to determine the $IC_{50}$ for allantoinase. The activity of allantoinase continued to decrease as the concentrations of dihydroorotate (Fig. 3A) and hydantoin (Fig. 3B) increased. Only 1 mM of phthalimide was used as the maximal concentration for $IC_{50}$ determination because of its poor solubility (data not shown). Phthalimide did not inhibit the activity of allantoinase. The IC50 for allantoinase of dihydroorotate was 18.6 ± 1.1 mM and that of hydantoin was 230 ± 10 mM. Thus, the inhibitory capability of dihydroorotate toward allantoinase was 12-fold higher than that of hydantoin, based on their $IC_{50}$ (Table 2).

### 3.4. $K_d$ of allantoinase bound to dihydroorotate, phthalimide, and hydantoin

From our initial inhibition study, some substrate analogs were identified as competitive inhibitors of allantoinase (Table 1 and Fig. 2). To determine whether their inhibitory capabilities are correlated with their binding abilities, the dissociation constants ($K_d$) of allantoinase for dihydroorotate, phthalimide, and hydantoin were determined through fluorescence quenching. The fluorescence emission spectra of allantoinase significantly quenched with hydantoin are shown in Fig. 4A. The fluorescence intensity of allantoinase also decreased remarkably with increasing dihydroorotate concentration, but not phthalimide (data not shown). Adding hydantoin and dihydroorotate resulted in a blue shift (~5 nm) of the allantoinase emission wavelength ($\lambda_{em}$), which indicates that dihydroorotate and hydantoin interact with allantoinase and suggest that dihydroorotate and hydantoin can form stable complexes with allantoinase. The $K_d$ values of allantoinase bound to dihydroorotate and hydantoin, as determined through

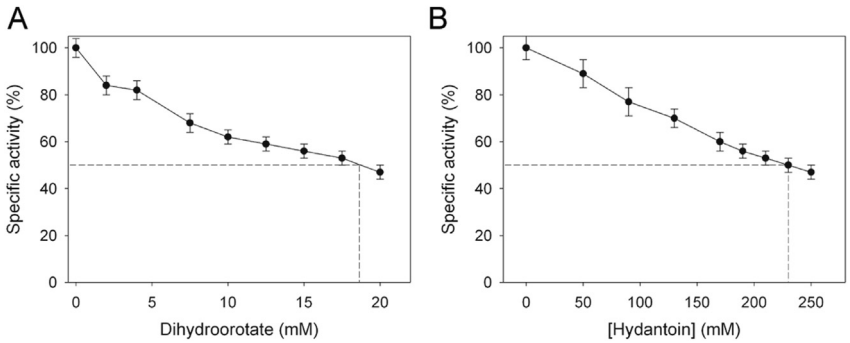


**Fig. 3.** $IC_{50}$ determinations for allantoinase (A) The concentration of dihydroorotate required for 50% inhibition of the activity of allantoinase was directly determined using graphic analysis. (B) $IC_{50}$ determination of hydantoin for allantoinase. The errors are standard deviation determined at 3 measurements.

Please cite this article in press as: W.-F. Peng, C.-Y. Huang, Allantoinase and dihydroorotase binding and inhibition by flavonols and the substrates of cyclic amidohydrolases, Biochimie (2014), http://dx.doi.org/10.1016/j.biochi.2014.01.001

**Table 2**
Effect of the flavonols and the substrate of other cyclic amidohydrolases on the activity of allantoinase and dihydroorotase.

| Compound | $IC_{50}$ (mM) | |
|---|---|---|
| | Allantoinase | Dihydroorotase |
| Dihydroorotate | 18.6 ± 1.1 | – |
| Phthalimide | – | – |
| Hydantoin | 230 ± 10 | – |
| Myricetin | ND | 0.040 ± 0.001 |
| Quercetin | ND | ND |
| Kaempferol | 0.035 ± 0.003 | 0.031 ± 0.002 |
| Galangin | ND | ND |

–: No effect under the concentration range of the compound.
ND: due to solubility, the $IC_{50}$ value was not determined.

**Table 3**
Binding of allantoinase and dihydroorotase to the substrate of other cyclic amidohydrolases and kaempferol.

| Compound | $K_d$ (mM) | |
|---|---|---|
| | Allantoinase | Dihydroorotase |
| Dihydroorotate | 3.89 ± 1.15 | ND |
| Hydantoin | 6.06 ± 1.18 | 39.5 ± 6.8 |
| Allantoin | ND | 57.7 ± 2.3 |
| Kaempferol | 0.028 ± 0.004 | 0.021 ± 0.004 |

The decrease in intrinsic fluorescence of protein was measured at 330 nm upon excitation at 280 nm and 25 °C with a spectrofluorimeter. At least seven data points were used to calculate each $K_d$. Each data point was an average of 2–3 determinants, and the difference of the determinants was within 10%. The $K_d$ was obtained by the equation: $\Delta F = \Delta F_{max} - K_d(\Delta F/[\text{compound}])$, and then the standard error was given.
ND, not determined.

their titration curves (Fig. 4B), were 3.89 ± 1.15 and 6.06 ± 1.18 mM, respectively (Table 3). Therefore, dihydroorotate exhibits the strongest binding and inhibitory capabilities toward allantoinase.

### 3.5. Allantoin and hydantoin bind to dihydroorotase, but does not inhibit its activity

Dihydroorotase cannot use hydantoin, phthalimide, and allantoin as a substrate. To test the dihydroorotase inhibitory capability of these compounds, allantoin (10 mM), phthalimide (1 mM), and hydantoin (50 mM) were individually included in the standard assay for dihydroorotase. However, unlike allantoinase, hydantoin, phthalimide, and allantoin did not affect dihydroorotase activity. Allantoin at 1 mM–40 mM and hydantoin at 1 mM–100 mM did not affect dihydroorotase activity. Thus, hydantoin, phthalimide, and allantoin were not inhibitors of dihydroorotase.

Fluorescence quenching was used to determine the $K_d$ of dihydroorotase for hydantoin and allantoin. The fluorescence emission spectra of dihydroorotase significantly quenched with hydantoin are shown in Fig. 5A. The fluorescence intensity of dihydroorotase also decreased remarkably with increasing allantoin concentration (data not shown). Adding hydantoin and allantoin resulted in a blue shift (~10 nm) of the emission wavelength ($\lambda_{em}$) of dihydroorotase, which indicates that dihydroorotase interacts with allantoin and hydantoin. The $K_d$ values of dihydroorotase bound to allantoin and hydantoin determined using titration curves (Fig. 5B) were 57.7 ± 2.3 and 39.5 ± 6.8 mM, respectively (Table 3). Thus, dihydroorotase can bind to allantoin and hydantoin, but cannot hydrolyze these compounds. Given that the $V_{max}$ and $K_m$ of dihydroorotase, determined from the titration curves (Fig. 5C), were 11.8 ± 0.4 μmol/mg/min and 0.13 ± 0.02 mM, respectively, the binding of allantoin and hydantoin to dihydroorotase is possibly too weak (<100 folds) to compete with dihydroorotate for the dihydroorotase active site.

### 3.6. Use of flavonols in allantoinase and dihydroorotase inhibition

Substrate analogs for any enzyme are usually potential inhibitors. Although we found that substrate analogs such as dihydroorotate and hydantoin inhibit allantoinase activity, their $IC_{50}$ values were at the mM range, which is not significant for designing inhibitors. To determine whether a natural product is an inhibitor for allantoinase and dihydroorotase, the inhibitory capability of the flavonols myricetin, quercetin, kaempferol, and galangin toward allantoinase and dihydroorotase were tested (Fig. 6A).

### 3.7. Identification of the flavonol inhibition of allantoinase and dihydroorotase

Flavonols are known to have antioxidant [30], antiradical [31], and antibacterial activities [35]. To determine whether flavonols inhibit allantoinase and dihydroorotase, myricetin, quercetin, kaempferol, and galangin at different concentrations were included in the standard assay. The titration curves shown in Fig. 6B suggest that kaempferol most strongly inhibited allantoinase. The order of the inhibitory capability of the flavonols is as follows: kaempferol > galangin > quercetin > myricetin. For dihydroorotase, kaempferol also exhibited the strongest inhibition of enzyme activity. The order of inhibitory capability of the flavonols is as follows: kaempferol > myricetin > galangin > quercetin (Fig. 6C). Thus, flavonols, especially kaempferol, are novel inhibitors of allantoinase and dihydroorotase. In addition, the inhibitory capability of these flavonols (at the μM range) was significantly higher

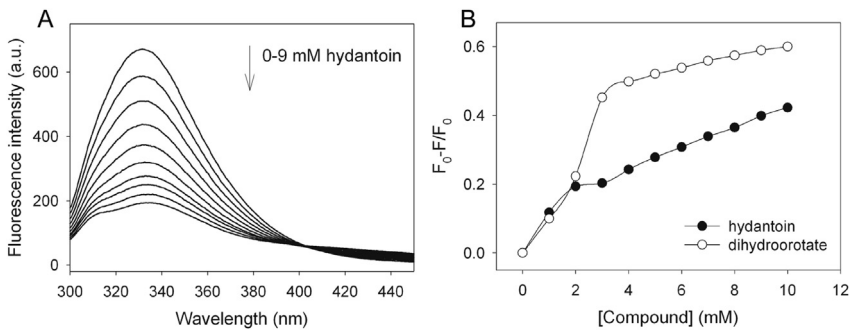


**Fig. 4.** Binding of allantoinase to the substrate of other cyclic amidohydrolases. (A) The fluorescence emission spectra of allantoinase with hydantoin of different concentrations (0–9 mM). The decrease in intrinsic fluorescence of protein was measured at 330 nm upon excitation at 280 nm and 25 °C with a spectrofluorimeter. The fluorescence intensity emission spectra of allantoinase significantly quenched with hydantoin. (B) An aliquot amount of hydantoin and dihydroorotate was individually added to the enzyme solution for each $K_d$. The $K_d$ was obtained by the equation: $\Delta F = \Delta F_{max} - K_d(\Delta F/[\text{compound}])$. Data points are an average of 2–3 determinations within 10% error.

Please cite this article in press as: W.-F. Peng, C.-Y. Huang, Allantoinase and dihydroorotase binding and inhibition by flavonols and the substrates of cyclic amidohydrolases, Biochimie (2014), http://dx.doi.org/10.1016/j.biochi.2014.01.001

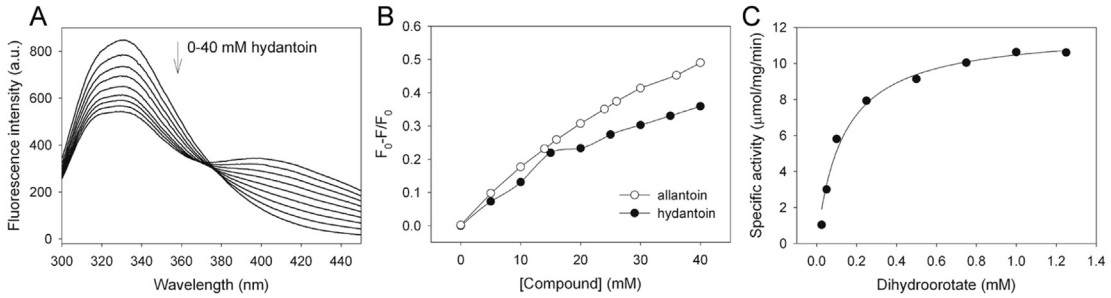


**Fig. 5.** Allantoin and hydantoin can bind, but cannot inhibit the activity of dihydroorotase. (A) The fluorescence emission spectra of dihydroorotase with hydantoin of different concentrations (0–40 mM). The decrease in intrinsic fluorescence of protein was measured at 330 nm upon excitation at 280 nm and 25 °C with a spectrofluorimeter. The fluorescence intensity emission spectra of dihydroorotase significantly quenched with hydantoin. (B) An aliquot amount of hydantoin and allantoin was individually added to the enzyme solution for each $K_d$. The $K_d$ was obtained by the equation: $\Delta F = \Delta F_{max} - K_d(\Delta F/[\text{compound}])$. (C) Kinetic analysis of dihydroorotase using dihydroorotate of different concentrations (0–1.25 mM) with the $V_{max}$ value of 11.8 ± 0.4 μmol/mg/min and the $K_m$ value of 0.13 ± 0.02 mM. Data points are an average of 2–3 determinations within 10% error.

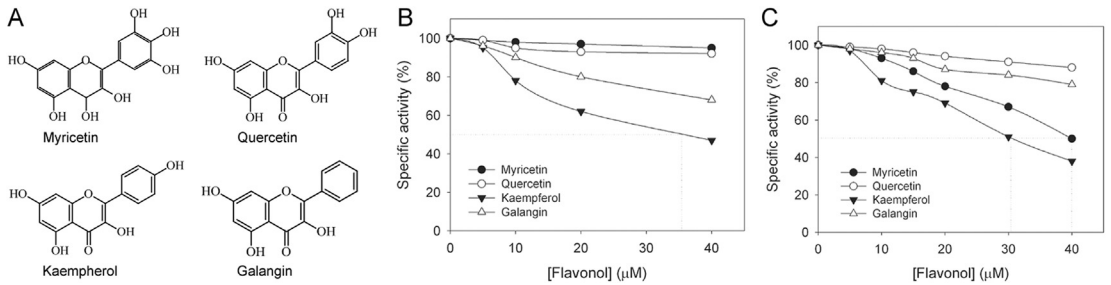


**Fig. 6.** The flavonol inhibitions of allantoinase and dihydroorotase. (A) Molecular structure of the flavonols, myricetin, quercetin, kaempferol, and galangin. They have a similar structure but contain different numbers of hydroxyl substituents on the aromatic rings. (B) $IC_{50}$ determination of flavonols for allantoinase. Due to solubility, $IC_{50}$ of some flavonols was not determined from the graphic analysis. (C) $IC_{50}$ determination of flavonols for dihydroorotase. Data points are an average of 2–3 determinations within 10% error.

than that of the substrate analogs (at the mM range) of allantoinase and dihydroorotase. However, because of the poor solubility of these flavonols, only some $IC_{50}$ values for allantoinase and dihydroorotase were determined (Table 2). Based on our knowledge, kaempferol remains the best inhibitor for allantoinase, with an $IC_{50}$ of 35 ± 3 μM, and for dihydroorotase, with $IC_{50}$ of 31 ± 2 μM.

### 3.8. $K_d$ of allantoinase and dihydroorotase bound to kaempferol

The initial inhibition study of flavonols indicated that allantoinase and dihydroorotase were both significantly inhibited by kaempferol. To determine whether the inhibitory capabilities are correlated with their binding abilities, the $K_d$ values of allantoinase and dihydroorotase for kaempferol were determined through fluorescence quenching. The $K_d$ values of allantoinase and dihydroorotase bound to kaempferol determined using titration curve (Fig. 7) were 28.3 ± 3.8 and 20.9 ± 3.9 μM, respectively (Table 3). Thus, kaempferol can inhibit and bind to allantoinase and dihydroorotase with $IC_{50}$ and $K_d$ values at the μM range, significantly higher than those of the substrate analogs of allantoinase and dihydroorotase (at the mM range).

### 3.9. Kaempferol is a competitive inhibitor of allantoinase

From our initial inhibition screening, the flavonol kaempferol was identified as an inhibitor of allantoinase for the first time. To determine which type of inhibitor kaempferol is, this flavonol (40 μM) was included in the standard assay for allantoinase with different concentrations of allantoin, and the kinetic parameters of allantoinase were calculated from the double reciprocal of the Lineweaver–Burk plot. As shown in Fig. 8, inhibition of allantoinase by kaempferol resulted in Lineweaver–Burk plots with lines that cross the y-axis at a similar point, which indicates that kaempferol is a competitive inhibitor for allantoinase. Thus, similar to hydantoin and dihydroorotate, kaempferol can compete with allantoin for the active site of allantoinase, but with significantly stronger activity.

### 3.10. Kaempferol is an uncompetitive inhibitor for dihydroorotase

In this study, the flavonol kaempferol was identified as an inhibitor of dihydroorotase for the first time. To determine whether kaempferol competitively inhibits dihydroorotase, as with allantoinase, kaempferol (40 μM) was included in the standard assay for

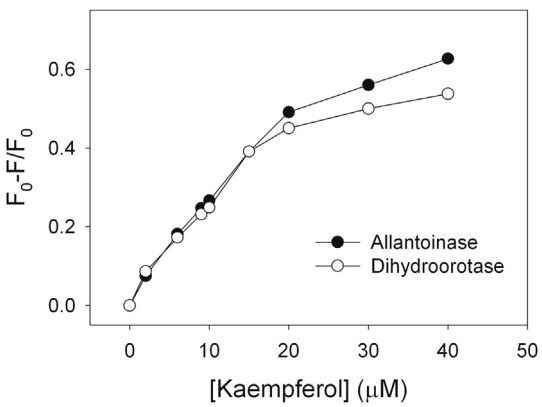


**Fig. 7.** Fluorescence titrations of kaempferol with allantoinase and dihydroorotase. An aliquot amount of kaempferol was added to the enzyme solution for each $K_d$. The $K_d$ was obtained by the equation: $\Delta F = \Delta F_{max} - K_d(\Delta F/[\text{kaempferol}])$. Data points are an average of 2–3 determinations within 10% error.

Please cite this article in press as: W.-F. Peng, C.-Y. Huang, Allantoinase and dihydroorotase binding and inhibition by flavonols and the substrates of cyclic amidohydrolases, Biochimie (2014), http://dx.doi.org/10.1016/j.biochi.2014.01.001

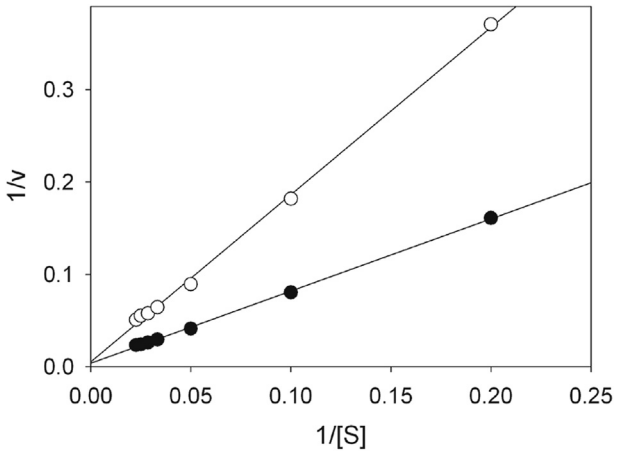


**Fig. 8.** Kaempferol is a competitive inhibitor for allantoinase. Inhibition of allantoinase by kaempferol resulted in Lineweaver–Burk plots where the lines are cross the *y*-axis at the similar point, indicating that kaempferol is a competitive inhibitor for allantoinase. Data points are an average of 2–3 determinations within 10% error.

dihydroorotase with different dihydroorotate concentrations. Unexpectedly, the inhibition of dihydroorotase by kaempferol resulted in Lineweaver–Burk plots with lines parallel that intersect the *y*-axis at different points, which indicates that kaempferol is an uncompetitive inhibitor (Fig. 9). Dihydroorotase in the presence of 40 μM kaempferol had a $V_{max}$ of 4.24 ± 0.06 μmol/mg/min and a $K_m$ of 0.048 ± 0.004 mM. Based on these kinetic results, kaempferol binds to the dihydroorotase–dihydroorotate complex rather than acts to a free enzyme, and then allosterically inhibits dihydroorotase. Taken together, kaempferol is a competitive inhibitor of allantoinase and an uncompetitive inhibitor of dihydroorotase.

### 3.11. Binding mode of allantoinase to kaempferol

To understand the inhibitory mechanism of kaempferol on allantoinase, the structure of allantoinase was built through homology modeling. Kaempferol, which is found in the DrugBank, was then computationally docked into the three-dimensional model of allantoinase using PatchDock (http://bioinfo3d.cs.tau.ac.il/PatchDock/) [45]. Docking was automatically performed after uploading the coordinate and topology file of flavonol and allantoinase. The three docking models (Supplementary materials) with the highest score for allantoinase interacting with kaempferol are shown in Fig. 10A. Kaempferol with different binding poses was docked into the active site pocket of allantoinase. For solution 1 with the highest docking score, the hydroxyl groups of kaempferol on the ring interact with Ser286 and Ser317 (Fig. 10B). Ser317 is a critical substrate binding site for allantoinase [14]. Thus, the docking study shows that kaempferol partially occupies the allantoinase active site. Consistent with the kinetic evidence, the docking study also shows that kaempferol competitively inhibits allantoinase.

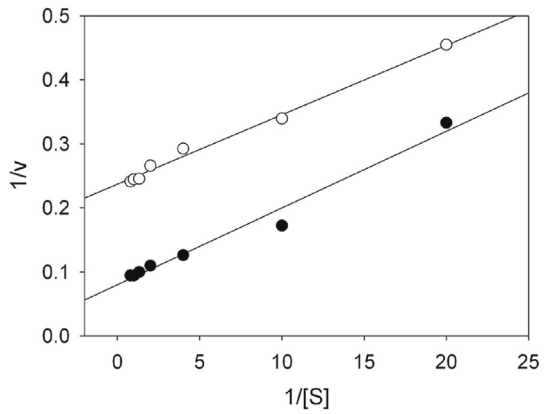


**Fig. 9.** Kaempferol is an uncompetitive inhibitor for dihydroorotase. Inhibition of dihydroorotase by kaempferol resulted in Lineweaver–Burk plots where the lines are parallel and cross the *y*-axis at different points, revealing an uncompetitive inhibitor. Data points are an average of 2–3 determinations within 10% error.

### 3.12. Binding mode of dihydroorotase to kaempferol

To study the inhibitory effect of kaempferol on dihydroorotase and the dihydroorotase–kaempferol complex, the model of *K. pneumoniae* dihydroorotase was computationally docked with kaempferol using PatchDock, as was done for allantoinase. The three dihydroorotase docking models (Supplementary materials) with the highest score for interacting with kaempferol are shown in Fig. 11A. Unlike allantoinase, the binding poses of kaempferol were all found to be docked outside the active site pocket of dihydroorotase. For solution 1 with the highest docking score, the hydroxyl groups of kaempferol on the ring interacted with E35, G277, and V346 (Fig. 11B). The docking study shows that kaempferol does not interact with the active site of dihydroorotase, a result consistent with the kinetic study (see Discussion).

## 4. Discussion

The development of clinically useful small-molecule antibiotics has been a seminal event in the field of infectious diseases [48]. DNA metabolism is one of the most basic biological functions and should be a prime target in antibiotic development. Considering allantoinase and dihydroorotase are required for metabolizing purines and pyrimidines, blocking their activities would be detrimental to bacterial survival. In addition, allantoinase is not found in humans; hence, these inhibitors are potentially safe for human use. The distinct differences between mammalian and prokaryotic dihydroorotases make bacterial dihydroorotases suitable targets for antibiotic development [16]. Although some chelators, such as 8-HQSA [42], inhibit allantoinase, such chelators are harmful to humans. In this study, we have shown that some flavonol compounds inhibit the catalytic activities of allantoinase (Fig. 6B) and dihydroorotase (Fig. 6C). Furthermore, the metabolic effects and safety of the flavonols are well established, making such flavonols beneficial for humans [28]. Thus, flavonols inhibit allantoinase and dihydroorotase, as well as potential antibiotics for further development.

We found that the flavonols myricetin, quercetin, kaempferol, and galangin, which contain different numbers of hydroxyl substituents on their aromatic rings (Fig. 6A), have different inhibitory effects on allantoinase and dihydroorotase (Fig. 6B and C). The catalytic activities of allantoinase and dihydroorotase were inhibited by flavonols in the following order: kaempferol > galangin > quercetin > myricetin for allantoinase, and kaempferol > myricetin > galangin > quercetin for dihydroorotase, respectively. Kaempferol, which contains one hydroxyl substituent on the flavonol aromatic ring, was the best inhibitor for allantoinase, with an $IC_{50}$ of 35 ± 3 μM, and for dihydroorotase, with an $IC_{50}$ of 31 ± 2 μM (Fig. 5A). Although flavonols are known to have several hydroxyl groups, thus, they have remarkable potential for binding any protein, the strength of the inhibitory effect ($IC_{50}$) on allantoinase and dihydroorotase did not correlate with the number of hydroxyl substituents on the flavonol aromatic rings.

The docking experiments of allantoinase and dihydroorotase suggested that kaempferol docks into the active site pocket of

Please cite this article in press as: W.-F. Peng, C.-Y. Huang, Allantoinase and dihydroorotase binding and inhibition by flavonols and the substrates of cyclic amidohydrolases, Biochimie (2014), http://dx.doi.org/10.1016/j.biochi.2014.01.001

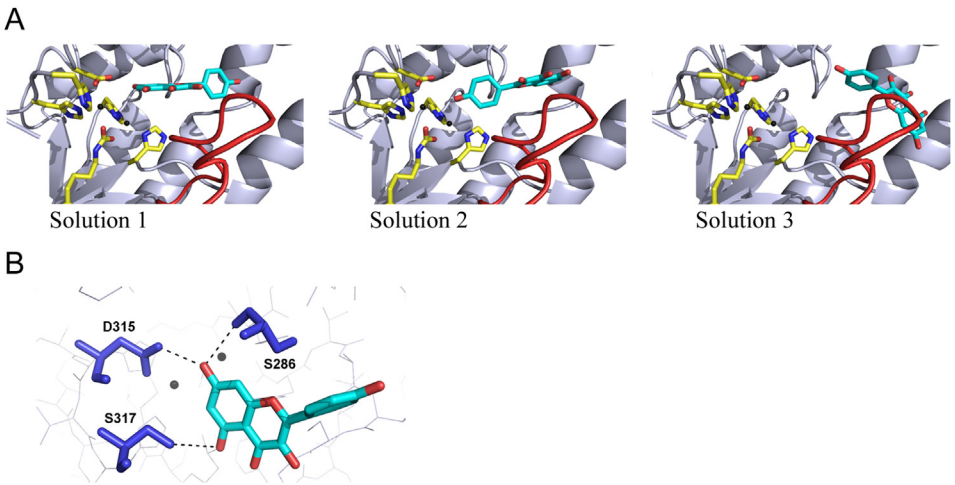


**Fig. 10.** Representation of the docking models of allantoinase–kaempferol complex from PatchDock. (A) The three docking models with the highest score for allantoinase interacting with kaempferol are shown. The active site residues of allantoinase are colored in yellow, and the substrate binding loop is colored in red. Kaempferol is colored in cyan. (B) Binding environment of kaempferol to allantoinase for Solution 1. The hydroxyl groups of kaempferol on the ring interact with S286, D315, and S317 of allantoinase.

allantoinase, but outside the active site pocket of dihydroorotase. Consistent with the docking results, the kinetic studies further identified kaempferol as a competitive inhibitor of allantoinase, but an uncompetitive inhibitor of dihydroorotase. Three docking solutions with the highest scores all show that kaempferol partially occupies the active site of allantoinase by interacting with the putative substrate-binding loop (Fig. 10). For dihydroorotase, kaempferol was bound to the loop with an unknown function. However, the corresponding positions of dihydroorotase for dihydropyrimidinase are structurally near the place for the conformational change of dihydropyrimidinase [49]. Thus, kaempferol may inhibit dihydroorotase allosterically. No potent inhibitor has been identified for these cyclic amidohydrolases. Thus, inhibitors designed to target the loop(s) to lock the conformation of the cyclic amidohydrolases may be worth to test in the future.

The cyclic amidohydrolases, at least hydantoinase [25,46,47], dihydropyrimidinase [50,51], and imidase [7,8,10,11], are known to catalyze the hydrolysis of a wide range of substrates and exhibit some overlapping substrate specificities. Our study clearly indicates that hydantoin, dihydroorotate, and phthalimide are not substrates, but are competitive inhibitors of allantoinase (Fig. 2). Unlike allantoinase, although hydantoin, allantoin, and phthalimide are not dihydroorotase substrates, they did not affect dihydroorotase activity. Nevertheless, dihydroorotase still binds to hydantoin and allantoin (Fig. 5A and Table 3).

The chemical mechanism of the binuclear metal center–containing amidohydrolase [2] likely has three steps (Fig. 1C): (1) the hydrolytic water molecule must be activated for nucleophilic attack, (2) the amide bond of the substrate must be made more electrophilic by the polarization of the carbonyl–oxygen bond, and (3) the leaving group nitrogen must be protonated as the carbon–nitrogen bond is cleaved. Thus, a single group must be unprotonated for the catalytic activity [52]. Based on the crystal structures of hydantoinase [53], dihydropyrimidinase [51], dihydroorotase [23], and allantoinase [14], the bimetal ion likely functions as a Lewis acid for polarizing the carbonyl group of the substrate of the imide group [13,24,25]. The carbonyl oxygen of the substrate that directly interacts with the metal center will diminish the electron density and facilitate nucleophilic attacks by the bridging the hydroxide. In the final step, the amide nitrogen of the substrate must be protonated. The conserved Asp in the active site of these cyclic amidohydrolases is responsible for proton transfer (Fig. 1B and C).

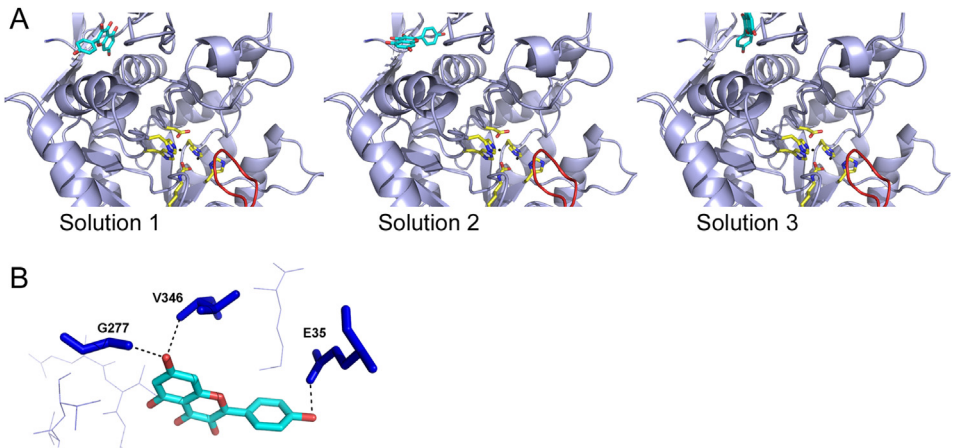


**Fig. 11.** Representation of the docking models of dihydroorotase–kaempferol complex from PatchDock. The three docking models with the highest score for dihydroorotase interacting with kaempferol are shown. The active site residues of dihydroorotase are colored in yellow, and the substrate binding loop is colored in red. Kaempferol is colored in cyan. (B) Binding environment of kaempferol to dihydroorotase for Solution 1. The hydroxyl groups of kaempferol on the ring interact with E35, G277, and V346 of dihydroorotase.

Please cite this article in press as: W.-F. Peng, C.-Y. Huang, Allantoinase and dihydroorotase binding and inhibition by flavonols and the substrates of cyclic amidohydrolases, Biochimie (2014), http://dx.doi.org/10.1016/j.biochi.2014.01.001

This residue has been proposed as the group that shuttles the proton from the bridging hydroxide to and from the substrate and product during catalysis. However, an important question remains as to why even at more than 100 mM, hydantoin can bind to, but absolutely cannot be hydrolyzed by, allantoinase and dihydroorotase. In addition, hydantoin can be docked into the active site of allantoinase (data not shown). Does the 5′ side chain of allantoin play an important role not only in interacting with the substrate binding loop of allantoinase but also involve in electron/proton delocalization as the driving force for imide hydrolysis? Further studies are needed to investigate the substrate specificity, selectivity, and the catalytic mechanism of allantoinase and dihydroorotase.

In conclusion, we identified a novel inhibitor, the flavonol kaempferol, and demonstrated its inhibitory mechanism on allantoinase and dihydroorotase using kinetic and docking experiments. We also found that allantoinase and dihydroorotase cannot use the substrates of other cyclic amidohydrolases as substrate. The significant inhibitory effect of kaempferol on allantoinase and dihydroorotase (>3 orders of magnitude than hydantoin) make it a promising drug lead for developing antibiotics targeting bacteria.

## Disclosure statement

The authors have no conflicts of interest.

## Acknowledgments

We would like to thank four anonymous reviewers and the editor for their comments. This research was supported by a grant from the National Science Council, Taiwan (NSC 102-2320-B-040-019 to C.Y. Huang).

## Appendix A. Supplementary data

Supplementary data related to this article can be found at http://dx.doi.org/10.1016/j.biochi.2014.01.001.

## References

[1] J.A. Gerlt, K.N. Allen, S.C. Almo, R.N. Armstrong, P.C. Babbitt, J.E. Cronan, D. Dunaway-Mariano, H.J. Imker, M.P. Jacobson, W. Minor, C.D. Poulter, F.M. Raushel, A. Sali, B.K. Shoichet, J.V. Sweedler, The enzyme function initiative, Biochemistry 50 (2011) 9950–9962.
[2] C.M. Seibert, F.M. Raushel, Structural and catalytic diversity within the amidohydrolase superfamily, Biochemistry 44 (2005) 6383–6391.
[3] J.A. Gerlt, P.C. Babbitt, Divergent evolution of enzymatic function: mechanistically diverse superfamilies and functionally distinct suprafamilies, Annu. Rev. Biochem. 70 (2001) 209–246.
[4] G.J. Kim, H.S. Kim, Identification of the structural similarity in the functionally related amidohydrolases acting on the cyclic amide ring, Biochem. J. 330 (1998) 295–302.
[5] L. Holm, C. Sander, An evolutionary treasure: unification of a broad set of amidohydrolases related to urease, Proteins 28 (1997) 72–82.
[6] J. Altenbuchner, M. Siemann-Herzberg, C. Syldatk, Hydantoinases and related enzymes as biocatalysts for the synthesis of unnatural chiral amino acids, Curr. Opin. Biotechnol. 12 (2001) 559–563.
[7] Y.W. Shi, X.Q. Liu, P. Shi, X.Y. Zhang, Characterization of zinc-binding properties of a novel imidase from *Pseudomonas putida* YZ-26, Arch. Biochem. Biophys. 494 (2009) 1–6.
[8] C.Y. Huang, Y.S. Yang, A novel cold-adapted imidase from fish *Oreochromis niloticus* that catalyzes hydrolysis of maleimide, Biochem. Biophys. Res. Commun. 312 (2003) 467–472.
[9] C.Y. Huang, Y.S. Yang, The role of metal on imide hydrolysis: metal content and pH profiles of metal ion-replaced mammalian imidase, Biochem. Biophys. Res. Commun. 297 (2002) 1027–1032.
[10] J. Ogawa, C.L. Soong, M. Honda, S. Shimizu, Imidase, a dihydropyrimidinase-like enzyme involved in the metabolism of cyclic imides, Eur. J. Biochem. 243 (1997) 322–327.
[11] Y.S. Yang, S. Ramaswamy, W.B. Jakoby, Rat liver imidase, J. Biol. Chem. 268 (1993) 10870–10875.
[12] S. Hayashi, S. Fujiwara, T. Noguchi, Evolution of urate-degrading enzymes in animal peroxisomes, Cell. Biochem. Biophys. 32 (2000) 123–129.
[13] Y.Y. Ho, Y.H. Huang, C.Y. Huang, Chemical rescue of the post-translationally carboxylated lysine mutant of allantoinase and dihydroorotase by metal ions and short-chain carboxylic acids, Amino Acids 44 (2013) 1181–1191.
[14] K. Kim, M.I. Kim, J. Chung, J.H. Ahn, S. Rhee, Crystal structure of metal-dependent allantoinase from *Escherichia coli*, J. Mol. Biol. 387 (2009) 1067–1074.
[15] I. Ramazzina, L. Cendron, C. Folli, R. Berni, D. Monteverdi, G. Zanotti, R. Percudani, Logical identification of an allantoinase analog (puuE) recruited from polysaccharide deacetylases, J. Biol. Chem. 283 (2008) 23295–23304.
[16] D.R. Evans, H.I. Guy, Mammalian pyrimidine biosynthesis: fresh insights into an ancient pathway, J. Biol. Chem. 279 (2004) 33035–33038.
[17] T. Nara, M. Hashimoto, H. Hirawake, C.W. Liao, Y. Fukai, S. Suzuki, A. Tsubouchi, J. Morales, S. Takamiya, T. Fujimura, H. Taka, R. Mineki, C.K. Fan, D.K. Inaoka, M. Inoue, A. Tanaka, S. Harada, K. Kita, T. Aoki, Molecular interaction of the first 3 enzymes of the de novo pyrimidine biosynthetic pathway of *Trypanosoma cruzi*, Biochem. Biophys. Res. Commun. 418 (2012) 140–143.
[18] M.I. Mally, D.R. Grayson, D.R. Evans, Catalytic synergy in the multifunctional protein that initiates pyrimidine biosynthesis in Syrian hamster cells, J. Biol. Chem. 255 (1980) 11372–11380.
[19] R.I. Christopherson, M.E. Jones, The overall synthesis of L-5,6-dihydroorotate by multienzymatic protein pyr1-3 from hamster cells. Kinetic studies, substrate channeling, and the effects of inhibitors, J. Biol. Chem. 255 (1980) 11381–11395.
[20] M.W. Washabaugh, K.D. Collins, Dihydroorotase from *Escherichia coli*. Purification and characterization, J. Biol. Chem. 259 (1984) 3293–3298.
[21] P. Zhang, P.D. Martin, C. Purcarea, A. Vaishnav, J.S. Brunzelle, R. Fernando, H.I. Guy-Evans, D.R. Evans, B.F. Edwards, Dihydroorotase from the hyperthermophile *Aquifex aeolicus* is activated by stoichiometric association with aspartate transcarbamoylase and forms a one-pot reactor for pyrimidine biosynthesis, Biochemistry 48 (2009) 766–778.
[22] D. McPhail, M. Shepherdson, The aspartate transcarbamoylase-dihydroorotase complex in *Deinococcus radiophilus* has an active dihydroorotase, Arch. Microbiol. 185 (2006) 78–81.
[23] J.B. Thoden, G.N. Phillips Jr., T.M. Neal, F.M. Raushel, H.M. Holden, Molecular structure of dihydroorotase: a paradigm for catalysis through the use of a binuclear metal center, Biochemistry 40 (2001) 6989–6997.
[24] T.N. Porter, Y. Li, F.M. Raushel, Mechanism of the dihydroorotase reaction, Biochemistry 43 (2004) 16285–16292.
[25] C.Y. Huang, C.C. Hsu, M.C. Chen, Y.S. Yang, Effect of metal binding and post-translational lysine carboxylation on the activity of recombinant hydantoinase, J. Biol. Inorg. Chem. 14 (2009) 111–121.
[26] V. Kumar, N. Saxena, M. Sarma, K.V. Radha Kishan, Carboxylated lysine is required for higher activities in hydantoinases, Protein Pept. Lett. 18 (2011) 663–669.
[27] K. Bush, Alarming beta-lactamase-mediated resistance in multidrug-resistant *Enterobacteriaceae*, Curr. Opin. Microbiol. 13 (2010) 558–564.
[28] J.A. Ross, C.M. Kasum, Dietary flavonoids: bioavailability, metabolic effects, and safety, Annu. Rev. Nutr. 22 (2002) 19–34.
[29] F. Teillet, A. Boumendjel, J. Boutonnat, X. Ronot, Flavonoids as RTK inhibitors and potential anticancer agents, Med. Res. Rev. 28 (2008) 715–745.
[30] K.L. Wolfe, R.H. Liu, Structure-activity relationships of flavonoids in the cellular antioxidant activity assay, J. Agric. Food. Chem. 56 (2008) 8404–8411.
[31] S. Burda, W. Oleszek, Antioxidant and antiradical activities of flavonoids, J. Agric. Food Chem. 49 (2001) 2774–2779.
[32] M.S. Yu, J. Lee, J.M. Lee, Y. Kim, Y.W. Chin, J.G. Jee, Y.S. Keum, Y.J. Jeong, Identification of myricetin and scutellarein as novel chemical inhibitors of the SARS coronavirus helicase, nsP13, Bioorg. Med. Chem. Lett. 22 (2012) 4049–4054.
[33] Y.S. Keum, Y.J. Jeong, Development of chemical inhibitors of the SARS coronavirus: viral helicase as a potential target, Biochem. Pharmacol. 84 (2012) 1351–1358.
[34] C.C. Chen, C.Y. Huang, Inhibition of *Klebsiella pneumoniae* DnaB helicase by the flavonol galangin, Protein J. 30 (2011) 59–65.
[35] T.P. Cushnie, A.J. Lamb, Antimicrobial activity of flavonoids, Int. J. Antimicrob. Agents 26 (2005) 343–356.
[36] C.C. Wang, H.W. Tsau, W.T. Chen, C.Y. Huang, Identification and characterization of a putative dihydroorotase, KPN01074, from *Klebsiella pneumoniae*, Protein J. 29 (2010) 445–452.
[37] H.H. Lin, C.Y. Huang, Characterization of flavonol inhibition of DnaB helicase: real-time monitoring, structural modeling, and proposed mechanism, J. Biomed. Biotechnol. 2012 (2012) 735368.
[38] Y.H. Huang, Y.H. Lo, W. Huang, C.Y. Huang, Crystal structure and DNA-binding mode of *Klebsiella pneumoniae* primosomal PriB protein, Genes Cells 17 (2012) 837–849.
[39] Y.H. Huang, C.Y. Huang, Characterization of a single-stranded DNA-binding protein from *Klebsiella pneumoniae*: mutation at either Arg73 or Ser76 causes a less cooperative complex on DNA, Genes Cells 17 (2012) 146–157.
[40] C.Y. Huang, C.H. Hsu, Y.J. Sun, H.N. Wu, C.D. Hsiao, Complexed crystal structure of replication restart primosome protein PriB reveals a novel single-stranded DNA-binding mode, Nucleic Acids Res. 34 (2006) 3878–3886.
[41] P.K. Smith, R.I. Krohn, G.T. Hermanson, A.K. Mallia, F.H. Gartner, M.D. Provenzano, E.K. Fujimoto, N.M. Goeke, B.J. Olson, D.C. Klenk, Measurement of protein using bicinchoninic acid, Anal. Biochem. 150 (1985) 76–85.

[42] Y.Y. Ho, H.C. Hsieh, C.Y. Huang, Biochemical characterization of allantoinase from *Escherichia coli* BL21, Protein J. 30 (2011) 384–394.
[43] K. Arnold, L. Bordoli, J. Kopp, T. Schwede, The SWISS-MODEL workspace: a web-based environment for protein structure homology modelling, Bioinformatics 22 (2006) 195–201.
[44] C. Knox, V. Law, T. Jewison, P. Liu, S. Ly, A. Frolkis, A. Pon, K. Banco, C. Mak, V. Neveu, Y. Djoumbou, R. Eisner, A.C. Guo, D.S. Wishart, DrugBank 3.0: a comprehensive resource for 'omics' research on drugs, Nucleic Acids Res. 39 (2011) D1035–D1041.
[45] D. Schneidman-Duhovny, Y. Inbar, R. Nussinov, H.J. Wolfson, PatchDock and SymmDock: servers for rigid and symmetric docking, Nucleic Acids Res. 33 (2005) W363–W367.
[46] U. Engel, C. Syldatk, J. Rudat, Stereoselective hydrolysis of aryl-substituted dihydropyrimidines by hydantoinases, Appl. Microbiol. Biotechnol. 94 (2012) 1221–1231.
[47] J.M. Clemente-Jimenez, S. Martinez-Rodriguez, F. Rodriguez-Vico, F.J. Heras-Vazquez, Optically pure alpha-amino acids production by the "Hydantoinase Process", Recent Pat. Biotechnol. 2 (2008) 35–46.
[48] A. Koul, E. Arnoult, N. Lounis, J. Guillemont, K. Andries, The challenge of new drug discovery for tuberculosis, Nature 469 (2011) 483–490.
[49] Y.C. Hsieh, M.C. Chen, C.C. Hsu, S.I. Chan, Y.S. Yang, C.J. Chen, Crystal structures of vertebrate dihydropyrimidinase and complexes from *Tetraodon nigroviridis* with lysine carbamylation: metal and structural requirements for post-translational modification and function, J. Biol. Chem. 288 (2013) 30645–30658.
[50] S. Martinez-Rodriguez, A.I. Martinez-Gomez, J.M. Clemente-Jimenez, F. Rodriguez-Vico, J.M. Garcia-Ruiz, F.J. Las Heras-Vazquez, J.A. Gavira, Structure of dihydropyrimidinase from *Sinorhizobium meliloti* CECT4114: new features in an amidohydrolase family member, J. Struct. Biol. 169 (2010) 200–208.
[51] B. Lohkamp, B. Andersen, J. Piskur, D. Dobritzsch, The crystal structures of dihydropyrimidinases reaffirm the close relationship between cyclic amidohydrolases and explain their substrate specificity, J. Biol. Chem. 281 (2006) 13762–13776.
[52] D.W. Christianson, J.D. Cox, Catalysis by metal-activated hydroxide in zinc and manganese metalloenzymes, Annu. Rev. Biochem. 68 (1999) 33–57.
[53] Y.H. Cheon, H.S. Kim, K.H. Han, J. Abendroth, K. Niefind, D. Schomburg, J. Wang, Y. Kim, Crystal structure of D-hydantoinase from *Bacillus stearothermophilus*: insight into the stereochemistry of enantioselectivity, Biochemistry 41 (2002) 9410–9417.

Please cite this article in press as: W.-F. Peng, C.-Y. Huang, Allantoinase and dihydroorotase binding and inhibition by flavonols and the substrates of cyclic amidohydrolases, Biochimie (2014), http://dx.doi.org/10.1016/j.biochi.2014.01.001